

2016

Task switching in the prefrontal cortex

<https://hdl.handle.net/2144/19067>

Boston University

BOSTON UNIVERSITY
SCHOOL OF MEDICINE

Dissertation

TASK SWITCHING IN THE PREFRONTAL CORTEX

by

ERIC L. DENOVELLIS

B.A., University of California, Santa Barbara, 2007

B.S., University of California, Santa Barbara, 2007

Submitted in partial fulfillment of the

requirements for the degree of

Doctor of Philosophy

2016

© 2016
ERIC L. DENOVELLIS
All rights reserved

Approved by

First Reader

Daniel Bullock Ph.D.
Professor, Department of Psychological and Brain Sciences

Second Reader

Helen Barbas, Ph.D.
Professor, Department of Health Sciences

Third Reader

Uri Eden, Ph.D.
Associate Professor, Department of Mathematics & Statistics

ACKNOWLEDGMENTS

Every dissertation is the product of the work of many people and mine is no exception. Although it is traditional to use the pronoun “I” in the dissertation with reference to the person writing the work, this does not encompass the people that contributed to the work and the gratitude that I feel towards those people. Please note that every time I use the pronoun “I” in my dissertation, I intend it to be with acknowledgement to the all the people that helped me along the way.

I would like to thank my parents, Richard and Angela Denovellis, for raising me and pushing me to be a person who perseveres. This latter part turned out to be quite instrumental in the process of obtaining a doctoral degree.

I would also like to thank my advisor, Daniel Bullock, who gave me the freedom to do work outside of the scope of his own work and was patient with my struggles to wrangle that work into a coherent dissertation.

I would also like to thank the other members of my committee: David Somers for providing direction for my committee; Helen Barbas for educating me and providing insight into the ever confusing anatomy of the prefrontal cortex; Uri Eden for guiding me to the right statistical path, particularly in Chapter III; and finally, Earl Miller for trusting me with his data and providing the framework for which a lot of this work is based. I would also like to informally include Timothy J. Buschman as part of this group for all the mentorship he provided me in the first half of graduate school and for the work he did on Chapter II of this dissertation.

Lastly, I want to thank my friends: Emily P. Stephen for not only being my partner and co-conspirator throughout graduate school, but providing valuable advice that shaped the direction of my work; Caroline Moore-Kochlacs for being a rock-solid friend and one of the toughest people I know; Austin Soplata for all the coffee breaks and random discussions; Samantha Michalka for grumbling through graduate school with me; and Franne Kahmi for her constant support and willingness to grab lunch. Nan Jia, Kayle Sawyer, EmilyKate McDonough, Yohan John, Stefan Berteau, Elizabeth McCarthy, Spencer Torene, Nicholas James, and Chris and Gretchen Markewicz also greatly enriched my graduate school experience.

TASK SWITCHING IN THE PREFRONTAL CORTEX

ERIC L. DENOVELLIS

Boston University School of Medicine, 2016

Major Professor: Daniel Bullock, Ph.D., Professor, Department of Psychological and Brain Sciences

ABSTRACT

The overall goal of this dissertation is to elucidate the cellular and circuit mechanisms underlying flexible behavior in the prefrontal cortex. We are often faced with situations in which the appropriate behavior in one context is inappropriate in others. If these situations are familiar, we can perform the appropriate behavior without relearning how the context relates to the behavior — an important hallmark of intelligence. Neuroimaging and lesion studies have shown that this dynamic, flexible process of remapping context to behavior (task switching) is dependent on prefrontal cortex, but the precise contributions and interactions of prefrontal subdivisions are still unknown.

This dissertation investigates two prefrontal areas that are thought to be involved in distinct, but complementary executive roles in task switching — the dorsolateral prefrontal cortex (dlPFC) and the anterior cingulate cortex (ACC). Using electrophysiological recordings from macaque monkeys, I show that synchronous network oscillations in the dlPFC provide a mechanism to flexibly coordinate context representations (rules) between groups of neurons during task switching. Then, I show that, whereas the ACC neurons can represent rules at the cellular level, they do not play a significant role in switching between contexts —

rather they seem to be more related to errors and motivational drive. Finally, I develop a set of web-enabled interactive visualization tools designed to provide a multi-dimensional integrated view of electrophysiological datasets.

Taken together, these results contribute to our understanding of task switching by investigating new mechanisms for coordination of neurons in prefrontal cortex, clarifying the roles of prefrontal subdivisions during task switching, and providing visualization tools that enhance exploration and understanding of large, complex and multi-scale electrophysiological data.

TABLE OF CONTENTS

ACKNOWLEDGMENTS	iv
ABSTRACT.....	vi
TABLE OF CONTENTS.....	viii
LIST OF TABLES	xiii
LIST OF FIGURES	xiv
LIST OF ABBREVIATIONS.....	xvii
CHAPTER I. INTRODUCTION.....	1
1.1 Background: The role of ACC and dlPFC in supporting flexible behavior	1
1.1.1 Prefrontal cortex and flexible behavior.....	1
1.1.2 ACC and dlPFC	3
1.1.3 ACC as recruiter of attention for action.....	4
1.1.4 ACC as error detector	5
1.1.5 ACC as conflict detector	6
1.1.6 ACC as action-outcome predictor.....	9
1.1.7 Recent models of ACC	11
1.2 Background: The role of prefrontal rhythms and coherence in circuit-level communication.....	12
1.3 Background: Interactive Visualization for Neuroscience	14
1.3.1 The purpose of visualization in science	14

1.3.2	Limitations of static visualizations in neuroscience	17
1.3.3	Interactive visualizations can help us quickly make comparisons and deal with complexity.....	20
1.3.4	Dynamic visualizations, when combined with interactivity, can help us understand complex data by preserving relationships between data	21
1.3.5	Web-enabled visualizations are familiar, easily shareable, and enable analysis transparency	22
1.3.6	Related Visualization Work.....	24
1.4	Summary of Dissertation	27
CHAPTER II: SYNCHRONOUS OSCILLATORY NEURAL ENSEMBLES FOR RULES IN THE PREFRONTAL CORTEX		30
2.1	Summary	30
2.2	Introduction.....	30
2.3	Results.....	33
2.3.1	Behavioral and Single Unit Evidence for the Dominance of the Orientation Rule.....	33
2.3.2	Rule-Selective LFP Synchronization between Pairs of Electrodes	36
2.3.3	Task-Relevant Neurons were Synchronized to the Current Rule-Network.....	39
2.3.4	Beta Orientation Network Shows Stronger Alpha Color Selectivity.....	40
2.3.5	Rule-Dependent Synchrony Correlates with Behavioral Reaction Time	42
2.4	Discussion.....	44
2.4.1	Linking Task-Relevant Neurons with Rule-Dependent Synchrony	44

2.4.2	Coordination of Neural Ensembles	45
2.5	Experimental Procedures	46
2.5.1	Recording Locations and Techniques	46
2.5.2	Behavioral Task	48
2.5.3	Behavioral and Neural Analysis Methods	50
2.5.4	Synchrony Analysis Methods	51
2.6	Supplemental Information	53
2.6.1	Behavioral Analysis	53
2.6.2	Rule-, Stimulus-, and Switch-Selectivity in Prefrontal Cortex Neurons	58
2.6.3	Time course of Neural Selectivity	60
2.6.4	Time-Frequency Decomposition of Local Field Potentials	61
2.6.5	Identification of Synchronous Sub-networks.....	63
2.6.6	Synchronous Sub-networks do not Reflect Differences in Evoked Potential..	67
2.6.7	Quantification of Synchronous Sub-network Structure.....	68
2.6.8	Alpha-Band Synchrony May Reflect a Suppressive Mechanism	72
2.6.9	Rule-Selective and Stimulus-Selective Neurons Synchronize with Currently Relevant Rule Sub-network	74
2.6.10	Sub-network Synchrony Changes with Behavior	76
CHAPTER III: THE ROLE OF ACC IN TASK SWITCHING.....		79
3.1	Summary	79
3.2	Introduction.....	79
3.3	Results.....	82

3.3.1 Cognitively demanding factors affect task performance	83
3.3.2 Single neurons respond to cognitive demand	87
3.3.3 ACC and dlPFC populations respond to cognitive demand	89
3.3.4 Within trial dynamics of cognitive demand selectivity	93
3.3.5 Does the ACC care about the number of trials from error (error distance) or the recent history of errors?	97
3.3.6 Can the current context affect ACC neurons?	99
3.4 Discussion	102
3.5 Materials and Methods	105
3.5.1 Subjects and Recordings	106
3.5.2 Task	106
3.5.3 Behavioral Analysis	108
3.5.4 Permutation Analysis	109
3.5.5 Spiking Model Parameters and Fitting	110
3.5.6 Spike Prediction	111
 CHAPTER IV: NEW TOOLS FOR WEB-ENABLED INTERACTIVE VISUALIZATIONS OF ELECTROPHYSIOLOGICAL DATA	
4.1. Summary	114
4.2. Introduction	115
4.3 Materials and Methods	119
4.3.1 Design	119
4.3.2 Configurable	120

4.3.3 Shareable.....	122
4.3.4 Modular and Extendable.....	123
4.4 Results.....	124
4.4.1 SpectraVis.....	124
4.4.2 RasterVis.....	130
4.4.3 GLMVis.....	133
4.5 Discussion.....	137
4.5.1 Importance of Visualization for Open Neuroscience.....	137
4.5.2 Future Directions.....	138
CHAPTER V: CONCLUSION.....	140
5.1 Summary.....	140
5.2 Significance.....	141
5.3 Future Directions.....	143
5.3.1 The Role of Alpha Oscillations.....	143
5.3.2 Cognitive Demand in Monkeys versus Humans.....	143
5.3.3 Task Switching and the Auditory Connections of ACC.....	144
5.3.4 Building Better Interactive Visualizations.....	145
BIBLIOGRAPHY.....	147
CURRICULUM VITAE.....	162

LIST OF TABLES

Table 2.S1, related to Figure 2.1.....	56
--	----

LIST OF FIGURES

Figure 1.1 An example of the importance of model checking – Anscombe’s Quartet.....	16
Figure 2.1. Task Design and Behavioral Performance.	33
Figure 2.2. PFC Neurons Encode Task-Relevant Information, Including the Current Rule and Stimulus.....	35
Figure 2.3. Rule-Selective Synchrony in PFC.....	36
Figure 2.4. Magnitude of Rule-Selective Changes in Synchrony.....	38
Figure 2.5. Single Neurons Carrying Task-Relevant Information Synchronize to the Currently Relevant Ensemble	40
Figure 2.6. Independent, Rule-Specific PFC Ensembles.....	42
Figure 2.7. Strength of Prefrontal Synchrony Selectivity Correlates with Reaction Time.	43
Figure 2.S1, related to Figure 2.2.	57
Figure 2.S2, related to Figure 2.3.	66
Figure 2.S3, related to Figure 2.4. Raw coherence plots showing rule-selective changes in synchrony between pairs of prefrontal cortex electrodes.	68
Figure 2.S4, related to Figure 2.6.	74
Figure 3.1 Task description and factors that can change cognitive demand	83
Figure 3.2. Effect of cognitive demand factors on behavior.....	85
Figure 3.3 Examples of single neurons responding to cognitive demand in ACC (left two columns) and dlPFC (right two columns).....	86

Figure 3.4 Average firing rate for each dlPFC and ACC neuron comparing high and low cognitive demand for the entire cue epoch (after the rule is cued and before the saccade is initiated) except for Congruency, which only considers the within-trial time epoch after the test stimulus appeared.	89
Figure 3.5 Neuronal model estimated changes in firing rate over the trial for each cognitive demand factor.	92
Figure 3.6. The majority of neurons increased their firing rate in response to recent errors and the change of the rule during the cue epoch.	96
Figure 3.7 Taking into account the past history of errors (Error History) rather than the number of trials from the error (Error Distance) improves spike prediction accuracy in ACC, but not dlPFC.	97
Figure 3.8 Representative neurons showing rule-related activity in ACC (left two columns) and dlPFC (right two columns) relative to the rule cue onset and test stimulus onset.	99
Figure 3.9 Average rule-related differences and percentage of significantly changing neurons for the rule.	101
Figure 3.10 Comparison of spike prediction accuracy for a set of models for ACC (top row) and dlPFC (bottom row) during the rule cue epoch.	102
Figure 4.1 Example of an electrophysiological dataset.	116
Figure 4.2. An example workflow (a) and JSON data structure (b).	121
Figure 4.3. A screenshot of the SpectraVis interface.	125
Figure 4.4 Different layouts for understanding associative networks.	128

Figure 4.5 A screenshot of the RasterVis interface.	130
Figure 4.6. RasterVis can align the raster plots to different trial events (saccade onset in darker pink vs. visual stimulus onset in light blue) and aggregate the spikes with different amounts of precision (15 ms standard deviation Gaussian smoothed kernel density estimate left, 50 ms standard deviation Gaussian smoothed kernel density estimate right).	132
Figure 4.7 Dynamic sorting by task factors.	132
Figure 4.8. A screenshot of the GLMVis interface.	133
Figure 4.9 Interacting with parallel coordinate plots on GLMVis.	136

LIST OF ABBREVIATIONS

ACC.....	Anterior Cingulate Cortex
AS.....	Arcuate Sulcus
AUC.....	Area Under the Curve
BOLD	Blood Oxygen Level Dependent
CSS.....	Cascading Style Sheets
dlPFC	dorsolateral Prefrontal Cortex
FI.....	Firing Rate-Input
fMRI.....	functional Magnetic Resonance Imaging
GLM.....	Generalized Linear Model
GNU	GNU's Not Unix
HTML	Hypertext Markup Language
ITI.....	Intertrial Interval
JSON.....	JavaScript Object Notation
LFP	Local Field Potential
MATLAB.....	Matrix Laboratory
MRI.....	Magnetic Resonance Imaging
PEV	Percent Explained Variance
PFC	Prefrontal Cortex
PLV	Phase Locking Value
PS.....	Principal Sulcus
ROC	Receiver Operating Characteristic

ROI	Region Of Interest
SPM	Statistical Parametric Mapping
STE	Standard Error of the Mean
SVG.....	Scalable Vector Graphics
t-SNE	t-Distributed Stochastic Neighbor Embedding
TB	Terabyte
URL.....	Uniform Resource Locator
XML.....	Extensible Markup Language

CHAPTER I. INTRODUCTION

Humans can change their behavior based on context and internal goals. This ability consists of two main components: (1) the ability to prioritize internal goals and resist reflexive behaviors and (2) the ability to flexibly change behavior when circumstances or goals change. A fundamental question of cognitive neuroscience is how the brain enables this flexibility. What are the neural mechanisms for selecting the appropriate behavior for a given context and for resisting reflexive behaviors?

This dissertation examines those questions with respect to two subdivisions of the macaque prefrontal cortex – the anterior cingulate cortex (ACC) and the dorsolateral prefrontal cortex (dlPFC). In this chapter, I will first review the motivation for studying ACC and dlPFC and the relevant hypothesis about their roles in supporting flexible behavior. Then I discuss a potential neural mechanism for selecting the relevant context at the circuit-level. Next I motivate interactive visualizations tools that will help us investigate the ACC and dlPFC data. I conclude with a summary of the remaining chapters.

1.1 Background: The role of ACC and dlPFC in supporting flexible behavior

1.1.1 Prefrontal cortex and flexible behavior

Whereas flexible behavior undoubtedly involves the coordination of many brain areas (sensory, motor, and cognitive), a key node in this network is the prefrontal cortex (Cole and Schneider, 2007; Miller and Cohen, 2001). In a seminal study,

Milner (1963) had human patients with lesions perform the Wisconsin Card Sorting Task – a task designed to test the patient’s ability to switch between task contexts. Subjects were given cards – each of which had at least one shape drawn on them. These cards varied by color of the shape, number of shapes, and type of shapes. Patients had to learn – by trial and error – to match a set of four stimulus cards along a particular dimension (color, number, type). This task context (dimension) changed unbeknownst to the patients after ten consecutive correct answers. Milner found that patients with prefrontal lesions were inflexible – they tended to not be able to switch between task contexts – whereas patients with lesions in parietal and temporal cortices were much better.

Importantly, this effect also varied by the subdivision of prefrontal cortex that contained the lesions. Patients with dorsolateral prefrontal lesions tended to perseverate on the incorrect task context more than patients with orbitofrontal lesions, indicating some degree of specialization of function within the prefrontal cortex. Dias et al. (1996) further tested the specialization of prefrontal subdivisions by ablating the dorsolateral prefrontal cortex or the orbitofrontal cortex in two groups of macaques. Dias and colleagues found the monkeys with dorsolateral lesions had trouble shifting between contexts in a task similar to the Wisconsin Card Sorting Task, but not during reversal learning – simply changing the associations between stimuli and reward. The orbitofrontal cortex showed the opposite effect. Monkeys with orbitofrontal lesions performed as well as

monkeys without lesions in the Wisconsin Card Sorting analog, but performed poorly in the reversal learning task.

What these lesions studies highlight is that it is important to understand the differences in function between prefrontal subdivisions. Different subdivisions of prefrontal cortex may contribute to different kinds of behavior. At the same time, we know that prefrontal subdivisions are intimately connected with each other (Barbas and Pandya, 1989; Medalla and Barbas, 2010), so it is also important to understand how prefrontal subdivisions work together. In the next section, I discuss the two prefrontal subdivisions this dissertation focuses on.

1.1.2 ACC and dlPFC

The dorsal ACC (areas 24 and 32 in the macaque monkey) and dlPFC (area 46) are prefrontal subdivisions that are simultaneously active in attentionally-demanding tasks and anatomically connected (Bates and Goldman-Rakic, 1993; Medalla and Barbas, 2010, 2009). Their roles in supporting flexible behavior are thought to be distinct, but complementary. To motivate our approach, we review the current hypotheses about the role of context in ACC and dlPFC.

The dlPFC is the prefrontal subdivision most commonly associated with visual attention. It receives sensory input from the dorsal and ventral visual streams and projects to motor areas such as supplementary motor area, basal ganglia and superior colliculus (Jacobson and Trojanowski, 1977; Schwartz and Goldman-Rakic, 1984; Yeterian and Pandya, 1994) – putting it in an ideal

position to influence visual sensory information and motor outputs (Miller and Cohen, 2001). Neurons in dlPFC are selective to context (even if the context is cued under different modalities) and sustain their activity over delays in tasks that require the memory of a cue (Fuster, 1973; Wallis et al., 2001). Moreover, lesions of the dlPFC impair the ability to cognitively adjust to changed contexts (Dias et al., 1996). Thus, the role ascribed to dlPFC is that of context maintenance/updating and attentional biasing of other brain areas (Miller and Cohen, 2001).

The role of ACC is more controversial — as evidenced by the sheer number of hypotheses about its role. There are four main categories of hypothesized functional roles for ACC: ACC as a recruiter of attention for action, ACC as error detector, ACC as conflict detector, ACC as action-outcome predictor.

1.1.3 ACC as recruiter of attention for action

An early idea for the role of ACC is that it selects the contextually-relevant sensory information for performing the appropriate response, much like the hypothesized role for dlPFC. This idea seems to have quickly fallen out of favor, but two studies have suggested this role. Using PET and a semantic word monitoring task (subjects had to report the percentage of words that fell into a particular category), Petersen et al. (1989) found that increasing the number of words to be monitored resulted in greater blood flow to ACC. They interpreted this increase in ACC activity as supporting the need for increased attention in the task. A later fMRI study by Luks et al. (2002) found ACC more active when the

cues were informative for the upcoming task (versus neutral cues), indicating that ACC can use context-related task information. While both of these studies are hardly conclusive for the idea of attention for action, the idea has received some revival in recent models (see section 1.1.7 on Recent models of ACC and in particular, Shenhav et al. (2013)).

1.1.4 ACC as error detector

Electroencephalography (EEG) studies have found that, as early as 50-150 ms after human subjects make an error, a strong negative deflecting potential occurs that is often localized to ACC. This led to the hypothesis that ACC acted as a comparator between the response made and the correct response (Bush et al., 2000; Carter et al., 1998; Carter and Veen, 2007; Gehring and Fencsik, 2001; Scheffers and Coles, 2000). A later formulation extended this to a model where basal ganglia signal “surprise” via phasic dopamine and ACC learns to select the correct process based on this dopamine signal (Holroyd and Coles, 2002). Brown and Braver (2005) similarly proposed that ACC learns to associate error with the stimulus-response representation active just prior to the error, meaning ACC detects the situations in which an error is more likely.

There is much neurophysiological evidence that ACC responds to error, going back to the earliest studies of ACC. Niki and Wantanabe (1979) found that cingulate neurons increased their firing rate when the monkey made an error or when a juice reward was omitted for a correct response. Shima and Tanji (1998) found that neurons in the cingulate motor areas (notably area 24c) increased

their firing only when the reward was reduced and the task changed. Michelet et al. (2009) found that ACC neurons showed increased activity both immediately after the error and during the next trial when a non-contextual warning stimulus signaling the start of the trial. Because this was also correlated with reduced error rates, they took this to indicate the ACC is involved in adjusting the level of attention needed on the next trial. While subsequent hypotheses (conflict detection and action-outcome) agree that ACC responds to error, they have tried to subsume that function under both the conflict and action-outcome hypothesis.

1.1.5 ACC as conflict detector

Another influential hypothesis suggests that ACC acts as a detector of conflict between information processing pathways; that is, anytime there are two or more competing processes (such as when deciding between two possible responses), the ACC signals the need for greater attention to resolve the conflict (Botvinick et al., 2001). The original hypothesis focuses on conflict between response processes and error processes, but in a later paper, Botvinick et al. (2004) suggest this can be extended to conflict between stimuli processes (such as when there are irrelevant but salient stimuli) and conflict between tasks or rules.

The support for the conflict theory primarily comes from human neuroimaging. In an often-cited fMRI study, MacDonald et al. (2000) trained subjects on a cued Stroop task. The subjects were cued to either name the color of the word stimulus or to read the word stimulus. On congruent trials, the color of the word stimulus and the word were the same. On incongruent trials, the color

of the word stimulus and the word were different. MacDonald and colleagues showed that ACC had a greater blood-oxygen-level dependent (BOLD) response to incongruent stimuli versus congruent stimuli, but found no such response in dlPFC. Because incongruent stimuli involved two possible competing responses (read the word versus name of the color of the word), the author took this to mean that ACC, but not dlPFC, responds to conflict. Kerns et al. (2004) further investigated the congruency effect by using a cued Stroop task to find trial-by-trial adjustments by ACC and dlPFC. Kerns and colleagues showed that incongruent trials preceded by congruent trials produced greater ACC activation compared to two incongruent trials in a row. They also showed that the increased ACC activity predicted both faster responding and dlPFC activity on the next trial.

Some fMRI studies also investigated the possibility of conflict between competing task sets in the ACC. Hyafil et al. (2009) used a spatial Stroop task and found ACC had stronger activity on the first trial after the task changed (the switch trial) regardless of the current or prior trial congruency. Similarly, (Woodward et al., 2006) found a linear decrease of activity in ACC as a function of the number of trials from the most recent task switch.

Primate neurophysiology studies have had less success finding evidence of conflict in single neurons. Ito et al. (2003) trained monkeys on a saccade countermanding task in which the monkeys saccaded to a target unless a stop-signal was given. Error neurons were defined as those neurons that were more active on stop-signal trials when the monkey incorrectly saccaded. Reinforcement

neurons were defined as those that were more active after receiving primary or secondary rewards. Conflict neurons were defined by the amount of change in firing after cancelling the saccade that was inversely proportional to the probability of cancelling the saccade. They recorded in ACC area 24c and found error-related neurons and reinforcement-related neurons, but no conflict-related neurons. Nakamura et al. (2005) similarly found no evidence of conflict in ACC. They trained two monkeys on a task where a cue indicated the correct direction of saccade and recorded in ACC and SEF. The cue was placed in the correct direction of the saccade (no response conflict) or the incorrect direction (response conflict). ACC activity was the same for both conditions, but nearby SEF neurons increased their firing in the conflict condition, suggesting that SEF, but not ACC, is responsive to conflict.

However, several recent studies suggest that conflict-related neurons do exist in ACC. Sheth et al. (2012) used fMRI and single neuron recordings to show that human dorsal ACC neurons fire more frequently with increasing degrees of conflict, and, like Kerns et al. (2004), this activity was greater if the preceding trial had no conflict. Amemori and Graybiel (2012) also found evidence of decision conflict-related neurons in the ventral bank of ACC. They trained monkeys to respond to two cues that informed them of the relative amount of liquid reward and airpuff they were about to receive. The monkeys could choose to avoid or receive the reward and airpuff. To measure decision conflict, they modeled the probability of the monkey choosing to receive the reward and airpuff

given the cues. They found this predicted well for a small subset of the neurons, but they never address its effect on firing rate. Finally, Ebitz and Platt (2015) found that, in a visually guided saccade task, task-relevant distractors on average induced a greater increase in ACC neuron firing rate compared to task-irrelevant distractors presented during the intertrial interval. They interpreted this to mean that ACC signals task conflict – conflict between the current goal, in this case saccading to a target, and stimuli not aligned with the goal, such as the distractor.

1.1.6 ACC as action-outcome predictor

Controversial evidence of conflict signals in the non-human primate ACC and the observation that the ACC responds both to error and reward prompted yet another formulation of ACC function – that of action-outcome predictor. The action-outcome hypothesis posits that ACC neurons learn to associate possible responses (actions) with the reinforcement values of their outcomes, both positive and negative reinforcement. Thus, ACC neurons predict when revisions to the response need to be made (Alexander and Brown, 2011; Brown and Braver, 2005; Rushworth and Behrens, 2008). Supporting this, Matsumoto (2003) found many neurons in medial prefrontal cortex (1) have a preference for reward or absence of reward and (2) show preferences for specific motor-reward combinations. Compared to lateral PFC neurons, these medial prefrontal neurons fired earlier after the presentation of a visual cue, which signaled the anticipated reward. The authors argue that this difference (between medial and lateral PFC) implies medial PFC is important for response based on expected reward, because

medial PFC cells that detected reward-response contingencies were active at the earliest time in which the monkeys could choose a response. A later study by Matsumoto and colleagues (2007) found that ACC neurons responded to positive and negative reinforcers and responded in a manner consistent with reward prediction errors; the neurons fired more for a reward when there was more uncertainty in the correct choice. This reward prediction error may be specific to ACC, as it was not found in OFC or dlPFC (Kennerley et al., 2011).

Neurons in ACC also track the history of errors multiple trials into the past. For example, Kennerley et al. (2006) lesioned ACC and had monkeys perform a motor-reward reversal task. The monkeys had to choose between turning and lifting a joystick in order to receive a reward and the rewarded motor action was changed after 25 correct responses. Surprisingly, although the lesioned monkeys did not perform as well, they were still able to change between the tasks at almost the same performance level as the control monkeys. According to the authors, the difference between the lesion and control monkeys lay in their ability to repeat the same movement, even though it was being rewarded. Lesioned monkeys did not continue to repeat the same movement after an error while control monkeys did. Kennerley and colleagues interpreted this to mean that the monkeys were failing to track the past history of errors. Seo and Lee (2007) reported more direct neurophysiological evidence of neurons responding to reward history. They observed that that 66% of neurons in ACC significantly modulated their firing rate in response to an error on the previous

trial and 26% modulated their firing rate to an error two trials previous. Johnston and colleagues (2007) further found that making an error in the preceding trial increased task-related selectivity in ACC on the next subsequent trial but not dlPFC (dlPFC activity was similar to that of an error trial). Similarly, Michelet (2009) also found that errors in the previous trial enhanced ACC activity in response to a non-task-related warning cue in a Wisconsin Card Sorting-like task.

1.1.7 Recent models of ACC

Finally, more recent views of ACC function have tried to reconcile these disparate hypotheses. Alexander and Brown (2011) suggest that conflict, error likelihood, and reward findings can be explained by ACC (and other medial prefrontal areas) detecting unexpected outcomes — more specifically, ACC learns to predict the probability and timing of responses and outcomes for a given context. Holroyd and Yeung (2012) propose that ACC learns to value, select and maintain the appropriate context and the amount of attention needed. Shenhav et al. (2013), taking a related approach, propose that ACC weighs the expected costs and rewards of increasing attention in a given context and chooses the appropriate amount of attention and biasing signal.

While all of the recent hypotheses propose different roles for ACC, there are several commonalities, especially with regard to the role of context. First, each proposes that context plays an important function in ACC — either in determining the possible responses and outcomes likely to occur, maintaining and selecting context, or evaluating the amount of attention needed for a given

context. Second, each proposes that ACC activity varies with the predicted amount of attention needed — the "cognitive demand" — in a context-dependent manner — either because more than one possible response-outcome might occur or because there are different values of attending in that context. Third, each hypothesis proposes that dlPFC (along with basal ganglia) is responsible for implementing context-dependent attentional signals from ACC. An important focus of this dissertation is investigating how cognitive demand and context signals affect ACC and dlPFC (chapter III).

1.2 Background: The role of prefrontal rhythms and coherence in circuit-level communication

Neurons tend to fluctuate rhythmically in excitation – both through intrinsic currents at the cellular level and as groups (Ainsworth et al., 2012). This rhythmicity has been observed throughout the brain and changes with cognitive, sensory and motor state (Buschman and Miller, 2007; Lakatos et al., 2008; Pesaran et al., 2008). A benefit of rhythmic excitation is that whenever multiple excitatory inputs arrive at nearly the same time to a target neuron, the effect on the targeted neuron's firing rate maybe supralinear, i.e. is greater than a simple addition of the effect of asynchronous inputs (Nettleton and Spain, 2000; Salinas and Sejnowski, 2000).

Neuronal rhythms also influence the temporal effectiveness of inputs to a group of neurons. If inputs arrive at peak times of group excitability, there is an increased chance of neurons in the group firing. Conversely, if the inputs arrive

when the group is less excitable, either due to inhibition from interneurons or refractory currents, there is less chance of neurons in the group firing (Burchell et al., 1998).

These observations have led to the suggestion that stable phase relationships (measured by phase-coherence) between groups of neurons enable selective communication between the groups — the so-called **Communication through Coherence** hypothesis (Fries, 2005). If two groups of neurons are coherent at the same frequency and the conduction delays between the groups are sufficiently short, the groups can mutually excite each other at times of peak excitability, allowing effective communication between the groups. If the groups are not coherent, their oscillations are not sufficiently narrowband, or the conduction delays are long enough to result in anti-phase coherence, then signals between the groups are less effective and communication is diminished.

An important feature of phase-coherence is that it enables rapid and flexible routing of information between groups of neurons, allowing them to be selected and de-selected in a task-dependent manner (Akam and Kullmann, 2014, 2010, 2012). Moreover, this selection of neuronal groups does not strictly depend on the underlying anatomical connectivity, which can only change on a much slower timescale. This makes phase-coherence an ideal mechanism for the context-dependent linking of neurons. Context switches and shifts of attention can occur in hundreds of milliseconds, so the mechanism that supports them must also be able to operate on this timescale (Singer, 2013).

Supporting this, several studies have found evidence for increased coherence between prefrontal cortex and distant brain areas during tasks that require visual attention. For example, Buschman and Miller (2007) found that beta (22-34 Hz) coherence was stronger between parietal and prefrontal cortex of monkeys when the task required top-down attention. Similarly, Gregoriou et al. (2009) found that spike-field coherence between LFPs in prefrontal cortex and neurons in visual cortex was enhanced when attending to a stimulus in their shared receptive field. Attentionally-enhanced coherence between prefrontal cortices and other areas also appears to be wide-spread among subdivisions of prefrontal cortex — electrodes placed in multiple subdivisions of prefrontal cortex were coherent in a content-specific manner with electrodes in the parietal lobe during a visual working memory task (Salazar et al., 2012). Another focus of this dissertation is how coherence varies with task within prefrontal cortex and how this might help coordinate subpopulations of neurons when switching between tasks.

1.3 Background: Interactive Visualization for Neuroscience

1.3.1 The purpose of visualization in science

Visualization is a fundamental tool for analysis and communication in science (Cleveland and McGill, 1985). Visualization serves two primary purposes: First, we use visualization to quickly make multiple, simultaneous comparisons (Gelman and Unwin, 2013; Tukey, 1993). While it is easy to compare and reason about a few numbers, this becomes more difficult as the amount of data or the

number of dimensions increases. Visualization eases the cognitive burden on our working memory by efficiently encoding properties of the data into features salient to the human visual perceptual system (Card et al., 1999; Cleveland and McGill, 1985). This involves exploiting easily processed, pre-attentive visual features such as color, line orientation, and line width as well as higher level perceptual grouping cues such as symmetry and proximity to reduce the search for information (Card et al., 1999; Fekete et al., 2008; Healey et al., 1996). By doing so, we are able to more accurately and quickly answer questions about the data compared to data tables (Spence and Lewandowsky, 1991), solve problems related to the data, and make predictions about future data.

Second, we use visualization to assist in the understanding and checking of statistical assumptions — it helps qualify our knowledge and uncertainty about the data and the procedure(s) used to summarize the data. All numerical statistical summaries rely on assumptions about the structure of the data (our implicit/explicit mental model of the data), but inspection of such summaries alone cannot tell us about violations of those assumptions (Anscombe, 1973). Visualization complements the use of statistical summaries by revealing differences between the expected structure of the data and the observed data (Tukey, 1977). This is important, from the initial stages of analysis to publication, for revising our assumptions and models and for understanding and communicating where and how often our models fail (Gelman, 2004).

A canonical example of the problem with numeric summaries and the benefit of visualization is a set of four datasets known as Anscombe's Quartet (Anscombe, 1973).

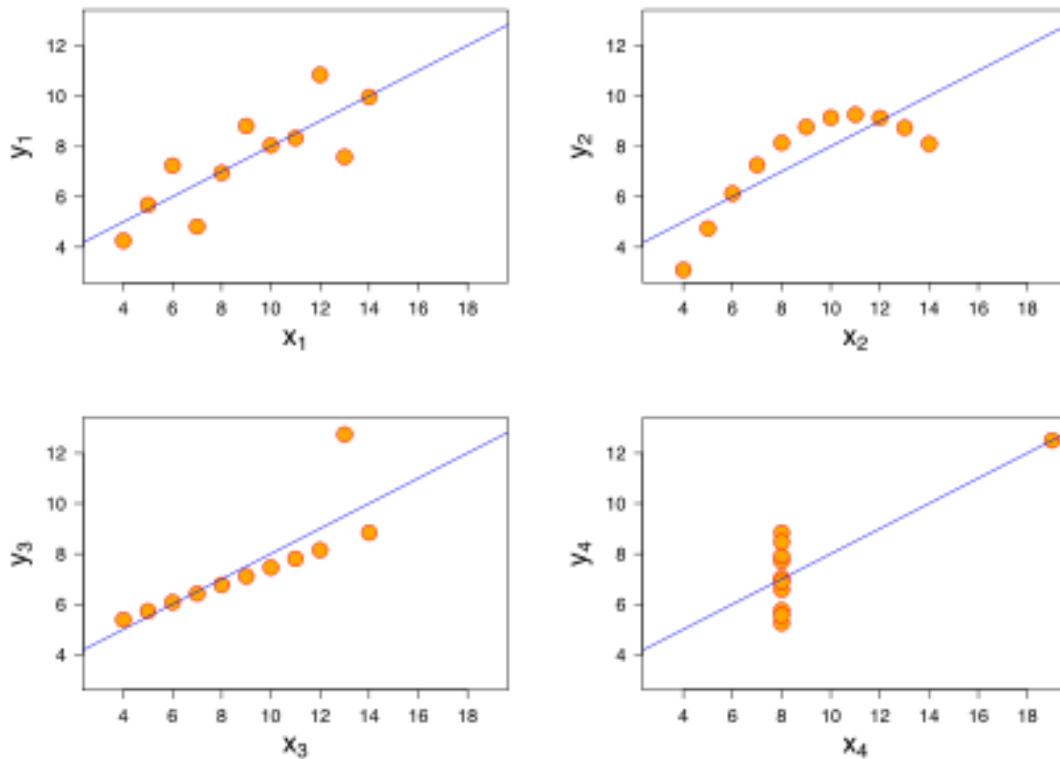


Figure 1.1 An example of the importance of model checking – Anscombe's Quartet.

Each box consists of one dataset in Anscombe's Quartet. Data points are orange filled-circles. The data have the same mean and variance in the x-dimension as well as the same regression line (blue line). These statistical summaries (mean, variance, regression line) do not explain the clear differences in structure between the four datasets. Credit: Wikimedia Commons

Each dataset consists of 11 observations of two variables — x and y . Across all four datasets, the x - and y -variables have the same mean and variance between each dataset. Within each dataset, the x - and y -variables are also identically correlated and fit by the same regression line. Thus, the numerical statistical summaries are identical. However, visual inspection of the datasets

reveal strikingly different structure in each dataset (**Figure 1.1**). In particular, the second and third dataset (going clockwise around **Figure 1.1**) respectively show a quadratic pattern, and a pattern in a single datapoint has an inordinate effect on the statistical summary.

1.3.2 Limitations of static visualizations in neuroscience

Static visualizations — visualizations where the state of the visualization cannot change by user interaction or animation — have been the *de facto* standard in neuroscience. Static visualizations are used at the early stages of analysis in examining the quality of raw signals (e.g. voltage changes on an electrode, BOLD signals in fMRI), in formulating preliminary hypotheses and in communicating refined analyses in publication. In general, they play a central role in the iterative, sense-making process of data analysis and communication of results.

Advances in technology and computing have made generating static visualizations easier, but those same advances have led to more data, more complex analyses and more sophisticated hypotheses (Freeman, 2015). In electrophysiology, implantation of multielectrode arrays with upwards of 100 electrodes are becoming common (Einevoll et al., 2012; Miller and Wilson, 2008; Siegel et al., 2015) and the number of simultaneously recorded neurons is projected to double every seven years (Stevenson and Kording, 2011). Laminar recordings have also become standard and add a spatial dimension of data per electrode. Whole brain two-photon imaging experiments in zebrafish can yield up to 1.2 TB of data per hour (Freeman, 2015). In fMRI, the amount of data per

brain is already high and there already have been efforts to analyze more than 1000 subjects (Van Dijk et al., 2012).

Consequently, analyses are growing in complexity, because with more data, there is greater statistical power to resolve finer differences in the data; we can partition the data into smaller subsets (more dimensions), make comparisons between these subsets, and still not be overcome by noise. Advances in computational power have reduced the time to compute these differences and allow for more sophisticated algorithms to detect differences. Thus, we can ask more complicated questions and form more sophisticated hypotheses.

So why is this a problem for static visualizations? Complex analyses and hypotheses necessitate an increase in the number of static visualizations or further summarization of the data (dimensionality reduction) to deal with the number of dimensions — often both. For example, a common visualization of spiking data from a neuron would be a raster plot or, as a summary, a histogram. These are typically visualized with respect to a particular experimental stimulus or event (e.g. a saccade); when there are sequences of such events, each event requires a new visualization. To investigate the firing rate of 1000 neurons in multiple conditions implies visualizations for each neuron, or aggregation in some form (e.g summarization by brain area) once the visualization becomes too ineffective to support perceptual comparison. Because analysis is an iterative process, a typical analysis might require hundreds of visualizations as different sets of experimental conditions are examined or as more data are added.

A large number of static visualizations results in more time spent switching between visualizations, which can not only extend the time to analyze the data, but also has a meaningful impact on our ability to explore and understand the data. For example, Liu and Heer (2014) found that even a 500 millisecond delay between visualizations could reduce the amount of the dataset explored and affect the number of hypotheses and observations formed. Similarly, Brutlag (2009) found that users performed fewer web searches if there was as little as a 200 millisecond delay in the return of search results.

Summarization, while often necessary, can obscure complexity and variability in the data — as in the case of Anscombe’s dataset. It does not obviate the need to understand and check statistical assumptions. This can be a problem with large datasets, where going back and forth between raw data and summaries is difficult because of the amount of data.

Moreover, high-dimensional summaries require careful checking and understanding of assumptions as more structure in the data is assumed (Gelman, 2004) and overfitting — fitting to more parameters than the data can support resulting in lack of generalizability of results — becomes a concern. Finally, the sophisticated computational algorithms used to compute the summaries can result in errors and visualizations play an important role in catching such errors.

1.3.3 Interactive visualizations can help us quickly make comparisons and deal with complexity

Interactive visualizations are visualizations where the viewer can manipulate the state of visualization — typically through the use of a computer mouse, keyboard or touch interface. Interaction triggers state changes that may provide alternate views and data, detail about a particular datapoint, or selection — a filtered set of the data (Heer and Shneiderman, 2012).

For example, [Google Maps](#) is an interactive visualization that provides alternate views by allowing the user to zoom to see map data at different scales (e.g. a single street block, streets in a city, an entire state) and toggle between a satellite overview, a street level view, and the typical map. A user can hover the mouse over a location datapoint to show the name of that location. Clicking on a location selects that datapoint and provides even more detailed information such as user reviews and ratings.

From the Google Maps example, we can see the primary advantages of an interactive visualization over a static visualization. Interactivity allows the user to navigate between alternate views with minimal delay. This allows the user to quickly make comparisons between complex representations of the data such as a map of the neighborhood and a map of the city or between satellite and mapping views. Compare this to using paper road atlases with hundreds of pages of static maps. Interactive visualization users can also gain detailed information about individual datapoints without losing the context of the entire map by hovering or

clicking on a location (selection). This is particularly advantageous in a rich dataset with multiple levels of information, because instead of obscuring the complexity of the data, the interactivity reveals the complexity in manageable stages.

1.3.4 Dynamic visualizations, when combined with interactivity, can help us understand complex data by preserving relationships between data

Dynamics — also known as animation — are important in interactive visualizations because they are extremely salient and they preserve the identity of datapoints when the state of the visualization changes (object constancy) (Heer and Robertson, 2007). They give the data analyst another perceptual dimension in which to display information. This can be important when dealing with the dimension of time, as well-designed dynamics have been shown to improve accuracy of estimates of change over time (Heer and Robertson, 2007).

For example, a typical display of a network may encode *nodes* (corresponding to electrodes implanted in a brain for instance) as circles, and *edges* (corresponding to correlation between electrodes) as lines between the circles. One option to show changes in the network would be to show static “snapshots” of the network as time progresses. While this is fine for a limited number of time points, dynamics can extend the number of time points displayed, because it occupies the same amount of space on the screen.

Dynamics can also be used to preserve a sense of place and context within a complex dataset (Tversky et al., 2002). In the Google Maps example, clicking on

an object centers the map around that object. This centering effect is achieved dynamically, slowly panning to the location in question to preserve the location of other objects relative to the object of interest. Google Maps also uses these dynamics with photos by first zooming in to the map location of the photo, tilting the perspective to imitate a landscape view, then rapidly zooming in on the photo – informing the user of the correspondence between map and photo. Like interactivity, this multi-stage dynamic helps reveal the complexity of the data in manageable stages.

It must be noted that, like other perceptual encodings of data, dynamics do not always facilitate comprehension. Complicated dynamics, unpredictable dynamics, difficult to perceive dynamics (e.g. due to speed of the animation), or dynamics that violate the user’s internal model of the data are all cases where dynamics may not enhance, or even detract from, static visualizations (Heer and Robertson, 2007). Careful design is necessary to make sure the dynamics contribute to the understanding of the data.

1.3.5 Web-enabled visualizations are familiar, easily shareable, and enable analysis transparency

Web browsers are an ideal interface for interactive dynamic visualizations. Web browsers are nearly ubiquitous applications on computers and their usage is familiar to users. Additionally, users are already familiar with dynamic interactive visualizations in the form of “web apps” in their browsers such as the aforementioned Google Maps. Because “web apps” are common on the browser,

there already exist tools for constructing dynamic, interactive visualizations.

Finally, because these apps are web-enabled, they are easily shareable over the internet. Shareability is important because science is a collaborative process. To maximize shareability, it is vital that communication of results require as little specialized software as possible.

Basic canonical web-enabled visualizations of neuroscience data can also contribute to transparency in the scientific process. Journals such as Proc. Nat. Acad. Sci. USA now [require](#) authors to make their datasets available. Two barriers to understanding these openly accessible datasets are that the amount of data provided can be overwhelming, and the time to process this data into an interpretable format can be costly. A possible way to alleviate these problems is to enforce common formats and provide basic canonical visualizations of the data that can be quickly accessed and understood. For example, a web-enabled raster plot of neuronal spiking data would be a useful visualization for understanding raw data in electrophysiology studies.

This transparency is also important for high-dimensional analyses. As the complexity of analyses grows, the chance of making an error increases. Greater transparency of the underlying data and data transformations combined with ease of access over the internet (shareability) allows easy spotting and correction of errors.

1.3.6 Related Visualization Work

There have been previous attempts to make web-enabled dynamic, interactive visualizations in neuroscience. Here we describe several notable visualizations.

The [pycortex webGL MRI viewer](#) (Gao et al., 2015) is a web-enabled interactive visualization tool that displays the results from Huth et al. (2012). In the study, Huth and colleagues had subjects view two hours of movie trailers. They then categorized objects and actions in the movies, regressed the categories on the BOLD fMRI signals collected on the subjects watching the movies, and performed a principal components dimensionality reduction to recover a “semantic space”. The visualization displays a single subject’s color-coded 3D cortical surface representation of this semantic space where similar colors indicate similar categorical representations. The visualization also displays a map of the semantic space itself.

The visualization has interactive controls that allow the user to click on a category to see how it is represented throughout the cortical surface. Conversely, the user can click on a voxel on the cortical surface to see the different categories associated with that voxel. The visualization also provides button controls that dynamically transform the view of the cortical surface (e.g. from inflated to superinflated or from superinflated to flat) and sliders that control the thresholding of the surface colors. The cortical surface can be rotated by holding a mouse-click on a point and moving the mouse. A user can also obtain a

permanent web link to a particular voxel of interest by clicking a button. Code for the pycortex viewer is available on [Github](#).

The [Allen Cell Types Database](#) is a visual interface for a database of neuronal cell types in mouse lateral geniculate nucleus and primary visual cortex. The visualization has several interlinked views including an anatomical cell location view, a parallel coordinate plot of cell features, and a list of cells with more detailed information about the experiment and a brief visual summary of its morphology and electrophysiological response pattern to a step current.

Interactive controls allow the user to filter results for layer type, mouse line, and hemisphere. Clicking on cells in the anatomical cell location view, highlights that cell in the list of cells and in the parallel coordinate plot. The parallel coordinate plot provides a way to visually filter by cell features such as FI curve slope or rheobase. Clicking on cell summary brings the user to another web page with more detailed information about that neuron such as the cell's response to different types of currents, and comparisons to common computational models (e.g. leaky integrate and fire) fit to the data.

The [Allen Mouse Brain Connectivity Atlas](#) is a similar interface that allows the user to explore the results of 2173 tracer injection experiments on mouse brains. The visualization consists of a 3D cortical surface with labeled injection sites, a brain section image and whole brain projection image corresponding to a specific experiment, and a list of all the projection sites. A user can filter by target

or source of the injection or click on an injection site to get the corresponding section and projection image.

Lastly, Freeman and colleagues have incorporated interactive visualizations into their library of distributed computing tools for large scale neuroscience (Freeman et al., 2014). Their tools — [Lightning](#) and [Thunder](#) — allow for basic chart types such as line graphs, network force diagrams, and heatmaps and custom visualizations to be constructed and updated in real time from data pushed from a server. They demonstrated on whole brain zebrafish recordings how these can be made into interactive visualizations. For example, using [tuning curves](#) estimated from moving stimuli in different directions, they visualized the spatial layout of the preferred direction of all neurons in the zebrafish. Mousing over the spatial layout shows the firing rate time course of a neuron in that region. Code for Lightning and Thunder are also available on [Github](#).

Chapter IV of this dissertation focuses on the development of interactive visualizations for neuroscience data. These visualizations are unique, because they focus on visualizing functional, task-dependent electrophysiology data recorded from multiple electrodes, rather than general charting tools as with Freeman and colleagues, cell properties as with the Allen database visualizations, or neuroimaging data as with Gao et al. (2015).

1.4 Summary of Dissertation

The rest of the dissertation is comprised of four chapters. Chapters II and III describe two analyses of electrophysiological data collected in the macaque monkey ACC and dlPFC while the monkeys performed a cued task switching experiment. Chapter IV describes web-enabled, interactive visualizations tools for the analysis of electrophysiological data, developed during the course of the data analyses in Chapters II and III. Chapter V again summarizes the findings of the dissertation and discusses future directions for the work.

In Chapter II, I seek to identify circuit-level coordination within and between ACC and dlPFC during task switching. Phase coherence is a potential mechanism by which ensembles of neurons communicate and functionally organize (Fries, 2005). I hypothesized that the phase coherence of local field potentials (LFPs) within and between dlPFC and ACC is context-dependent and is a useful mechanism for coordinating ensembles of neurons when switching between tasks. I find that: (1) ensembles of dlPFC neurons coordinate in the beta band (19-40 Hz) depending on the context, (2) ensembles of neurons in dlPFC that synchronized during the more dominant context also synchronized in a preparatory fashion in the alpha band (6-16 Hz), perhaps reflecting the inhibition of the more dominant rule, and (3) ACC ensembles did not show the same context-dependent synchronization as dlPFC neurons.

Chapter III investigates the functional differences between ACC and dlPFC at the single neuron level during the task switching paradigm. Motivated by the

lack of consistent task-dependent phase coherence differences in Chapter II, I ask (1) if there are any other aspects of the task that could be driving ACC neurons such as changes in cognitive demand (which may not be as easily detectible by coherence because coherence requires averaging over many trials to achieve sufficient power and cognitively demanding conditions are infrequent) and (2) if context-dependent differences could still be important for ACC neurons at the single neuron level.

Of particular interest is the role of ACC neurons in switching between tasks. While previous studies have implied that ACC could be important for switching between tasks (Ebitz and Platt, 2015; Johnston et al., 2007; Shenhav et al., 2013), no study has definitely shown that the ACC neurons are responsive to the switch *per se* and not the past history of errors. I find that in a visually cued context switch, ACC neurons, compared to dlPFC neurons, are not responsive to the context switch. Rather, ACC neurons are more responsive to the past history of errors. In addition, I find evidence that the task context can affect ACC neurons at the single neuron level and is important for predicting the firing rate of ACC neurons. This task context signal is preferentially boosted in preparatory fashion in ACC when the monkeys make an error in past trials (particularly if the errors were made in the previous two trials). These results support reinforcement learning views of ACC and highlight its importance in complex tasks where context matters.

Chapter IV is a departure from the experimental analyses of Chapters II and III. Chapter IV is focused on developing tools for the future of data analysis of electrophysiological data. In section 1.3 of this chapter, I outlined an argument for why web interactive visualization tools will be important as electrode technology and computational power increases. In Chapter IV, I discuss three visualization tool prototypes I developed as an extension of that argument: RasterVis, GLMVis, and SpectraVis. Each of these tools was developed from the experience of performing the data analyses in Chapters II and III. RasterVis is the interactive version of two canonical data plots for electrophysiological data – the raster plot and the peri-event time histogram. GLMVis is an interactive display for regression model results – allowing for compact summaries of regression models and linking to raw data or model-generated data via RasterVis. SpectraVis is a network exploration tool that allows users to quickly move between networks at different times and frequencies and compare individual electrode data to the network as a whole.

Finally, Chapter V concludes the dissertation with a summary and a discussion of the significance of the work on the respective roles of ACC and dlPFC. I will also discuss some possible future experiments that could be performed to further differentiate dlPFC and ACC functioning.

CHAPTER II: SYNCHRONOUS OSCILLATORY NEURAL ENSEMBLES FOR RULES IN THE PREFRONTAL CORTEX

2.1 Summary

Intelligent behavior requires acquiring and following rules. Rules define how our behavior should fit different situations. To understand its neural mechanisms, we simultaneously recorded from multiple electrodes in dorsolateral prefrontal cortex (PFC) while monkeys switched between two rules (respond to color vs. orientation). We found evidence that oscillatory synchronization of local field potentials (LFPs) formed neural ensembles representing the rules: there were rule-specific increases in synchrony at ‘beta’ (19-40 Hz) frequencies between electrodes. In addition, individual PFC neurons synchronized to the LFP ensemble corresponding to the current rule (color vs. orientation). Furthermore, the ensemble encoding the behaviorally dominant orientation rule showed increased ‘alpha’ (6-16 Hz) synchrony when preparing to apply the alternative (weaker) color rule. This suggests beta-frequency synchrony selects the relevant rule ensemble while alpha-frequency synchrony de-selects a stronger, but currently irrelevant, ensemble. Synchrony may act to dynamically shape task-relevant neural ensembles out of larger, overlapping, circuits.

2.2 Introduction

A critical cognitive ability is the flexibility to change one’s behavior based on context. Day-to-day life is full of such situations. For example, one often answers their phone when it rings, but mutes it in a lecture. These context-dependent

stimulus-response mappings are called “rules”. By allowing us to quickly adapt to specific situations, rules endow the cognitive flexibility crucial for intelligent behavior.

The prefrontal cortex (PFC) is key to rule-based behaviors (Miller and Cohen, 2001). Rule-based tasks, especially those involving rule-switching, activate the human PFC (Dove et al., 2000; MacDonald et al., 2000; Sakai and Passingham, 2003) and are impaired following PFC damage (Milner, 1963; Stuss and Benson, 1984). Many PFC neurons encode task rules (Wallis et al., 2001; White and Wise, 1999), and can “multiplex”: encoding different task information (rule, stimulus, etc.) in different contexts (Cromer et al., 2010; Rainer et al., 1999). Recent theoretical work suggests that this diversity of PFC neuron properties underlies the capacity to encode a large number of diverse rules (Rigotti et al., 2010).

But this diversity raises the question of how PFC circuits satisfy two competing demands: Form the neural ensembles that represent the current rule while allowing for their flexible reconfiguration when the rule changes. One proposed solution is synchronized network oscillations. Oscillations can establish ensembles of neurons in a task-dependent, flexible, manner (Akam and Kullmann, 2010), allowing ensembles to be dynamically ‘carved’ from a greater, heterogeneous, population of neurons. In addition, coincident activity has a supralinear effect on downstream neurons (Aertsen et al., 1989), increasing the impact of neural ensemble activity on function (Fries, 2005). To investigate the

neural mechanisms underlying cognitive flexibility, we trained two monkeys to switch between two rules: respond to either the color or orientation of a stimulus (**Figure 2.1A**). After acquiring a central fixation target, a rule-cue indicated whether the color or orientation rule was now relevant. Two different cues were used for each rule in order to disassociate neural selectivity for the cue from the rule (see Materials and Methods). After a brief, randomized, interval, a test stimulus appeared. The test stimulus consisted of small shapes that were either red or blue and were either vertically or horizontally aligned (**Figure 2.1A**). Depending on the current stimulus and rule, monkeys made a leftward or rightward saccade (color rule: red=left, blue=right; orientation rule: horizontal=left, vertical=right; **Figure 2.1A**). On most trials (70%), the color and orientation of the test stimulus signaled incongruent responses to ensure that the animals consistently followed the rule (e.g. a red/vertical cued different saccade directions under different rules). The same rule was repeated for at least 20 trials before a probabilistic switch.

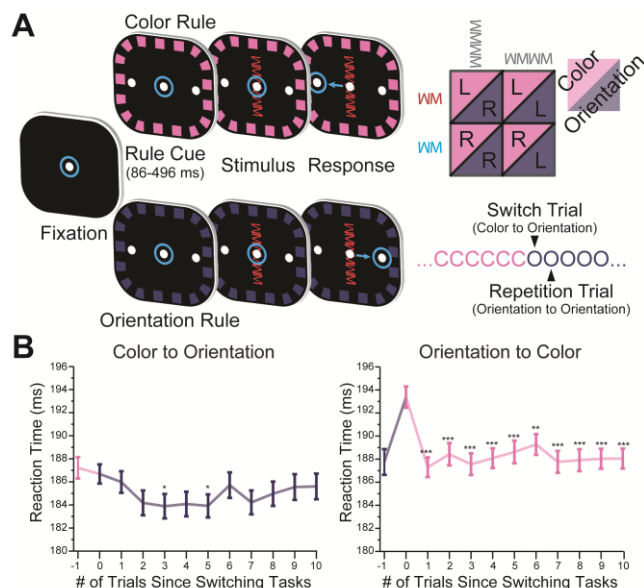


Figure 2.1. Task Design and Behavioral Performance.

(A) Task timeline. Eye position indicated by blue circle. Animals initiated trial by fixating the center dot. Following presentation of a border-cue indicating the rule, the stimulus was presented. The animal integrated the rule and stimulus in order to make a decision about the required saccade: under the color rule, red stimuli meant saccade left and blue meant saccade right; under the orientation rule, vertical meant saccade right and horizontal meant saccade left. The rule in effect was blocked and switched randomly after a minimum of 20 trials. (B) An asymmetric cost was observed when switching between rules, reflected in the speed at which the animals performed the task. Switching from orientation to color was significantly slower, but no cost was observed when switching from color to orientation. This suggests orientation was behaviorally dominant. All error bars are SEM. *** $p \leq 10^{-3}$, ** $p \leq 0.01$, * $p \leq 0.05$

2.3 Results

2.3.1 Behavioral and Single Unit Evidence for the Dominance of the Orientation

Rule

Monkeys performed well (~90% of trials were correct) but, like humans, were slower to respond on the first trial after switch, compared to repeated rule trials (Allport et al., 1994; Caselli and Chelazzi, 2011; Rogers and Monsell, 1995). This reaction time “switch cost” is thought to reflect the cognitive effort needed to change rules. However, it was only observed after a switch from orientation to color rule and not vice-versa (**Figure 2.1B**; $p=1.61 \times 10^{-4}$, GLM, Table 2.1). This

suggests the orientation rule was behaviorally dominant, as the animals had more difficulty switching away from it.

We quantified neural information about the cued rule using a bias-corrected percent explained variance statistic (ω PEV, see Supplemental Information for details). The majority of PFC neurons carried rule information (**Figure 2.2A**, PFC: 225/313, randomization test, cluster corrected for multiple comparisons, see **Figure 2.S1A** for an example neuron). Similar numbers of neurons had higher firing rates during orientation and color rule trials (108 and 117 respectively, $p=0.25$, binomial test). Across the population of PFC neurons, rule-selectivity increased following the rule cue, although some baseline rule information was observed due to the task-design: the rule repeated for multiple trials before a switch (**Figure 2.2A**). PFC neurons were also selective for the color or orientation of the test stimulus (104/313, 33%; 126/313, 40%, respectively). Orientation was behavioral dominant (see above) and neural selectivity for it was more common than color ($p= 3.9 \cdot 10^{-3}$, binomial test), stronger across the population (**Figure 2.2B** and **Figure 2.S1C**), and appeared slightly earlier (41.1 vs. 47.6 ms after stimulus onset; $p=0.0026$, permutation test).

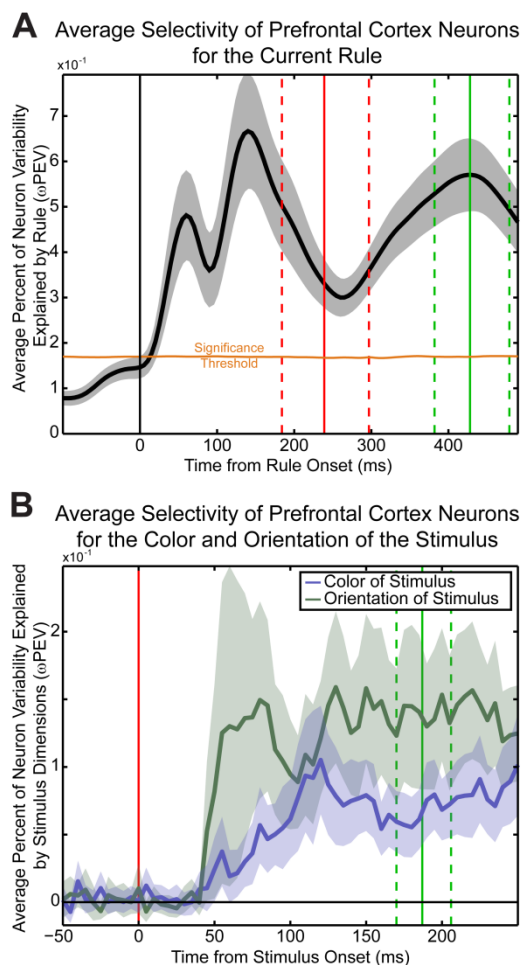


Figure 2.2. PFC Neurons Encode Task-Relevant Information, Including the Current Rule and Stimulus.

(A) Information about the current rule (black line) is captured using a bias-corrected percent-explained variance statistic (y-axis) and is determined in a sliding-window across the trial (x-axis). Shaded region indicates 95% confidence interval. As the rule often repeated on consecutive trials (see Figure 2.1A) there was some expectancy of the rule encoded by PFC neurons before rule-cue onset (although not significant across the population of recorded PFC neurons). (B) PFC neurons encode stimulus identity, both its orientation (green line) and color (blue line). Shaded regions indicate 95% confidence interval. Information about the orientation of the stimulus was more strongly represented across the population, possibly leading to the behavioral dominance of the orientation rule (see Figure 2.1B).

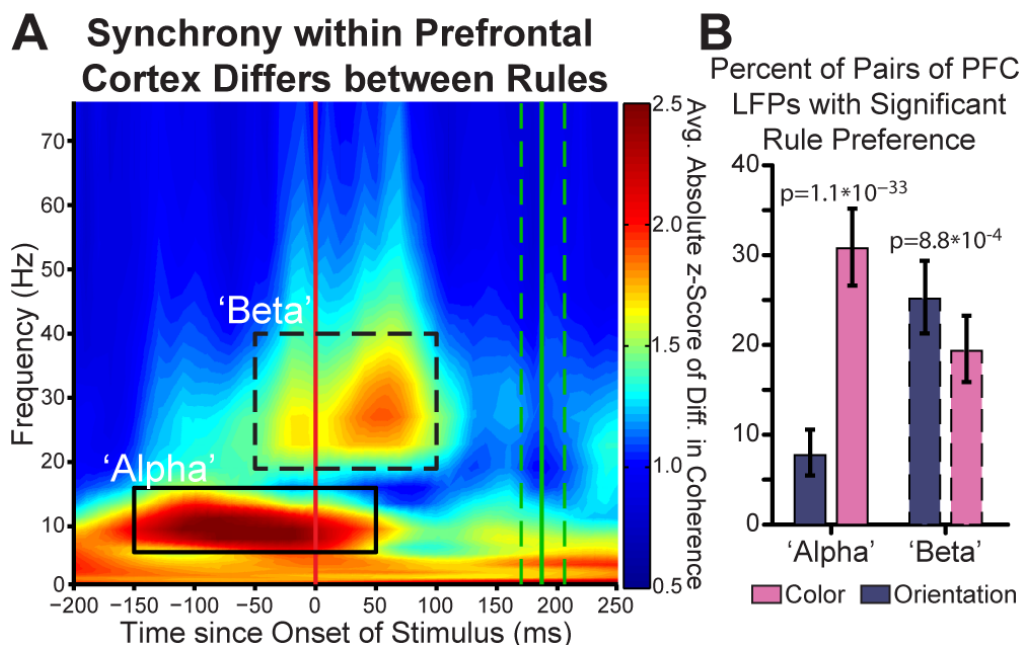


Figure 2.3. Rule-Selective Synchrony in PFC.

(A) Synchrony between electrodes within prefrontal cortex differs for rules. Synchrony is quantified by the coherence in simultaneously recorded local field potentials during each rule. The difference in synchrony (rectified to capture synchrony differences that prefer either rule) was compared to a trial-shuffled null distribution, resulting in a z-score of observed rule difference (color axis). Absolute synchrony differences are shown across time relative to stimulus onset (x-axis) and frequency (y-axis). Two time-frequency regions of interest (ROI) are seen – an ‘alpha’, 6-16 Hz, pre-stimulus ROI (solid outline) and a ‘beta’, 19-40 Hz, peri-stimulus ROI (dashed outline). (B) Percentage of recorded pairs of electrodes with a significant rule-preference during the ‘alpha’ and ‘beta’ time-frequency regions of interest (solid/dashed outlines in A). Significantly more electrode pairs prefer color within the alpha ROI and orientation within the beta ROI.

2.3.2 Rule-Selective LFP Synchronization between Pairs of Electrodes

We found rule-selective oscillatory synchronization of local field potentials between individual PFC electrode pairs. There were significant differences in synchrony between the rules in two frequency bands during two separate trial epochs: ‘alpha’ (6-16 Hz) after the rule cue and ‘beta’ (19-40 Hz) after test stimulus appeared (179/465 and 207/465 recorded pairs at $p < 0.05$ in alpha and beta, respectively; **Figure 2.3A** and **Figure 2.S2A**, alpha/beta shown as solid/dashed outlines). This was not due to differences in evoked potential

(**Figure 2.S2E**) or oscillatory power (see Supplemental Experimental Methods). It was also not due to volume conduction of an evoked potential: many rule-selective electrode pairs were spatially interspersed with electrodes with either the opposite or no synchronous rule preference (22/79 or 28%, see Supplemental Experimental Methods for details) and rule-selective synchrony did not monotonically decrease with distance (**Figure 2.S2C**).

Beta oscillations increase with cognitive effort (Buschman and Miller, 2007; Pesaran et al., 2008; Kopell et al., 2010). Thus, we sorted electrode pairs by which rule elicited significantly stronger beta synchrony. This identified two networks: one synchronized during the orientation rule (N=117 out of 465 pairs, $p < 10^{-15}$, binomial test against the number expected by chance) and one during the color rule (N=90, $p < 10^{-15}$, binomial test). There were significantly more electrode pairs with significantly stronger beta synchrony for the orientation rule than the color rule (**Figure 2.3B**, $p = 8.8 \times 10^{-4}$), again consistent with orientation being dominant. The magnitude of rule-selective increases in synchrony were comparable to those previously observed during attention (**Figures 2.4** and **2.S3**; Buschman and Miller, 2007; Gregoriou et al., 2009). Rule-selective synchrony between electrodes was not between isolated electrode pairs. Rather, synchrony occurred within interconnected networks: electrode sites were synchronized to an average of 2.6 and 1.8 other sites (out of a maximum of 5.0) for the orientation and color rule networks, respectively ($p < 10^{-3}$ for both, permutation test against random networks, see Supplemental Information).

These rule-dependent networks were highly overlapping spatially (see **Figure 2.S2D** for anatomical localization of networks). The majority of recording sites that selectively increased synchrony with one set of electrodes during one rule also increased synchrony with a different set of electrodes during the other rule (58% of electrodes participating in an orientation-rule-prefering pair, 52% of color-rule-prefering, see Supplemental Information).

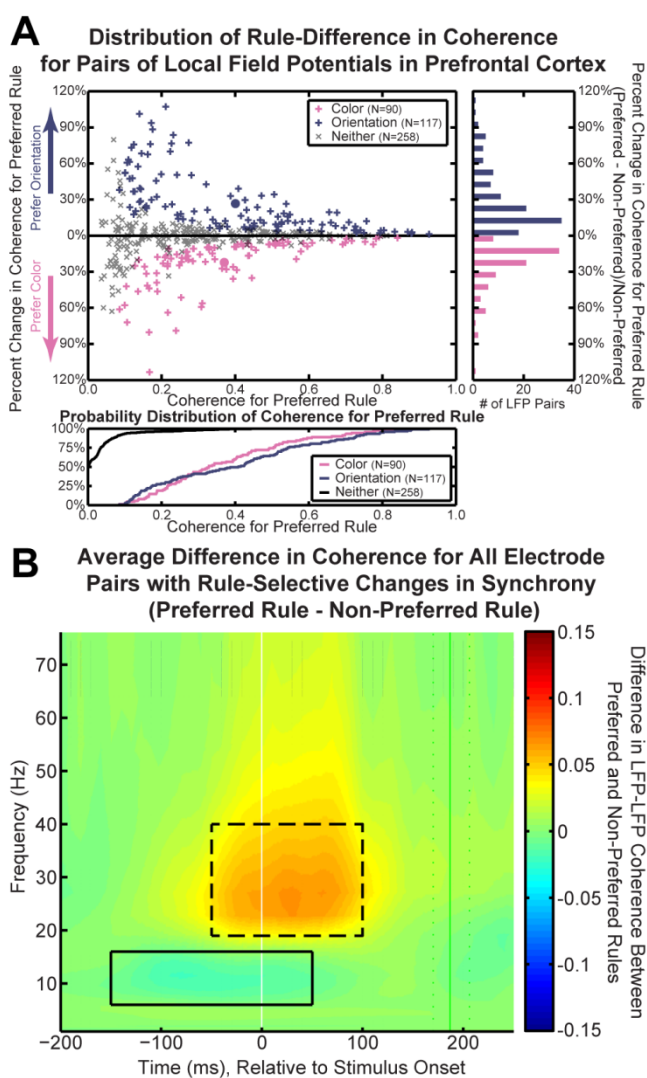


Figure 2.4. Magnitude of Rule-Selective Changes in Synchrony

(A) Individual electrode pairs in the beta ROI are highly synchronous and show significant rule-dependent change. Coherence between rule-dependent pairs of electrodes (pink and purple crosses, main panel; group averages, solid circles) in the beta ROI was high overall (cumulative probability distribution, bottom panel) and generally reflected a 10% or greater change in coherence over the non-preferred rule (histogram, right panel) compared to non-rule preferring electrode pairs (grey x's, main panel). (B) Average difference in coherence between preferred and non-preferred rules for all beta ROI electrode pairs.

2.3.3 Task-Relevant Neurons were Synchronized to the Current Rule-Network

LFP synchrony may reflect functional networks of spiking neurons (Fries, 2005). Indeed, we found that both stimulus- and rule-selective neurons showed rule-dependent spike-LFP synchrony. When the orientation or color rule was relevant, neurons with selectivity for the relevant test stimulus modality (**Figure 2.5A**) and/or the current rule (**Figure 2.5B**) were more synchronized to the currently activated beta-band color or orientation ensemble (see Supplemental Information for details). Spike-field synchrony was largely observed at beta-band frequencies, particularly for orientation rule trials (**Figure 2.5**, left column). During color rule trials synchrony was shifted slightly towards higher frequencies (**Figure 2.5**, right column). This may reflect differences in the underlying architecture of the rule-selective network either locally or between PFC and sensory/motor regions (Siegel et al., 2012).

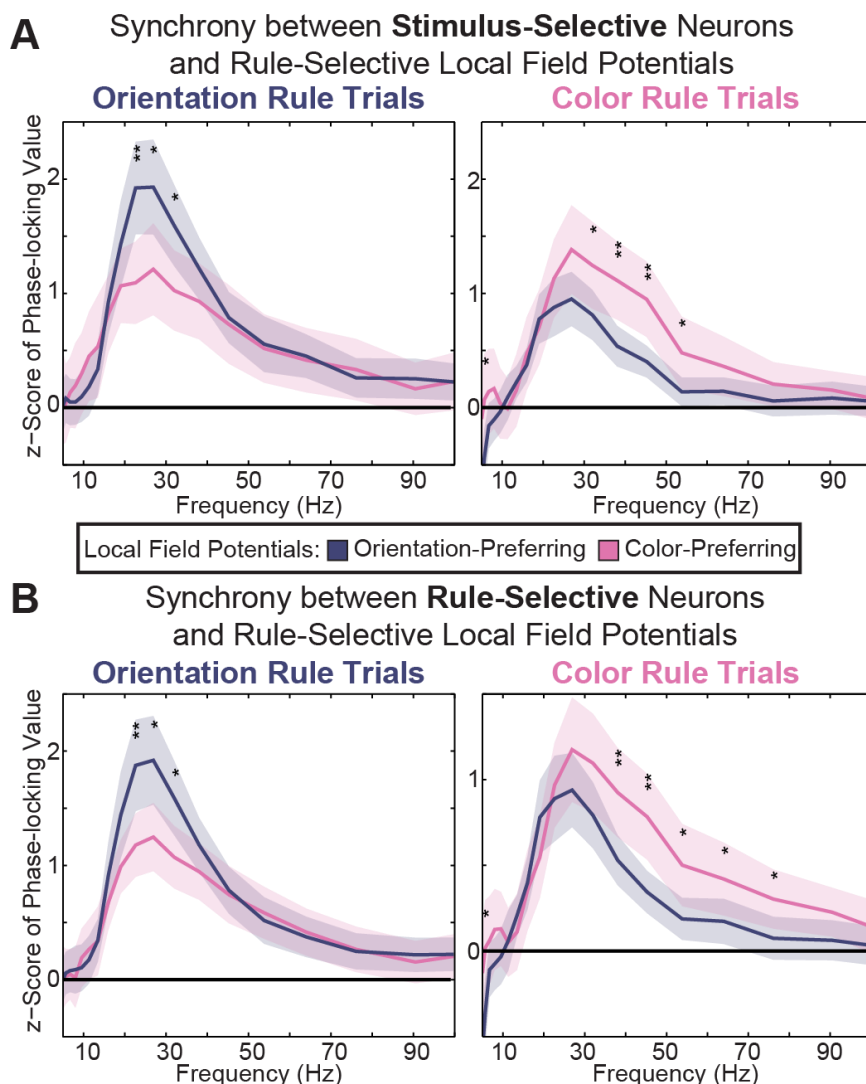


Figure 2.5. Single Neurons Carrying Task-Relevant Information Synchronize to the Currently Relevant Ensemble

Neurons encoding task-relevant information were more synchronized with the rule-selective ensemble preferring the current rule. Phase-locking of (A) stimulus-selective neurons and (B) rule-selective neurons to electrodes that either participated in the color-preferring ensemble (pink) or orientation-preferring ensemble (purple). Only electrodes that were exclusive to either ensemble were used (i.e. those electrodes participating in both ensembles were excluded). Phase-locking is shown for both orientation trials (left) and color trials (right). Shaded regions indicate 95% confidence intervals. Significant differences in phase-locking between the two ensemble is indicated at each frequency tested (*, $p < 0.05$; **, $p < 0.01$).

2.3.4 Beta Orientation Network Shows Stronger Alpha Color Selectivity

Alpha synchrony increases were primarily limited to color rule trials. **Figure**

2.3B shows that most of the electrode pairs that showed significant increases in

synchrony in the alpha band did so when the color rule was cued. To examine this more closely, we plotted the beta-synchrony defined orientation and color ensembles separately (**Figure 2.6**). When separated, it is clear that while increases in alpha synchrony were on color trials they were primarily limited to the orientation rule ensemble (**Figure 2.6**, left column). Indeed, electrode pairs with increased alpha synchrony during the color rule were more likely to show increased beta synchrony for the orientation rule than color rule (55/117 and 24/90 pairs, respectively; $p < 10^{-5}$, permutation test). Synchronized alpha activity may reflect inhibition of task-irrelevant processing (Haegens et al., 2011b; Klimesch, 1999; Palva and Palva, 2007; Pfurtscheller, 2001; Ray and Cole, 1985). Thus, alpha synchrony during color trials may reflect “de-selection” of the dominant (but currently irrelevant) orientation network, allowing the weaker (but currently relevant) color network to be boosted. Indeed, alpha increases in the orientation rule ensemble were associated with enhancement of individual color-rule neurons. Alpha power during the preparatory interval of color trials was positively correlated with the activity level of color-rule-preferring, but not orientation-rule-preferring, neurons during rule application to the test stimulus (**Figure 2.S4**, correlation coefficient of 0.014, $p = 0.0019$ vs. 0.003, $p = 0.47$, for color- and orientation-rule-preferring neurons, respectively, for 100 ms following stimulus onset; color > orientation, $p = 0.047$, see Supplemental Information for details). There was no direct evidence for suppression of the orientation network (e.g. a negative correlation between alpha power and the activity of orientation-

preferring neurons on color trials). However, these neurons are already suppressed during the color rule, so further suppression may be harder to detect.

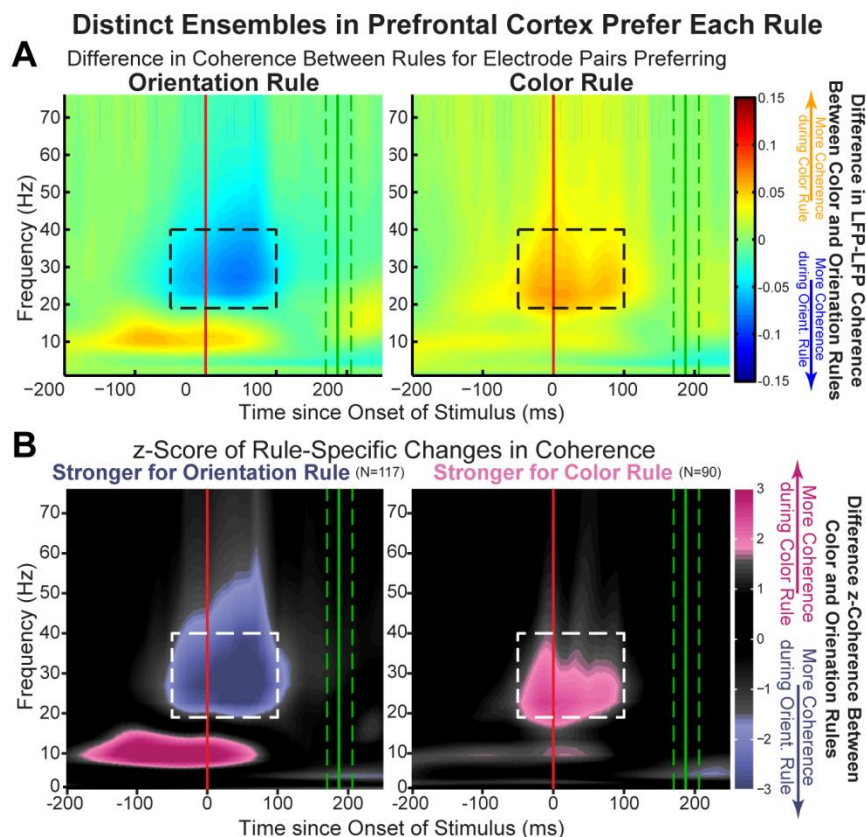


Figure 2.6. Independent, Rule-Specific PFC Ensembles.

Ensembles within PFC can be identified by rule selective synchrony in the peri-stimulus ‘beta’ ROI (dashed outline). One ensemble is more synchronous during orientation trials (A, left). This difference is significantly greater than expected by chance (B, left). A separate ensemble of electrodes is more synchronous during color trials (A, right). Again, this difference is significant (B, right). Alpha-band synchrony is observed in the orientation ensemble during the competing color rule (left panels, orange/pink), but not in the color ensemble (right) or during the orientation rule (Figure 2.2B). Axes are the same as Figure 2.3A, but now color axes are no longer rectified: orange/pink reflects greater synchrony during color rule trials, blue/purple during orientation rule trials. Please note the color axis of (B) is intentionally non-linear, showing only significant rule selectivity, beginning at a z-score of ± 1.67 ($p=0.05$) and fully saturated at ± 1.97 ($p=0.01$).

2.3.5 Rule-Dependent Synchrony Correlates with Behavioral Reaction Time

Synchrony at both alpha and beta was correlated with behavioral reaction time, further suggesting their functional role. There was significantly stronger rule-

selective synchrony in both bands on trials with shorter reaction times (**Figure 2.7**; alpha: $p=3.4310 \cdot 10^{-10}$, beta: $p=2.7110 \cdot 10^{-3}$, Wilcoxon signed-rank test), even after controlling for the effects of preparatory time and rule on reaction time (see Table 2.1). This stronger synchrony with faster reaction times occurred prior to test stimulus for both alpha and beta (**Figure 2.7**; stronger selectivity in beta: -20 to 0 ms, alpha: -240 to 0 ms prior to stimulus onset, Wilcoxon signed-rank test, $p < .05$, Bonferroni correction), suggesting preparatory facilitation of test stimulus processing.

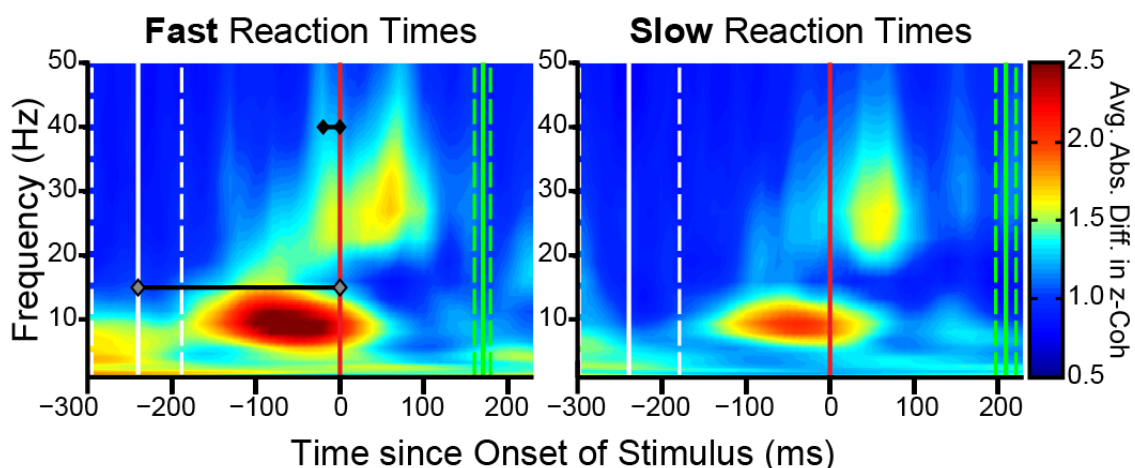


Figure 2.7. Strength of Prefrontal Synchrony Selectivity Correlates with Reaction Time.

Trials in which the monkeys responded faster (left) showed stronger rule-selective synchrony in the ‘alpha’ and ‘beta’ regions of interest compared to trials with slower reaction times (right). Green lines indicate reaction time quartiles and white lines indicate the corresponding preparatory period quartiles. Black lines on faster-reaction time trials (left) indicate when synchrony in the alpha and beta-frequency bands (gray and black diamonds, respectively) was significantly higher than synchrony during slower-reaction time trials.

2.4 Discussion

2.4.1 Linking Task-Relevant Neurons with Rule-Dependent Synchrony

Our results suggest distinct synchronous PFC networks support different rules. Rule-selective beta-band synchrony may help to dynamically link neurons in order to support task performance. Indeed, task-relevant (rule- and stimulus-selective) neurons were more synchronized to the corresponding network for the current rule. Similar organization of neural activity by synchronous population oscillations have been seen during sensory processing (Lakatos et al., 2008), and attention (Buschman and Miller, 2009). This synchrony-based linking of neurons into networks could be an ideal mechanism for cognitive flexibility, allowing ensembles of task-relevant neurons to be dynamically formed and reformed (Sejnowski and Paulsen, 2006; Womelsdorf et al., 2007).

Our results are consistent with recent evidence from humans and monkeys suggesting that beta oscillations play a major role in top-down organization of neural processing (Engel and Fries, 2010; Oswal et al., 2012). There is enhancement of beta oscillations in human sensorimotor cortices when maintaining posture (Androulidakis et al., 2007; Gilbertson et al., 2005), and when competing movements need to be inhibited (Pfurtscheller, 1981; Swann et al., 2009). Beta synchronization between frontal and parietal cortices increases during top-down attention (Buschman and Miller, 2009, 2007; Gross et al., 2006) and with increased working memory load (Axmacher et al., 2008; Babiloni et al., 2004). Further, beta synchronization increases in anticipation of an

upcoming stimulus and is stronger when a stimulus is more predictable (Gross et al., 2006; Liang et al., 2002; Zhang et al., 2008). Similarly, we observed rule-selective beta synchronization in anticipation of the test stimulus was correlated with the animal's reaction time.

2.4.2 Coordination of Neural Ensembles

Orientation seemed to be the dominant modality. This may be due to its relative saliency, much like word-naming in the Stroop test (MacLeod, 1991). We found the orientation network, which was synchronized at beta-band frequencies during the orientation rule, had increased alpha-band synchrony when color was relevant. Recent studies in humans have suggested a role for alpha oscillations in working memory (Freunberger et al., 2008; Jensen et al., 2002; Palva and Palva, 2011) and visual attention (Sadaghiani et al., 2010; Sauseng et al., 2005; Von Stein et al., 2000). In particular, alpha oscillations during attention are suppressed in the task-relevant sensorimotor cortices, enhanced in the task-irrelevant cortices, and can influence discriminability of stimuli (Gould et al., 2011; Haegens et al., 2011a; Worden et al., 2000). Because of this, it has been suggested that enhanced alpha synchronization creates an inhibition of irrelevant processes (Klimesch et al., 2007; Mathewson et al., 2011). Our study is consistent with this model: alpha synchronization may allow the weaker color network to be activated over the stronger (orientation) network when color is relevant. In support, we observed an increase in the activity of color-selective neurons following an increase in alpha in the orientation network. These results suggest a

dual model of competition between networks of neurons: beta synchrony selects the relevant network while alpha may de-select the irrelevant, but dominant, network so that a weaker, relevant one can be established. Similar dual mechanisms may bias competition between stimuli during focal attention, leading to high-frequency synchronization of neural activity representing attended stimuli (Fries et al., 2001) and slower-frequency synchronization of neural activity representing unattended stimuli (Cohen and Maunsell, 2009; Mitchell et al., 2009).

In sum, our results suggest that synchronous oscillations allow dynamic selection of currently relevant neural ensembles. This may be particularly important in prefrontal cortex, where neurons have highly diverse properties and thus a particular ensemble must be formed from neurons that are also members of other ensembles (Rigotti et al., 2010). The dynamic nature of synchronized oscillations may provide a substrate for the ensembles that allows that their rapid selection and de-selection and, hence, cognitive flexibility.

2.5 Experimental Procedures

2.5.1 Recording Locations and Techniques

Two macaque monkeys, one male (CC, *Macaca fascicularis*) and one female (ISA, *Macaca mulatta*), were trained on a cued task switching paradigm (**Figure 1A**). Neural activity was simultaneously recorded during task performance from two frontal regions: the dorsolateral prefrontal cortex (PFC, area 9/46) and the anterior cingulate cortex (ACC, areas 24c and 32). Only data from the

dorsolateral prefrontal cortex is reported here. The recording well targeting PFC was placed in the left hemisphere and was centered approximately 28 mm anterior to the interaural plane and 21 mm lateral from the midline. Stereotaxic positioning of the well was guided by structural magnetic resonance imaging.

Neural activity was recorded during 34 sessions (11 for monkey CC, 23 for monkey ISA). Arrays of up to sixteen epoxy-coated tungsten electrodes (FHC Inc, Bowdoin ME) were lowered into the PFC during each recording session (median # of electrodes with well-isolated single neuron activity was 5.5 per session). Electrodes were lowered in pairs by a custom built microdrive assembly and spaced at least 1 mm apart. Electrodes were lowered acutely each day through an intact dura and allowed to settle before recording. This ensured stable isolation of the single neuron activity. After each recording session, the electrodes were retracted and the microdrive assembly was removed from the well.

A Plexon Multichannel Acquisition Processor (MAP; Plexon Inc, Dallas, TX) was used to perform electrophysiological recordings. The signal from each electrode was filtered by the pre-amplifier between 154 Hz and 8.8 kHz to isolate spiking activity and between 3.3 and 88 Hz to isolate the local field potential. Both spiking activity and local field potentials were referenced to earth ground (although the same results were observed when re-referencing locally, within PFC). The raw spiking waveforms were digitized at 40 kHz and subsequently sorted into single units offline, based on waveform shape characteristics and principal components analysis (Offline Sorter, Plexon Inc, Dallas, TX). During

recording, electrodes were lowered to maximize the signal-to-noise ratio of spiking activity and were not guided by the task-relevance of neural responses. This ensured a representative sample of neural activity without selection bias. A total of 313 neurons were recorded in the PFC (99 in monkey CC and 214 in monkey ISA). The average firing rate of neurons recorded in PFC was 7.4 Hz (inter-quartile range of firing rate was 1.7 to 10.1 Hz). Only local field potentials from electrodes with at least one isolated unit were used for all of our analyses, ensuring the electrode was in the appropriate cell layer.

Animal eye position was monitored using an infrared eye-tracking system (Eyelink, SR Research Ltd., Ontario, Canada) which sampled the eye position at 240 Hz. Behavioral control was handled by Cortex (<http://www.cortex.salk.edu>). Animal procedures followed all guidelines set by the Massachusetts Institute of Technology Committee on Animal Care and the National Institute of Health. Code used in the analysis was custom-written in Matlab (Mathworks, Natick, MA) or R (R Foundation for Statistical Computing, Vienna, Austria).

2.5.2 Behavioral Task

The task began with the presentation of a fixation spot at the center of the screen. The monkeys were required to acquire and maintain fixation within three degrees of this spot until making a behavioral response. Immediately after fixation was acquired, both the rule cue and response targets appeared and remained on screen for the duration of the trial. The rule cue was a colored border around the display indicating the feature of the stimulus the monkey needed to discriminate

on the current trial. The animals were trained to perform two different rules: color and orientation. Each rule was associated with two different cues in order to distinguish rule-related activity from cue-related activity (see **Figure S1A** for example neurons encoding the rule and not the individual cues). After the presentation of the rule cue, the animals were required to maintain fixation for a 'preparatory' time-period before the onset of the stimulus. The duration of the preparatory period was randomized for each monkey (227 – 496 ms for monkey CC, 86 – 367 ms for monkey ISA; different ranges were the result of iteratively lowering the preparatory period during training while equalizing performance between animals).

At the end of the preparatory period, a test stimulus, oriented either vertically or horizontally and colored either red or blue, appeared at the center of the screen. The test stimulus consisted of small shapes (colored and aligned appropriately). The identity of these small items changed from session to session, ensuring the animals generalized the rules. After the onset of the stimulus, the monkeys were free to make their response: a single saccade to either the left or right target. The correct saccade direction depended on both the stimulus identity and the current rule in effect (**Figure 2.1A**). For the color rule, a red stimulus required a saccade to the right, a blue stimulus a saccade to the left. For the orientation rule, a horizontal stimulus required a saccade to the right, a vertical stimulus a saccade to the left. As each stimulus consisted of both an orientation and color dimension, the correct saccade for the two rules could either be the same (congruent trials)

or different (incongruent trials). For example, a red vertical stimulus is incongruent, requiring a rightward saccade under the color rule and a leftward saccade under the orientation rule. In contrast, a red horizontal stimulus requires a rightward saccade for both rules. The majority (70%) of trials were incongruent, ensuring the animal always followed the rule. After the animal made the correct saccade, a juice reward was delivered via a juice tube. There was an inter-trial interval of approximately 100 ms before the next trial began.

Although the rule was cued on each trial, the rule in effect was blocked into groups of trials. Each block consisted of a minimum of 20 trials of the same rule. After 20 trials, the rule switched randomly – with a 5% or 10% chance of switching rules on each trial for monkey ISA and CC, respectively. The average block consisted of 39 trials of the same-rule for ISA and 30 for CC.

2.5.3 Behavioral and Neural Analysis Methods

A generalized linear model (GLM) was used to quantify the effect of multiple task-related covariates on the animals' behavioral reaction time. A Gamma distribution was used in the model to as it is ideal for fitting strictly positive data with a constant coefficient of variation, such as reaction times (McCullagh and Nelder, 1989). The link function, which defines a non-linear transformation between the linear predictors and the mean of the observations, was chosen to be the log function to enforce the requirement that reaction times be strictly positive. A complete model was developed, fitting the reaction time with the all task-related covariates: the rule (color/orientation), preparatory period,

congruency of stimulus-response association across rules, monkeys, time in session, and whether it was a switch trial (see Supplemental Information for details). A bias-corrected percent explained variance statistic (ω PEV) was used to evaluate neural selectivity. ω PEV determines the portion of variance of a neuron's firing rate explained by a particular task variable (e.g. the current rule) but is analytically corrected for upward bias in percent explained variance with limited observations. Significance was determined by a permutation procedure (see Supplemental Information for details).

2.5.4 Synchrony Analysis Methods

The local field potential (LFP) was transformed into the time-frequency domain using Morlet wavelets. Synchrony was estimated by computing the spectral coherence between pairs of electrodes. Significant differences in coherence between the two rules were determined with a permutation test. The null-hypothesis is that no significant difference exists between rules, therefore a null-distribution was generated by permuting color and orientation trials and recalculating the coherence (this process was repeated at least 100 times for each pair of electrodes). The mean and variance of this null-distribution was used to estimate the likelihood of the observed synchrony (captured by a z-score statistic). Z-scores greater than 1.96 or -1.96 indicated significant changes in coherence for the color and orientation rule, respectively (see Supplemental Information for details). Time-frequency regions of interest (e.g. the 'alpha' and 'beta' bands) were defined such that they encapsulated the peaks in rule-selective

changes in synchrony (**Figures 2.2** and **2.S3**). Although the bands were not pre-defined, they closely follow the alpha and beta-bands defined in other studies, supporting conclusions about common mechanisms (see Discussion).

Phase locking value (PLV) was used to estimate spike-field synchrony. The phase-locking of task-relevant neurons (as identified by ω PEV, see above) to the LFP of electrodes participating in either the color or orientation network was estimated in a 200 ms window around the time of stimulus onset (-50 ms to 150 ms). In order to correct for the strong sample size bias in estimating spike-field synchrony, a stratification procedure was used (requiring 200 spikes in the window). Significant differences were determined by a permutation test, as above (see Supplemental Information for details). The relationship between rule-dependent LFP synchrony and reaction time was determined by first regressing-out the effect of preparation time on reaction time (see Supplemental Information for details). The resulting reaction time residuals were sorted into 'fast' and 'slow' trials (defined as the 65th-95th and 5th-35th percentile of the residual distribution for each session, respectively). As above, a permutation test was used to estimate a z-score of the observed rule-selective differences in synchrony (see Supplemental Information for details). Significant differences in rule-selectivity between fast and slow trials were determined by comparing the average absolute z-score in the beta (or alpha) frequency bands using a Wilcoxon signed rank test. To preclude dependence between electrodes recorded in the same session, we bootstrap resampled the electrode pairs 1000 times. After

establishing rule-selectivity was stronger on average in the alpha and beta bands respectively, we examined rule-selectivity for differences over time by testing for differences in rule-selectivity at each time point, again using a Wilcoxon signed rank test (see Supplemental Information for further details).

2.6 Supplemental Information

2.6.1 Behavioral Analysis

Both animals were able to perform the task with high performance, well above chance (~90% of trials were correct, $p < 2.20 \times 10^{-16}$ for both animals and both rules, binomial test). Performance was maintained even after a switch in rule (Figure 2.1B). However, consistent with human behavioral results (Monsell, 2003), there was a cost to switching between rules – both animals were significantly slower to respond when the rule in effect changed (Figure 2.1B). This suggests the animals slowed their response to maintain accuracy in the task. To fully quantify the effect of task switching on the reaction time, a generalized linear model (GLM) was fit to the data. A GLM was selected to model the reaction time because it allows for non-constant variance, can account for the effect of multiple time-dependent covariates, and can treat strictly positive data. In particular, we chose the Gamma distribution for our model fit because it is well-suited to model strictly positive continuous data with a constant coefficient of variation (McCullagh and Nelder, 1989). For GLMs, the link function defines a non-linear transformation between the linear predictors and the mean of the observations. We chose the log link function to enforce the requirement that

reaction times be strictly positive. A complete model was developed, fitting the reaction time with the following covariates:

$$\begin{aligned} \log(\text{ReactionTime}) &= \text{Intercept} + \text{Rule}(\text{levels: Color, Orientation}) \\ &+ \text{NormalizedPreparatoryPeriod} \\ &+ \text{Congruency}(\text{levels: Incongruent, Congruent}) \\ &+ \text{Monkey}(\text{levels: ISA, CC}) \\ &+ \text{SessionTime}(\text{levels: Early, Middle, LateinSession}) \\ &+ \text{SwitchTrial}(\text{levels: Repetition, Switch}) + \text{SwitchTrial: Rule} \end{aligned}$$

Preparatory period was normalized by subtracting the mean preparatory period for each monkey.

As with all of our analysis, trials in which the monkeys broke fixation and trials in which the monkey did not make a consistent attempt – defined as successful fixating in at least 80% of the five trials before the current trial – were excluded. Outlier reaction times (<100ms and >313ms), determined by examination of the raw reaction times, were also excluded. Reaction time analysis included only correct trials.

Table 2.S1 shows the estimated coefficients and standard errors. Similar to Figure 2.1B, the detailed GLM revealed a significant effect of switching rules on reaction time dependent on which rule was in effect: the GLM fit found that the switch cost occurred when the monkey switched from orientation to color but not vice-

versa (Table 2.S1, Switch Trial). This, along with the stronger neural selectivity (see Figure 2.2), suggests orientation might have been the ‘default’ behavior and may explain the differences observed in the synchronous sub-networks (Figure 2.6).

Similar to human behavioral results, the preparatory period duration also had a strong effect on reaction time (Monsell, 2003). Longer preparatory periods result in faster reaction times and shorter preparatory periods result in slow reaction times ($p < 2 \times 10^{-16}$, GLM). Finally, the model shows congruent stimuli led to slightly faster responding (Table 2.S1).

Although not included in the GLM, there was a slight decrease in time to respond during the first few trials following a switch into the orientation rule (this effect can be seen in **Figure 2.1B**). This likely reflects the animal’s increased certainty for the first few trials following a rule-switch (as they are guaranteed the rule repeats for a limited number of trials). Although this provides further behavioral support for a dominant orientation rule, the effect was not consistent across trials (only reaching significance at $p < 0.05$ for a few trials).

Parameter		Estimate	Std. Error	Pr(> t)
Intercept		195.00 ms	0.18 ms	$< 2*10^{-16}$
Rule	Orientation	----		
	Color	-3.89 ms	0.18 ms	$< 2*10^{-16}$
Congruency	Incongruent	----		
	Congruent	-1.88 ms	0.19 ms	$< 2*10^{-16}$
Switch Trial	Repetition	----		
	Switch (Orientation)	0.04 ms	0.77 ms	0.96
	Switch (Color)	4.14 ms	1.11 ms	$1.61*10^{-4}$
Monkey	ISA	----		$< 2*10^{-16}$
	CC	-26.14 ms	0.20 ms	
Preparation Time	Per 1 ms increase in Preparation Time	-0.18 ms	0.001 ms	$< 2*10^{-16}$
Session Time	Early-in-Session	----		0.23
	Mid-in-Session	-0.13 ms	0.11 ms	
	Late-in-Session	-0.26 ms	0.11 ms	

Table 2.S1, related to Figure 2.1.

Estimated coefficients (the first level is included in the baseline), standard errors, and p-values from the reaction time GLM. Since the log link function is used, effects are multiplicative rather than additive as in normal linear regression.

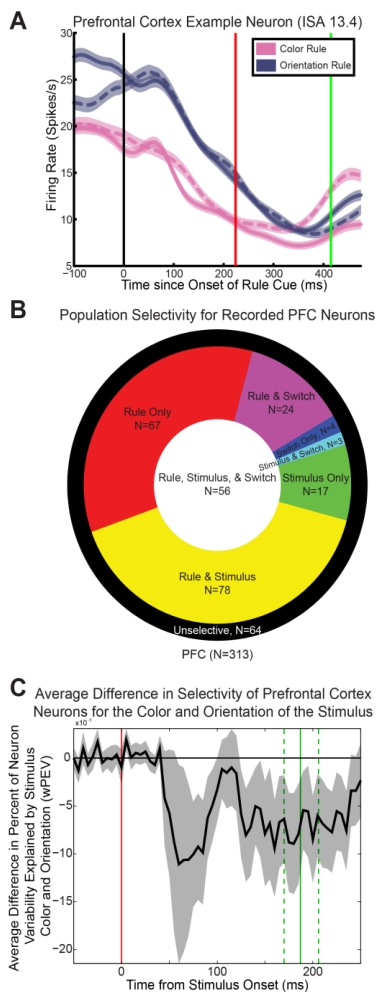


Figure 2.S1, related to Figure 2.2.

(A) Smoothed (20 ms Gaussian) firing rate histogram an example PFC neuron that responds differentially to the color rule (pink lines) and orientation rule (purple lines). Solid/dashed lines indicate response to two cues for each rule. Black line indicates onset of rule cue, red line indicates median time of stimulus onset and green line indicates median reaction time. (B) Distribution of neuron selectivity in population of recorded PFC neurons. Selectivity was quantified for the rule (red), stimulus (green), and switch (blue). Neurons with selectivity in multiple categories combined the appropriate colors. (C) PFC neurons encode more information about the orientation of the stimulus than the color of the stimulus. Information is captured by a percent explained variance (PEV) statistic (y-axis) over time (x-axis). The black line shows the average difference for all recorded PFC neurons (95% CI shown by shaded region). Vertical red line indicates time of stimulus onset, green line indicates median reaction time (with IQR shown by dashed green lines).

2.6.2 Rule-, Stimulus-, and Switch-Selectivity in Prefrontal Cortex Neurons

Single neuron activity was simultaneously recorded from up to 16 electrodes placed across PFC (see above for recording locations and techniques). Waveforms were digitized at 40 kHz for isolation and then spike times for each isolated neuron was decimated to a 1 kHz sampling rate. We were interested in determining if neurons carried information about task-relevant features and if so, the timing of this information. Three features were of interest: the current rule in effect, the stimulus identity, and whether the current trial was a switch trial (versus a repetition). The rule was cued on every trial, although the identity of the rule was blocked into trials of at least 20 of the same rule (see Behavioral Task above). However, exactly when a switch occurred was random, and therefore unknown to the animal. Similarly, the color and orientation of the stimulus was not known to the monkey before stimulus onset. We assessed selectivity for all three task-relevant features for each neuron using a percent explained variance (PEV) statistic (see Figure 2.S1A for example rule coding neurons).

The PEV reflects how much of the variance in a neuron's firing rate can be explained by the value of a particular task variable (e.g. whether the current rule is color or orientation). Typically, PEV is measured by eta-squared: $\eta^2 =$

$\frac{SS_{BetweenGroups}}{SS_{Total}}$, such as in an analysis of variance. Where $SS_{Total} = \sum_i^N (x_i - \bar{x})^2$ and

$SS_{BetweenGroups} = \sum_{group}^G n_{group} (\bar{x}_{group} - \bar{x})^2$. However, the eta-squared statistic

has a strong positive bias, particularly for lower sample sizes. Therefore, we used the omega-squared statistic (ω PEV) for determining neural selectivity instead:

$$\omega^2 = \frac{SS_{BetweenGroups} - d.f.* MSE}{SS_{Total} + MSE}$$

where d.f. is the degrees of freedom (i.e. the number of groups, G, minus 1) and MSE is the mean squared error, $MSE = \sum_i^N (x_i - \bar{x}_{group})^2$

Omega-squared is an unbiased measure (Keren and Lewis, 1979), resulting in a zero-mean statistic when there is no information (e.g. baseline of Figure 2.S2 is zero). This is crucial for averaging the selectivity across a population of neurons. The time course of ω PEV was calculated in a sliding window (a Gaussian with 20 ms standard deviation for rule and switch information and 10 ms for stimulus information, allowing for greater temporal resolution). As used here, the ω PEV statistic makes the assumption that neurons encode information by modulating their average firing rate within the analyzed window of time. Importantly, the statistic does not make any assumption about the consistency of neural response over time or the nature of the change relative to other time periods. To determine whether and when the observed level of ω PEV was significantly different from chance, we used a randomization test. The association between neural activity and the identity of the task-relevant variable was randomly permuted and the ω PEV was re-calculated. By repeating this process 1000 times a null distribution was constructed. A cluster-correction technique was used to correct for multiple comparisons across time. First, a time-varying threshold was set as the 95th percentile of the null distribution over time. Continuous periods of time when the observed ω PEV exceeded the 95th percentile threshold were identified as clusters. The size of the cluster was then determined by integrating the area

between the observed ω PEV and the threshold. The same process was repeated for each randomly permuted ω PEV time course. Only the maximum cluster size was taken for each ω PEV permutation. This corrects for multiple comparisons across time (Nichols and Holmes, 2002) and creates a null distribution of cluster size. The observed clusters are then compared to the null distribution in order to determine the likelihood of observing a cluster of that size. Neurons were classified as carrying significant information if they contained at least one observed cluster with a low probability of occurring by chance ($p \leq 0.05$).

Selectivity was determined for each neuron for all three task-relevant variables: rule, stimulus identity (either color or orientation), and switch/repetition. A significant number of PFC neurons carried information about each of the three variables (**Figure 2.S1B**). Individual PFC neurons often carried information about multiple dimensions of the task, with some neurons encoding all three (the white area of **Figure 2.S1B**).

2.6.3 Time course of Neural Selectivity

After the population of selective neurons were identified in each region, the time course of selectivity was determined for stimulus identity (**Figure 2.2B** and **2.S1C**). We were interested in determining the time at which the average information across PFC's population of selective neurons exceeded chance, and whether these times were significantly different for color and orientation information. First, each neuron's selectivity (as measured by ω PEV) was normalized by the randomly permuted, null distribution to create a z-score of

ω PEV over time. This allowed for selectivity to be weighted appropriately across the population. The time point when the population carried significant information was taken to be when this average z - ω PEV was significantly above zero (corrected for multiple comparisons across time) for at least 15 ms. It is important to note that the absolute time to significance is affected by non-physiological parameters (such as the threshold chosen or the smoothing kernel used). Therefore, all statements about timing are relative between different neural populations where these parameters were held constant. In order to estimate the uncertainty about the time to significance, we used a bootstrapping procedure. A pseudo-population of neurons was created for each area by drawing randomly, with replacement, from the population of observed neurons. The time at which this pseudo-population exceeded chance was then determined. This process was repeated 1000 times in order to generate a distribution around the observed time to significance for each region. Following this process, we determined that orientation information occurred at 41.1 ms after stimulus onset, significantly earlier than color information (47.6 ms, $p=0.0026$).

2.6.4 Time-Frequency Decomposition of Local Field Potentials

The estimation of coherence during the two rules (**Figures 2.2, 2.S2, 2.3, 2.4, and 2.6**) and the estimation of spike-field synchrony (**Figure 2.5**) rely on decomposing the local field potential (LFP) into its time-frequency components. The time-varying spectrum of the LFP was estimated by convolving the filtered signal with a series of Morlet wavelets:

$$\psi(f, t) = A e^{-\frac{t^2}{2\sigma^2}} e^{2\pi i f t}$$

where t is time, f is the center frequency, A is a normalizing constant to ensure unitary power, and σ^2 is the smoothness of the kernel in time. In time-frequency analyses, there is a necessary tradeoff between temporal and spectral resolution. Therefore, the smoothness in time (σ^2) is directly related to the smoothness in frequency $\sigma_f = \frac{1}{2\pi\sigma}$. The tradeoff between temporal and spectral resolution is captured by the constant q , such that $\sigma = \frac{f}{q}$. We set $q=3$ to balance good frequency resolution (FWHM $\sim 3/4$ of an octave) with good temporal specificity (FWHM $\sim 9/8$ of that frequency's wavelength) across a wide range of frequencies. For example, our 'beta' band (19-40 Hz) is smoothed in time with a Gaussian with a full-width half-max of 38 ms. No further smoothing in time or frequency was done for any of the spectral analyses. The choice of q directly impacts the spread of rule-selective changes in synchrony both in time and frequency (e.g. **Figure 2.3**). In particular, in order to achieve good temporal resolution at low frequencies we necessarily lose some degree of frequency resolution, leading to a slightly wider 'alpha' band (6-16 Hz) than what is typically reported (8-12 Hz, see Discussion). Note that this does not impact the center frequency (10 Hz in both cases).

The convolution of the Morlet wavelet with the local field potential estimated both the amplitude and phase of the ongoing LFP signal for each

frequency and for each time-point during the trial. Synchrony between two simultaneously recorded LFP signals was estimated using the coherence statistic:

$$C_{t,f}^{XY} = \left| \frac{S_{t,f}^{XY}}{\sqrt{S_{t,f}^{XX} * S_{t,f}^{YY}}} \right|$$

Where $S_{t,f}^{XY}$ is the cross-spectrum for two time-frequency transformed signals $X_{t,f}$ and $Y_{t,f}$ and $S_{t,f}^{XX}$ and $S_{t,f}^{YY}$ are their respective power spectra. X^* indicates the complex conjugate of X .

2.6.5 Identification of Synchronous Sub-networks

For each trial, the coherence between each pair of simultaneously recorded electrodes was determined for the color rule and orientation rules separately (see **Figure 2.3** for population distribution). Note that because we examined coherence on a trial-by-trial basis, extremely low frequency oscillations (< 3 Hz) are essentially “filtered out” of our analysis since one full cycle of the oscillation is slower than the length of the trials in the task (average trial length was 434 ms between monkeys). While oscillations at these frequencies are likely not functionally relevant on a trial-by-trial basis in this task, it is possible that these slower oscillations play a role across trials. However, our particular task and analysis leave us unable to comment on their relevance as the oscillations may reflect the rhythm of the task itself.

A permutation test was used to determine for each pair whether synchrony in color and orientation was significantly different. The null hypothesis is that

there is no difference between rules, and therefore the observed coherence is not the result of a special grouping of trials into color and orientation. Therefore, to generate a null distribution, trials were randomly assigned to either the color or orientation groups (with the relative number of trials in each group held constant) and the coherence statistic and its difference between groups were re-computed. This process was repeated 100 times to estimate the mean and variance of the difference statistic under the null hypothesis. These were then used to estimate the relative likelihood of our observed difference in coherence under the null hypothesis (quantified in the z-score of the coherence statistic). The average absolute-value of the z-coherence across the population of pairs of simultaneously recorded PFC electrodes can either be aligned on rule-cue onset (**Figure 2.S2A**) or stimulus-onset (**Figure 2.3A**). Both alignments show two time-frequency periods of interest where the synchrony between electrodes significantly differed between the two tasks: a 6-16 Hz, ‘alpha’ band that is time-locked to the onset of the rule cue and ends around the time of stimulus presentation (solid outline in **Figure 2.3A** and **Figure 2.S2A**) and a 19-40 Hz, ‘beta’ band around the presentation of the stimulus (dashed outline in **Figure 2.3A** and **Figure 2.S2A**). The differences in time course of the observed rule-selective synchrony when aligning trials on stimulus (**Figure 2.3A**) or rule-cue onset (**Figure 2.S2A**) suggests the beta band occurs around the stimulus onset while the alpha band follows rule-cue onset. The average coherence for each pair of electrodes within these regions of interest was compared to the null

distribution (see above), resulting in a z-score of the coherence (zCoh) observed for both the alpha and beta regions of interest. Based upon the zCoh for each pair, the pairs were classified as either being more synchronized during the color or orientation rule (117 pairs significantly preferred the orientation rule, 90 preferred the color rule; see **Figure 2.3B** for population and **Figure 2.S2B** for an example electrode pair).

One possible source of the observed rule-selective sub-networks is that the onset of the stimulus evokes a potential that differs between the rules for each group of recording sites. We controlled for this by subtracting each electrode's average evoked potential (for a given rule) from the local field potential recorded on every trial (of that rule). This was done before calculating the coherence statistic. Therefore, any remaining changes in coherence are due to trial-to-trial variability in the local field potential that co-varies within a subset of recording sites for each rule. In addition, the existence of two separate, but simultaneously observed, sub-networks, each with greater coherence during one of the learned rules, excludes a common, general source of this trial-to-trial variability (such as arousal).

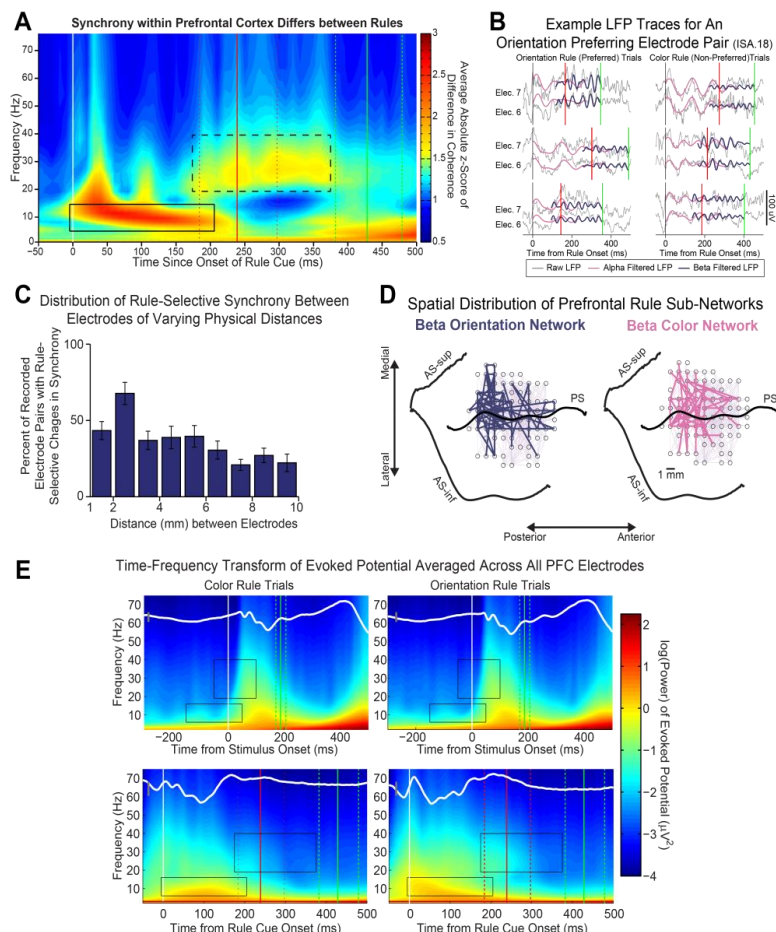


Figure 2.S2, related to Figure 2.3.

(A) Synchrony within PFC differed depending on which rule was in effect. Color axis indicates the average z-score of the observed difference between synchrony during the color and orientation rule. Synchrony is shown relative to rule-cue onset (gray vertical line) across frequency (y-axis). As seen relative to stimulus onset (Figure 2), two time-frequency regions of interest were found to carry rule information: a 6-16 Hz ‘alpha’ band (solid outline) and a 19-40 Hz ‘beta’ band (dashed outline). Median time and interquartile range of stimulus onset and saccade are shown in red and green, respectively. (B) Example local field potential traces of a prefrontal electrode pair (3 mm apart) participating in the orientation sub-network during example orientation (left) and color (right) trials. Local field potentials show peri-stimulus beta synchrony (purple) during orientation trials and rule-locked alpha synchrony (pink) during color trials. Red and green vertical lines indicate stimulus onset and time of saccade. (C) Rule-selective synchrony was observed on a high proportion of electrodes (y-axis) over all recorded distances between electrodes (x-axis). Error bars indicate STE over recording sessions. This distribution is not monotonically decreasing, arguing against the possibility the observed effects are due to volume conduction of local field potentials. (D) Spatial distribution and connectivity of synchronous electrodes. PFC electrode pairs within the rule-selective networks are spatially overlapping and often span the principal sulcus. Each circle represents an electrode location and each line represents significant rule selective coherence between two electrode locations. Electrodes from monkey ISA alone (precise anatomical locations for Monkey CC relative to sulci are unknown, only relative position were recorded). PS = principal sulcus, AS-inf = arcuate sulcus inferior, AS-sup = arcuate sulcus superior. (E) Average power distribution of the evoked field in both time and

frequency, relative to stimulus onset (top) and rule cue onset (bottom), for all PFC electrodes. White traces show average evoked potential across all PFC electrodes (gray scale bar is 5 μV). The time-frequency response does not show the same structure as observed in the coherence between electrodes (Figure 3), suggesting the observed rule-selective synchrony is not a direct modulation of the evoked potential.

2.6.6 Synchronous Sub-networks do not Reflect Differences in Evoked Potential

Two different mechanisms could underlie the observed rule-selective synchrony in the color and orientation networks. One possible mechanism is that the observed rule-selective coherence could reflect a preparatory process, similar to attending to the current rule in effect. Alternatively, the observed synchronous sub-networks could alter the processing of the stimulus (modulating the evoked field) in order to facilitate the execution of a given rule. Our current results provide evidence for a preparatory mechanism: although the beta-band synchrony occurred around stimulus presentation, **Figure 2.3A** shows an early peak in coherence before the stimulus onset, excluding the possibility of a purely evoked response. We isolated this peak by defining the sub-networks using only the pre-stimulus beta-band coherence (i.e. a window of -50 to 0 ms instead of the -50 to 100 ms window previously used). Indeed, the majority of electrodes pairs were still significantly rule-selective in both sub-networks (81/117 for orientation, 55/90 for color). Finally, the time-frequency power distribution of the average evoked field itself does not show the same structure as our observed coherence (**Figure 2.S2E**), suggesting the frequency response of the synchronous sub-networks are not just modulations of the stimulus response.

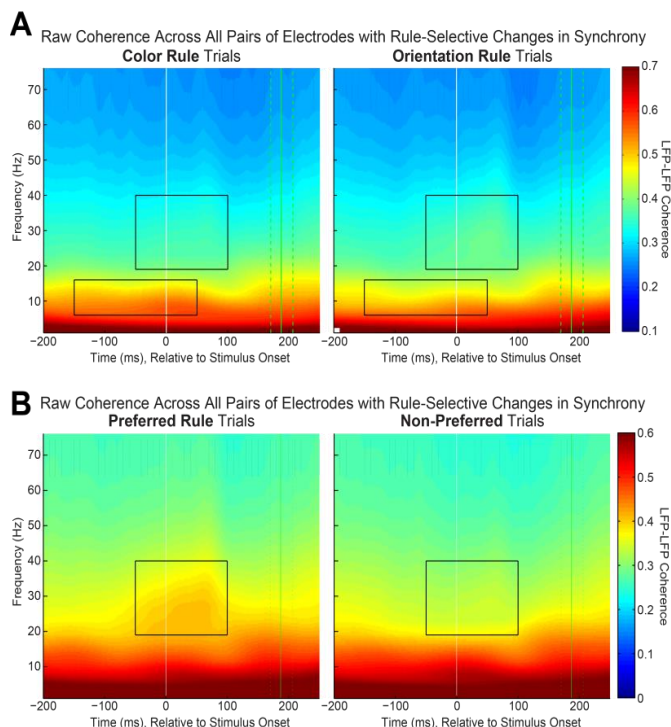


Figure 2.S3, related to Figure 2.4. Raw coherence plots showing rule-selective changes in synchrony between pairs of prefrontal cortex electrodes.

Color axes indicate the average coherence observed for all rule-selective electrode pairs. Coherence is shown relative to stimulus onset (white vertical line) across frequency (y-axis). Black boxes indicate the two time-frequency regions of interest (ROI) found to carry rule information (see Figure 3). Median time and interquartile range of saccade is shown by vertical green lines. The rule preference of an electrode pair was defined by their beta-band ROI, as for Figure 6. (A) Coherence for all pairs of PFC electrodes that were rule-selective (regardless of rule preference) during color rule trials (left) and orientation rule trials (right). Coherence is dominated by $1/f$ component due to referencing to earth ground. As both color- and orientation-preferring electrodes (defined by the beta ROI as in Figure 2.6), changes in coherence are largely canceled by each ensemble. (B) Coherence for all rule-selective electrode pairs during their preferred (left) and non-preferred (right) rules.

2.6.7 Quantification of Synchronous Sub-network Structure

As noted in the main text, our results indicate that abstract rules are not only encoded by the activity of single neurons in frontal cortex, but also in the pattern of synchronous activity within a sub-network. In addition to being rule-selective, these sub-networks showed non-random structure. For the orientation network each ‘node’ (i.e. recording site) in the network was synchronized with an average

of 2.57 other sites (in other words, the average ‘degree’ of the orientation sub-network was 2.57). In contrast, each recording site in the color network was synchronized with 1.76 other sites. The average number of possible pairs that an electrode could participate in was 5.05. The degree of both networks was greater than expected when compared to a randomly connected network with the same edge likelihood ($p < 10^{-3}$, randomization test where the observed coherence values are randomly assigned to pairs of electrodes). In addition, the observed network degree was significantly greater than random networks generated by shuffling coherence values within a given recording day (a more stringent test, $p < 10^{-3}$ for orientation, $p = 0.032$ for color). Although the orientation network had more pairs of synchronous recording sites, each site was synchronized with a greater number of other sites, resulting in less individual recording sites participating in the network ($N = 91$ for orientation, $N = 102$ for color). As noted in the main text, the two networks were not exclusive at the level of individual recording sites: the majority of recording sites that selectively increased synchrony during one rule with one set of electrodes also increased synchrony during the second rule with a different set of electrodes ($N = 53$). However, to fully test this possibility, we also limited our analysis to recording sites that showed no rule-selective changes in local LFP power. Although this quartered our population of electrode pairs ($N = 108$), we still found a highly significant number of pairs of these sites were synchronized in a rule-selective manner ($p = 0.0015$ for orientation, $p = 8.1 \times 10^{-5}$ for color, binomial test). Furthermore, across the entire population of electrode

pairs, there was no obvious correlation between the rule-preference (if any) of the local LFP power at each recording site in a pair and their rule-selective coherence. For example, 28% of pairs of recording sites where both electrodes, individually, showed an increase in beta LFP power during the orientation rule, were more synchronized with each other during the color rule, again arguing against rule-selective differences in local power as the sole explanation for the observed rule-selective synchrony and highlighting the dynamic nature of the observed sub-networks. As noted in the main text, such dynamic re-organization of neural activity is ideal for supporting cognitive flexibility.

Further support for our hypothesis that these rule-selective networks play a functional role comes from analysis of the electrode locations and their relative distances. Estimates of the area of integration for cortical field potentials vary from 250 μm to 3 mm (Berens, 2008; Katzner et al., 2009) meaning high spatial clustering of sub-network electrode pairs within this range would indicate our observed coherences and networks are spurious (although see (Kajikawa and Schroeder, 2011) for a challenge to the locality of the field potential). However, half of the sub-network electrode pairs are greater than 3 mm apart (color sub-network interquartile range = [2 mm, 3 mm, 4.24 mm], orientation sub-network interquartile range = [3 mm, 3.16 mm, 5.62 mm]) and we observe rule-selective synchrony as far as 10 mm apart in both sub-networks (see **Figure 2.S2** for full distribution). Moreover, many of the sub-network electrode pairs (with known anatomical location) were located on opposite sides of the principal sulcus and

there was little spatial difference between the networks (**Figure 2.S2D**).

Therefore, even under more liberal estimates for field potential integration area (3 mm), our analysis of electrode locations indicates that the observed networks are not entirely the result of common field signals at nearby electrodes.

One final possibility is that there are remote processes in other brain areas generating fields that differentially affect the recorded electrodes, causing the observed differences in coherence. However, several observations about the nature of our networks discount this possibility. First, the interdigitated nature of the rule-selective sub-networks (**Figure 2.S2D**) argues against a remote process, because presumably, a remote process should affect electrodes in the same way spatially. This is not what we observed. We quantified this more carefully by examining the selectivity of electrode pairs spatially located in-between rule-selective electrodes. Because “spatially in-between” can be difficult to define, we restricted our search to electrode pairs on the same columns, rows and diagonal of the recording array as the current electrode pairs (Recall that recording sites are spaced in a 1 mm grid located over the principal sulcus, see **Figure 2.S2D**). As reported in the main text, many electrode pairs had at least one pair of electrodes spatially interposed with either no differences in synchrony between the rules or the opposite preference. Second, we observed no rule-selective synchrony in the nearby anterior cingulate cortex, which should be affected by remote processes as well. Third, our results were qualitatively similar when using a common average reference instead of earth ground. Finally, as

discussed in the main text, task selective neurons synchronize more with the electrodes that showed task selective coherence (**Figure 2.5**) which would be unlikely if the coherences were not intrinsic to prefrontal cortex.

2.6.8 Alpha-Band Synchrony May Reflect a Suppressive Mechanism

Previous work suggests oscillations in the alpha-band (6-16 Hz) represent a de-selection process during sensation (see main text references, particularly (Palva and Palva, 2007)). Our results extend this model to cognitive processing: we observe increase alpha-band synchrony in the sub-network of the ‘dominant’ orientation rule during the competing color rule. We test two predictions of this model. First, we show that greater alpha coherence is correlated with a faster reaction time (**Figure 2.6**, see below for details on methods). Second, we show synchrony in the alpha-band during color trials is positively correlated with the strength of color rule representation later in the trial (**Figure 2.S4**). As coherence is a measure of correlation, it is difficult to estimate on a trial-by-trial basis. Therefore, for this analysis we used LFP power at a given frequency as our measure of synchrony. The LFP power on each trial was estimated for each frequency during a 200 ms window before the onset of the stimulus (i.e. during the preparatory period, see **Figure 2.S4A**). The trial-by-trial variability in this power was then correlated with the firing rate of rule-selective neurons on the same electrode. A shuffle-correction was used to remove the effect of correlations over time due to co-varying baselines. This process also determined the z-score of the observed correlation (z-correlation). The average z-correlation was

determined for rule-selective neurons that either preferred the color-rule (greater firing rate during color trials over orientation trials, **Figure 2.S4A**, left) or rule-selective neurons that preferred the orientation-rule (**Figure 2.S4A**, right). As can be seen in **Figure 2.S4B**, left, alpha-power before stimulus onset was more strongly correlated the activity of color-preferring neurons later in the trial, after stimulus onset. This difference was significant (**Figure 2.S4B**, right, p-value determined by unpaired t-test between z-correlation values). Summary correlation statistics presented in the main text were taken from the first 100 ms after stimulus onset. The observed correlation between power and firing rate is consistent with our model: preparatory alpha power during color trials increases the strength of color-rule representations later in the trial, during rule execution.

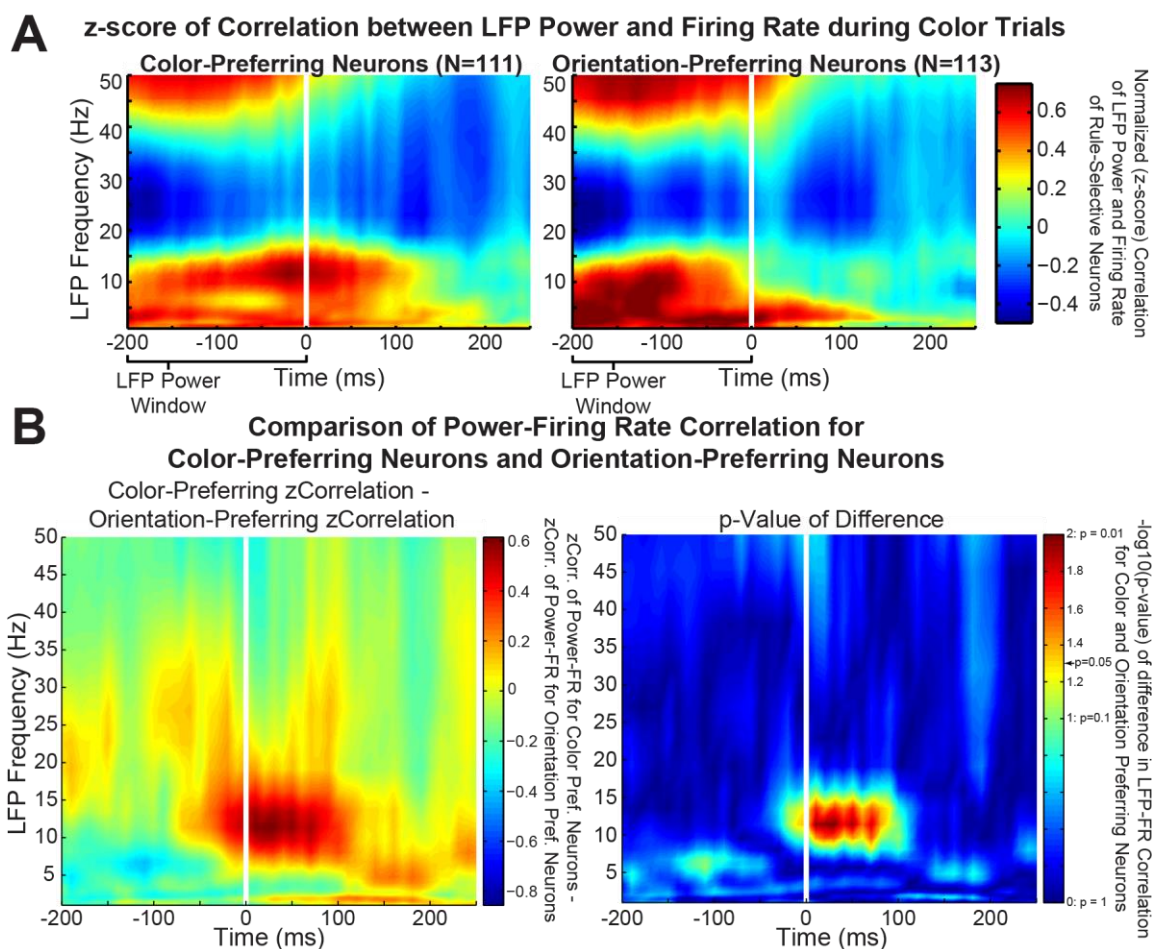


Figure 2.S4, related to Figure 2.6.

(A) Trial by trial LFP power at different frequencies (y-axis) was determined for the 200 ms window preceding stimulus onset (indicated by bracket under the x-axis). The power observed on each trial was correlated with the firing rate of rule-selective neurons in 100 ms windows slid over time (x-axis marks the center of this window). The z-score of the resulting correlation is shown for both color-rule-preferring neurons (left) and orientation-rule-preferring neurons (right). (B) Difference in correlation observed for color-preferring neurons and orientation preferring neurons. Greater pre-stimulus alpha synchrony was significantly more correlated with an increase in firing rate of color-selective neurons later in the trial (after the stimulus appeared and the animal was executing the rule).

2.6.9 Rule-Selective and Stimulus-Selective Neurons Synchronize with Currently

Relevant Rule Sub-network

Synchrony between the spiking activity from individual neurons and the ongoing local field potential were estimated for simultaneously recorded, neighboring electrodes (N = 465 pairs). Spikes were taken from a 200 ms wide peri-stimulus

time period starting 50 ms before the onset of the stimulus. This time-period was selected for when the greatest differentiation of rule-selective sub-networks is observed (**Figure 2.3**). Within this time window spike-field synchronization was estimated using the phase-locking value (PLV) statistic:

$$PLV(f) = \left| \frac{1}{N_S} \sum_{s_t \in S} e^{i\phi(f, s_t)} \right|$$

where $\phi(f, s_t)$ is the phase of the local field potential for frequency f at the time of the spike (s_t), as estimated from the wavelet-based time-frequency decomposition, N_S is the number of spikes, and S is the set of all observed spike times.

The phase-locking value is known to be strongly biased by the number of observations (e.g. a single spike would mistakenly be taken as perfect phase-locking). Therefore we required a minimum of 200 spikes to be observed for inclusion in the dataset. Furthermore, the total number of spike-phase estimates was balanced for all comparisons using a stratification procedure. When comparing across different neuron populations all estimates of PLV were made with the required minimum number of 200 observations. A null-distribution of phase-locking values was estimated by shuffling the trial associations between the neural activity and LFP, disrupting any trial-by-trial co-variation, and recalculating the PLV. This process was repeated 100 times and the mean and standard deviation of the resulting distribution was used to normalize observed phase-locking values.

One hypothesis is that the observed rule-selective sub-networks act to dynamically structure neural activity in order to support the current behavior. To test this hypothesis we determined whether neurons involved in the task were significantly more synchronized to the local-field potentials of electrodes involved in the currently cued rule sub-network (**Figure 2.5**). Both stimulus-selective (**Figure 2.5A**) and rule-selective (**Figure 2.5B**) neurons were significantly synchronized with the color- and orientation-preferring sub-networks in the beta-band. Furthermore, which network these neurons were synchronized to shifted with the current task: during execution of the orientation rule (**Figure 2.5A/B**, left column) both populations of neurons were more synchronized to the orientation-preferring sub-network. This preference was reversed during color trials (**Figure 2.5A/B**, right column).

2.6.10 Sub-network Synchrony Changes with Behavior

Our results suggest the observed rule-selective synchronous sub-networks encode the current rule and organize the activity of single neurons carrying task-relevant information (**Figure 2.5**). If true, then the animal's ability to perform the task should be correlated with the strength of synchrony in the observed sub-networks. In order to determine whether this was the case, we compared the rule-selective coherence in each sub-network for trials when the animal responded quickly or slowly (**Figure 2.6**). This procedure is detailed here. The largest impact on reaction time was the preparation time between rule-cue onset and stimulus onset. Longer preparation times resulted in faster reaction

times and shorter preparation times resulted in slower reaction times. In addition, there were slight differences in the animal's reaction time for the two rules (**Table 2.S1, Figure 2.1B**). However, we were interested in the relationship between the strength of synchrony in the rule-selective sub-networks and the animal's behavioral performance, not the preparatory time or current rule. Therefore, we accounted for the effect of the rule and preparatory time on reaction time by regressing out their effect. Specifically, we fit the linear model $\log(RT_i) = A * (PreparatoryPeriod_i) + B * (Rule_i) + C$ where log of the reaction time was used to stabilize the variance of the skewed reaction time distribution. After fitting this model, the residual difference between the observed reaction time and the fit reaction time captures the intrinsic variability in the animal's performance. These residuals were sorted into 'fast' and 'slow' trials (defined as the 65th-95th and 5th-35th percentile of the residual distribution for each session, respectively) and the rule-selective coherence was determined, as before (see above). As noted in the main text, synchrony in both the preparatory 'alpha' band and the rule-execution 'beta' bands was significantly greater when the animal performed the task quicker (**Figure 2.6**). Strength of rule selectivity was determined by taking the absolute value of the average zCoh within the alpha and beta regions of interest. A Wilcoxon signed rank test compared the zCoh values for fast and slow reaction times at each time point during the trial. We required at least 2 consecutive time points for the rule selectivity to be considered significant. As the black (significant beta differences) and grey lines (significant alpha

differences) on **Figure 2.6** indicate, faster reaction times were accompanied by stronger selectivity in both the alpha and beta bands ($p < 0.05$, Bonferonni corrected for multiple comparisons) before the onset of the test stimulus. These results support the hypothesis that the observed synchronous sub-networks are involved in representing and implementing the current rule.

CHAPTER III: THE ROLE OF ACC IN TASK SWITCHING

3.1 Summary

Adjusting attention to changing task demands is a key component of intelligent behavior. The dlPFC and ACC are prefrontal subdivisions implicated in the adjustment and directing of attention, but it remains unclear whether they are more important for certain types of task demands. To investigate this, we trained two monkeys on a cued task switching paradigm, which allows us to investigate several types of task demand such as attentional context switching, errors, and response conflict. We found that ACC neurons responded to the past history of errors, but not the switching of context or response conflict. dlPFC neurons responded to the switching of attention and the first trial after the error, but not the history of errors. We also found that ACC neurons can respond to the task attentional context, even in a visually cued task. Our results show that the ACC is not always responsible for identifying and switching the context -- different prefrontal subdivisions are important for switching between different types of internal / external signals (i.e. errors versus visual cues) and argue against the role of ACC as a task conflict detector.

3.2 Introduction

Complex behavior involves recognizing and adjusting for situations that demand more attention. This entails a careful balancing between maintaining goals in the face of distractions, switching between task contexts, and relinquishing control when behaviors are sufficiently automatic in order to minimize cognitive load.

The prefrontal cortex is necessary for supporting context-dependent behavior — prefrontal lesions result in perseverative, context-inappropriate behavior (Stuss and Benson, 1984) and neurons in prefrontal cortex are selective to context and behavioral responses (Wallis et al., 2001) — but how prefrontal subdivisions utilize context-related information with changing cognitive task demands is still not understood.

Recent models suggest that two subdivisions of the prefrontal cortex, the dorsal anterior cingulate cortex (ACC) and dorsolateral prefrontal cortex (dlPFC) play functionally distinct, complementary roles in enabling the mapping of context to behavior. The dlPFC is responsible for maintaining and biasing attention to context-relevant sensorimotor information and the ACC is responsible for selecting the relevant context and signaling the amount of attention needed to perform the task (Shenhav et al., 2013). These models predict that in situations where more attention is needed — such as when the expected value of meeting task demands increases (Shenhav et al., 2013), when there are multiple tasks or responses to choose from (Botvinick et al., 2004), or when unexpected outcomes occur (Alexander and Brown, 2011)— ACC and dlPFC act together to strengthen the contextual link between relevant sensory information and the appropriate response.

However, the role of ACC is still controversial. While it is well established that ACC neurons respond to multiple aspects of errors and reward (Kennerley et al., 2011, 2009; Niki and Watanabe, 1979; Shima and Tanji, 1998) — including

responding to errors several trials in the past (Johnston et al., 2007; Kennerley et al., 2011; Michelet et al., 2009; Seo and Lee, 2007; Shen et al., 2014) — and behavioral responses (Hayden and Platt, 2010; Luk and Wallis, 2013; Shima and Tanji, 1998), it is not clear that the ACC is important for (1) selecting the relevant task (as Shenhav and colleagues suggest) and (2) selecting the amount of attention needed in all cognitively demanding situations.

For example, a typical situation in which cognitive demand is thought to increase is when there are multiple potential competing responses, creating response conflict. However, numerous electrophysiologic studies of the macaque ACC have failed to find evidence of increased single neuron activity related to response conflict (Ebitz and Platt, 2015; Ito et al., 2003; Nakamura et al., 2005). Another situation in which cognitive demand is thought to increase is around the time of a context switch — this being an especially important event if ACC selects the relevant task. However, Rushworth et al. (2003) found that lesioning the ACC did not impair switching between task contexts, but did impair the ability to correct behavior after errors have been made. One important neurophysiological study in the macaque, Johnston et al. (2007), found task-selective ACC neurons that increased their selectivity both when the task changed and after errors on the preceding trial, but their experimental design limited their ability to distinguish between effects of errors on previous trials, response conflicts, and task switches. In particular, their experiment involved un-cued, error-driven switches between two tasks: pro-saccade and anti-saccade. Because the ACC is sensitive to errors in

previous trials, their finding of increased task selectivity after task switches could have been driven by an interaction between errors in previous trials, by anticipated response conflict between the saccade and anti-saccade, and/or by switching between the tasks. If ACC is important for selecting the relevant task and adjusting amount of attention needed to perform that task, then we would expect to see a task selectivity increase after a task switch even after controlling for errors in previous trials and response conflict.

Therefore, we sought to separate out the contributions of task switching, response conflict and errors by training two monkeys on a cued task switching paradigm. The cued task switching paradigm is ideal for probing cognitive demand because it can experimentally disassociate these cognitively demanding factors and we can explicitly model the effect of multiple task factors. Controlling for multiple task factors is particularly important for prefrontal neurons, because they often “multiplex” — they can be sensitive to combinations of task factors (Fusi et al., 2016; Rigotti et al., 2013). Surprisingly, our analyses reveal that while ACC neurons selectively respond to task context, the effect of changing between tasks does not increase task selectivity in a preparatory fashion. Instead, we find that with a visually cued task switch, the activity of ACC is more consistent with tracking the relevant rule and the past history of reward and errors.

3.3 Results

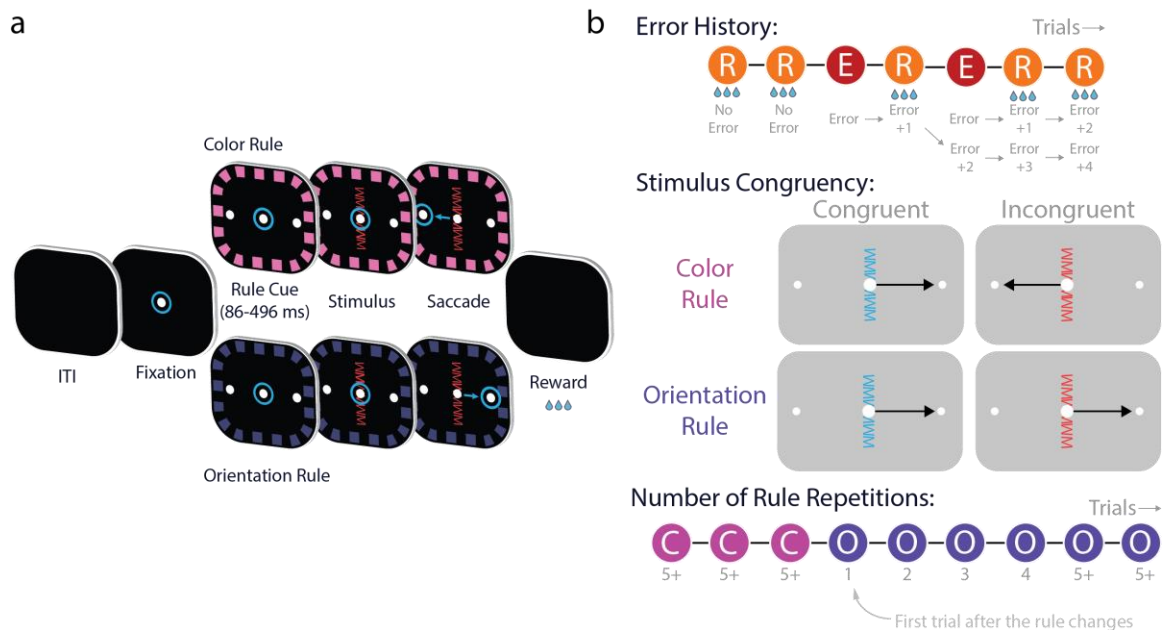


Figure 3.1 Task description and factors that can change cognitive demand

(a) Sequence of trial events. After a 100 ms intertrial interval (ITI), each trial begins with the presentation of a fixation spot. After fixation is acquired, one of two rules is cued, signaling the task context with a purple or pink border. A test stimulus is then presented after a variable delay. The combination of the test stimulus and rule stimulus informs the subject about the appropriate saccade direction. A juice reward is given after the correct saccade. (b) Factors that could affect cognitive demand. Error History encodes the impact of recent errors on current performance – making more errors should require more control. The Stimulus Congruency encodes whether attention to the rule is necessary to make the correct response. Incongruent trials require knowledge of the rule and are presumably harder and more demanding. Finally, the Number of Rule Repetitions encodes the number of trials since the rule has changed. The first rule repetition is of particular interest, because the initial switching of the rules typically causes increases in reaction time and deficits in accuracy and involves reconfiguration of the task context.

3.3.1 Cognitively demanding factors affect task performance

Two monkeys performed the cued task switching paradigm (**Figure 3.1a**, see Methods and Buschman et al. (2012) for more detail) at a high level – Monkey CC performed 85% trials correctly and Monkey ISA performed 88% trials correctly (**Figure 3.2a**). Although there was some variability in performance over sessions, none of these sessions were performed at chance (**Figure 3.2a**).

Cognitive demand is associated with task difficulty – in general, harder tasks are considered to require more executive control. To quantify the effect of cognitive demand factors on task performance, we fit a binomial generalized linear model to the correct / incorrect responses. We considered three different sources of demand (**Figure 3.1b**): Error History, Stimulus Congruency, and the Number of Rule Repetitions.

Our behavioral model revealed that all three cognitively demanding factors under consideration impacted task performance. Both monkeys were more likely to make errors on the first trial after the rule changed (**Figure 3.2c**, Number of Rule Repetition, Rep. 1, Monkey CC: 42% reduction in odds of correct response, $p=3.3 \times 10^{-7}$, Monkey ISA: 16% reduction, $p=0.01$, compared to greater than five rule repetitions), even as performance remained above chance levels (monkey CC : median 77% correct trials for on the first repetition, interquartile range [74%, 84%], monkey ISA: median 90% correct, interquartile range [77%, 94%], only one session with monkey CC at chance). Subsequent trials after the rule changed (Rule Repetitions 2-4) had a smaller effect on the odds of a correct response and were not significantly different from rule repetitions greater than 5. Stimulus congruency also significantly affected the monkeys' ability to perform the trials correctly. Trials with incongruent stimuli, where there was more than one possible response, were harder to perform correctly than congruent trials (**Figure 3.2d**, Monkey CC: 29% reduction in odds of correct response compared to congruent trials, $p=5.5 \times 10^{-12}$, Monkey ISA: 8% reduction, $p=5.8 \times 10^{-4}$).

Finally, making an error led to a greater chance of making an error on the next trial, but had minimal effect on two to four trials after the initial error (**Figure 3.2b**, Error History, Error+1 trial compared to No Error+1 trial, Monkey CC: 52% reduction in odds of correct response, $p=1.85 \times 10^{-22}$, Monkey ISA: 24% reduction in odds of a correct response, $p=1.23 \times 10^{-9}$). Although this effect was strong, like Rule Repetition, making an error on the previous trial did not result in chance behavior (monkey CC : median 74% correct trials for on the first trial after an error, interquartile range [73%, 75%], monkey ISA: median 86% correct, interquartile range [81%, 89%])

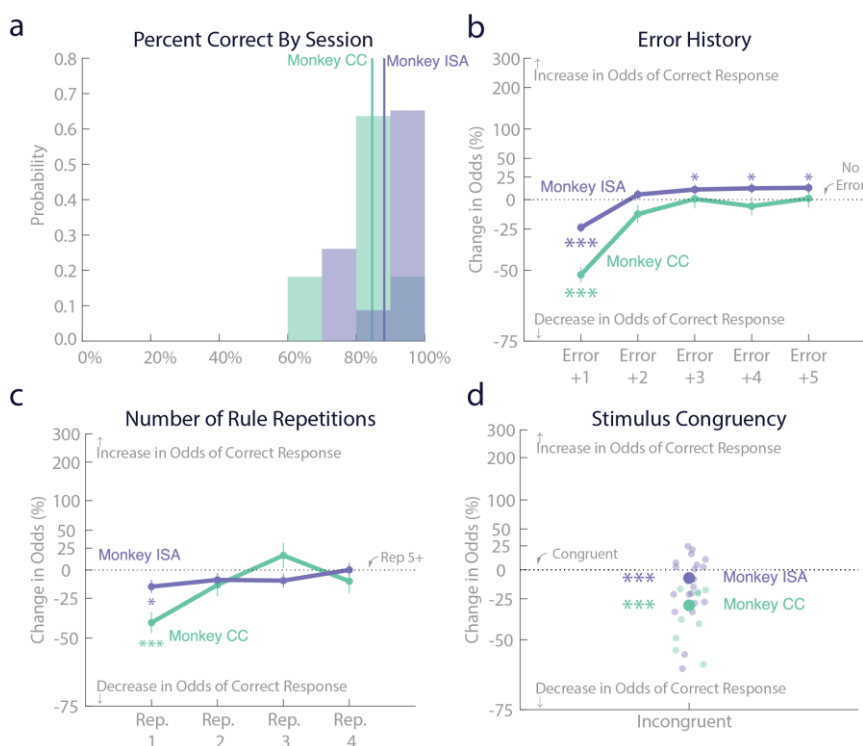


Figure 3.2. Effect of cognitive demand factors on behavior.

(a) Average performance of the monkeys over sessions. Both monkeys, ISA (green) and CC (purple), averaged over 80% correct (green and purple lines) over all sessions and only a few sessions were performed below 70% correct. (b) Model estimated change in performance after making an error in the past five trials. Both monkeys performed better after making an error (although not better than if there was no error in the previous trial) and returned to baseline

performance one to two trials after the error. (c) The trial immediately after the rule changed (Rep.1) was more likely to result in an error and performance returned to baseline (five or more repetitions, Rep 5+) by the second repetition of the rule. (d) Incongruent stimuli were more likely to result in an error for both monkeys (big dots), but the session-to-session variability of monkey ISA (smaller, faded purple dots) indicated that incongruency didn't always result in more errors. All uncertainty intervals are standard error of the mean.

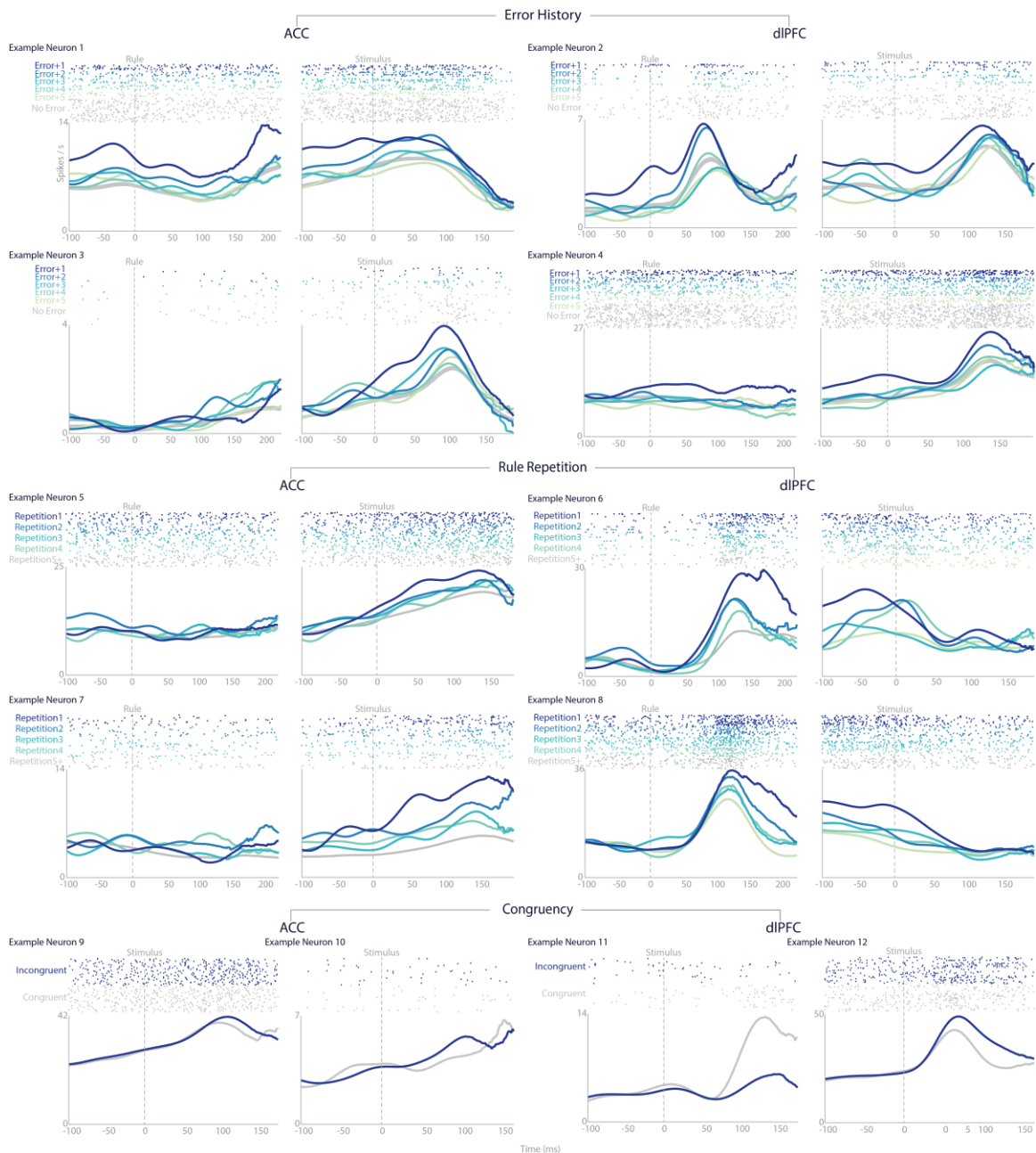


Figure 3.3 Examples of single neurons responding to cognitive demand in ACC (left two columns) and dlPFC (right two columns).

Each neuron is displayed relative to the onset of the rule cue (columns 1, 3) and test stimulus cue (columns 2, 4), except for congruency (bottom row), which is only a property of the test stimulus and therefore only displayed relative to the test stimulus. Each column displays a random sample of the spike raster corresponding to the cognitive demand factor of interest, with the condition corresponding to the highest cognitive demand at the top and the lowest at the bottom. A corresponding peri-event time histogram for each cognitive demand position is displayed directly below the spike raster.

3.3.2 Single neurons respond to cognitive demand

Neurons in ACC and dlPFC showed varied responses during the cue epoch (from the onset of the rule cue to the initiation of the saccade, which includes the test stimulus cue onset, see **Figure 1**) — with dlPFC neurons generally showing more sensory responses to the cues and ACC neurons more ramping and tonic responses. **Figure 3.3** shows typical firing patterns for single neurons in ACC and dlPFC in response to our three cognitive demand factors of interest.

First, regardless of the activity pattern, we observed neurons in both areas that increased their firing rate in response to errors in the preceding trials for up to three or four trials, gradually returning to the firing rate in which no previous error was committed (see **Figure 3.3**, Example Neurons 1-4). Second, we also observed neurons in both areas that exhibited increased firing in response to the switching of the rule — particularly on the first repetition of the rule after the rule had changed (see **Figure 3.3**, Example Neurons 5-8, Repetition1). Much like the response to the error, some of these neurons maintained an increased firing rate for the second and third repetitions (Repetition2 and Repetition3) of the rule before returning to a steady state (Repetition5+). Finally, we found test stimulus congruency had small effects on ACC neurons and inconsistent effects on dlPFC neurons (**Figure 3.3**, Example Neurons 9-12). For example, ACC example

neuron 9 in **Figure 3.3** does show a congruency related response. The neuron increases its firing rate roughly 50 ms after the onset of the test stimulus, its change in firing consistent with a prefrontal neuron selective for a visual stimulus, and its firing rate is higher for the incongruent condition. However, the increase in firing rate is small. For dlPFC, we observed larger changes in firing rates, but some of the neurons were more selective for the congruent condition (**Figure 3.3**, Example Neuron 11) than the incongruent condition, suggesting that the dlPFC neurons are more sensitive to visual features of the test stimulus rather than the increased cognitive demand created by having to pay attention to both the rule and the test stimulus to make the correct response.

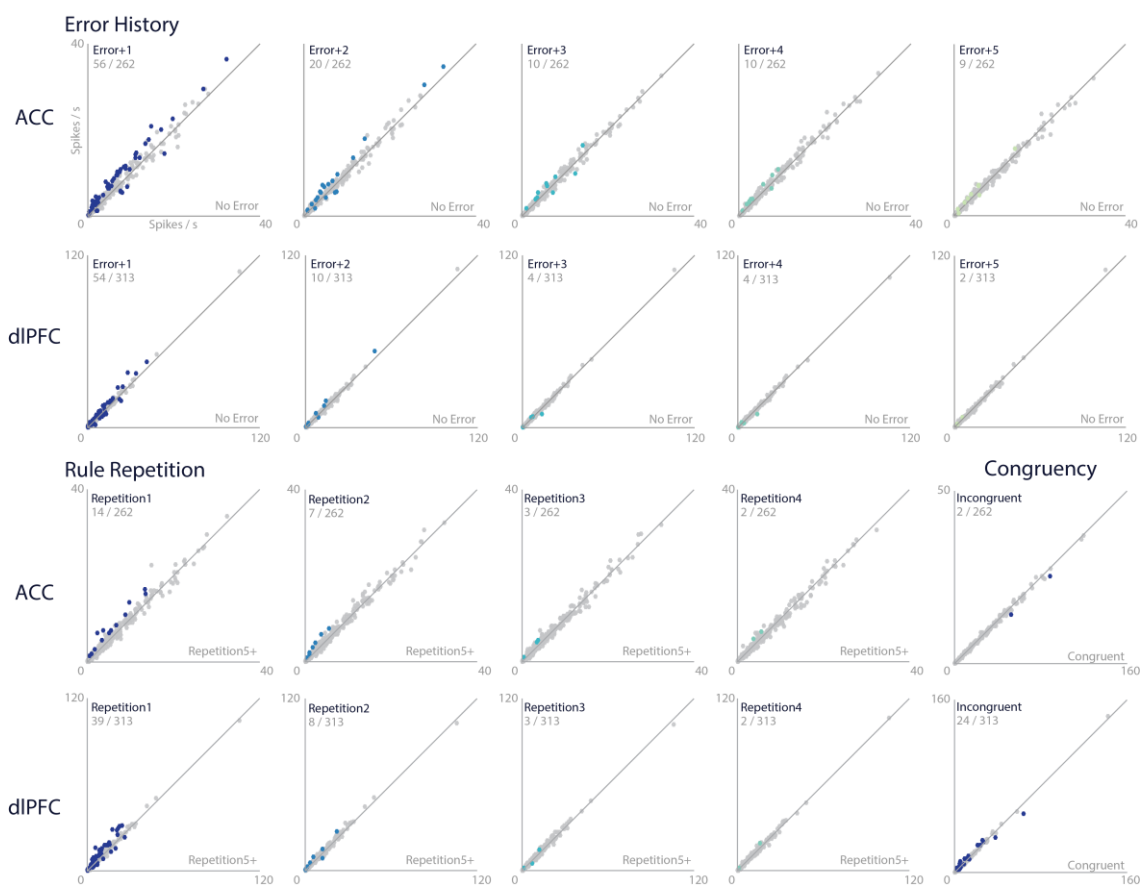


Figure 3.4 Average firing rate for each dlPFC and ACC neuron comparing high and low cognitive demand for the entire cue epoch (after the rule is cued and before the saccade is initiated) except for Congruency, which only considers the within-trial time epoch after the test stimulus appeared.

For each cognitive demand factor, the ordinate displays the firing rate for the higher cognitive demand condition (Error+1, Error+2, etc.) compared to the firing rate of the lowest cognitive demand condition (No Error, etc.) on the abscissa in spikes per second. Neurons that showed significant changes in firing rate using a permutation test are highlighted in non-grey colors (corrected for multiple comparisons using false discovery rate of $q=0.5$, see Methods for details) and the total number of significant neurons is noted below the condition name (below Error+1 for example). Both ACC and dlPFC populations had neurons that significantly changed in the highest demand condition for Error History and Rule Repetition (Error+1, Repetition1), but the ACC showed more significant changes in the Error+2 condition and the dlPFC showed more significant changes in the Repetition1 condition. Most ACC neurons did not significantly change firing rate for incongruent versus congruent conditions.

3.3.3 ACC and dlPFC populations respond to cognitive demand

To more quantitatively characterize the neural responses of ACC and dlPFC neurons in response to different sources of cognitive demand (Error

History, Rule Repetition, Congruency), we first used univariate permutation tests (corrected for multiple comparisons with false discovery rate, $q = 0.5$) to test for differences in firing rate between a high cognitive demand situation (such as the first few trials after the rule has changed or after an error has been made) versus a lower cognitive demand situation (such as when no error has been made in the previous trial or rule has not changed for more than five trials) during the cue epoch (onset of the rule cue to initiation of saccade). **Figure 3.4** shows the firing rate in the high cognitive demand situation (ordinate) compared to the low demand situation (abscissa) with the significant changes highlighted in color.

Many ACC neurons showed evidence of responding to errors in past trials, particularly one and two trials after an error (**Figure 3.4**, Error History, ACC). 21% (56 / 262) of ACC neurons significantly changed their firing rate on the first trial after an error compared to when there was no error in the past trials and 8% (20 / 262) of ACC neurons significantly changed their firing rate two trials after an error. There was little support for firing rate changes due to errors made more than three trials in the past (Error+3: 4% or 10 / 262 ACC neurons; Error+4: 4% or 10 / 262 neurons; Error+5: 3% or 9 / 262 neurons).

dlPFC neurons also showed evidence of responding to errors in past trials, particularly on the first trial after the error (**Figure 3.4**, Error History, dlPFC). 17% (54 / 313) of dlPFC neurons significantly changed their firing rate on the first trial after an error compared to not making an error in the previous trial. There was little evidence that errors made more than one trial in the past affected the

firing rate of dlPFC neurons (Error+2: 3% or 10 / 313 dlPFC neurons; Error+3: 1% or 4 / 313 neurons; Error+4: 1% or 4 / 313 neurons; Error+5: 1% or 2 / 313 neurons). Overall, our data suggests the firing rate of both ACC and dlPFC neurons can be modulated by errors in past trials.

We next examined if the change of rules could affect the firing rate of prefrontal neurons. There was little evidence of ACC neurons changing their firing rate in response to the rule change (**Figure 3.4**, Rule Repetition, ACC). Only 5% (14 / 262) of ACC neurons were compatible with the hypothesis of a difference in firing rate on the first trial after the rule change (Repetition1) compared to the firing rates of five or more trials after the rule change (Repetition 5+). ACC neuronal firing rates for subsequent trials after the rule change (Repetitions 2-4) compared to the firing rates of five or more trials after the rule change (Repetition 5+) were also incompatible with the hypothesis of a change in firing rate for those trials (Repetition2: 3% or 7 / 262 ACC neurons with significant changes; Repetition3: 1% or 3 / 262 neurons; Repetition4: 1% or 2 / 262).

Some dlPFC neurons showed evidence of responding to the change in rules. 12% (39 / 313) of dlPFC neurons significantly changed their firing rate on the first trial after the rule changed (compared to five or more trials after the rule change). Subsequent trials after the rule change did not significantly modulate firing rates of dlPFC neurons compared to five trials or more trials after the rule change (Repetition2: 3% or 8 / 313 dlPFC neurons significantly changed;

Repetition3: 1% or 3 / 313 neurons; Repetition4: 1% or 2 / 313 neurons). So, our data shows that dlPFC neurons can change their firing rate in response to a rule change, but provides no support for a similar change in ACC neurons.

Finally, there was little evidence of stimulus congruency affecting the firing rate of ACC neurons. Only 1% of ACC neurons were compatible with the hypothesis of a difference in firing rate between incongruent conditions and congruent conditions. dlPFC neurons also showed little evidence of firing rate changes due to stimulus congruency (8% or 24 / 313 of dlPFC neurons significantly changed due to stimulus congruency).

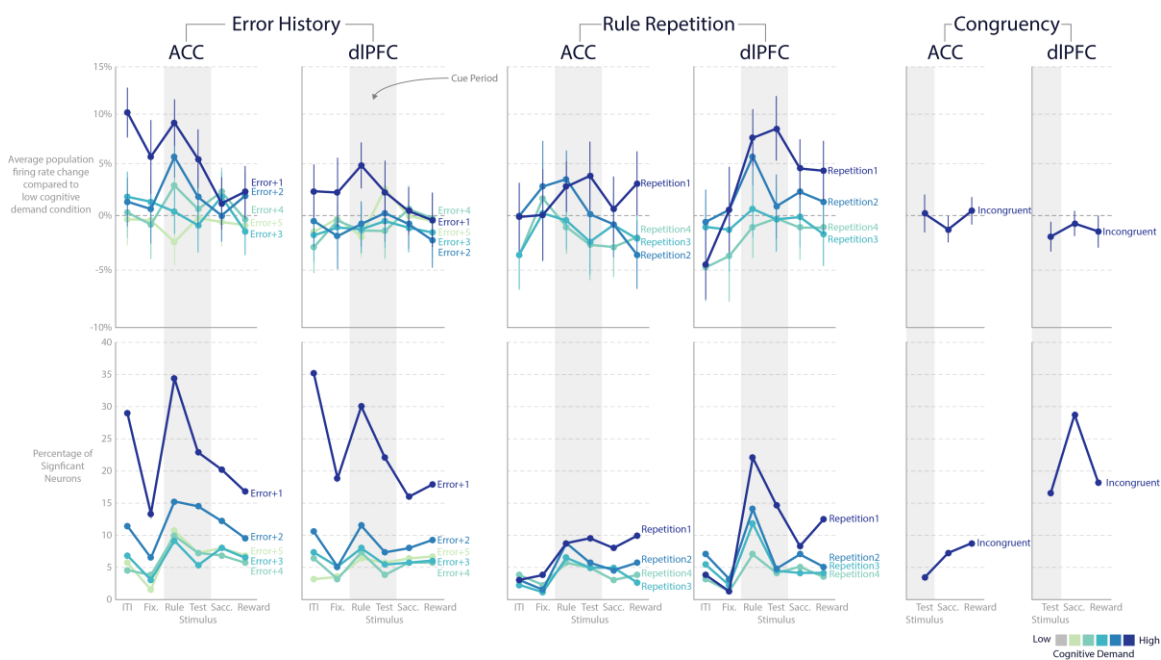


Figure 3.5 Neuronal model estimated changes in firing rate over the trial for each cognitive demand factor.

The top row ordinate displays the average normalized population percentage change in firing rate relative to the low demand condition (e.g. Error+1 versus No Error or Repetition1 versus Repetition5+). All confidence intervals are 95% confidence intervals. The bottom row ordinate shows the percentage of significant neurons for those conditions, corrected for multiple comparisons using a false discovery rate, $q=0.5$. The abscissa corresponds to the events in the trial as defined by Figure 3.1: ITI – intertrial interval, Fix. – fixation dot onset to rule cue onset, Rule – rule cue onset to test stimulus onset, Test Stimulus – test stimulus onset to saccade initiation, Sacc. – saccade initiation to reward, and Reward – reward to end of trial. The ACC has

stronger firing rate changes on average to Error+1 and Error+2. Those error-related changes come primarily in the rule epoch. dlPFC neurons show stronger firing rate changes on the first trial after the rule changes (Repetition1) and there are more neurons that are selectively significant for the Repetition1 condition. Congruency for both areas is not strongly biased toward increased or decreased firing rates and more neurons are significantly selective for incongruency in dlPFC compared to ACC.

3.3.4 Within trial dynamics of cognitive demand selectivity

Next, we were interested in characterizing the relative contributions of the different cognitive demand factors to changes in firing rate over the course of the trial. We were particularly interested in the portion of the trial after the rule was cued, but before the test stimulus was presented. This “preparatory epoch” (which we denote by Rule in **Figure 3.5**) is important because it represents the time epoch in which the animal can proactively adjust the amount of attention needed in the current trial in response to increased cognitive demand (Alexander and Brown, 2010; Rogers and Monsell, 1995; Ruge et al., 2013). We fit multivariate generalized linear models to each time epoch in the trial (as defined in Figure 3.1a) that accounted for the contributions of the cognitive demand factors of interest (see Methods for a full description of the model). This analysis yielded important differences between ACC and dlPFC neuronal populations.

On the first trial after an error, the average firing rate of the population of ACC neurons increased (relative to no error on the previous trial) from the intertrial interval to the initiation of the saccade, with the highest firing rate increases sustained in the intertrial and rule cue intervals (**Figure 3.5**, Error History, ACC, Error+1, average change in ACC neurons firing rate, intertrial interval: 10% [8%, 13%]; rule cue epoch: 9% [7%, 11%]). This increase was not due to large firing rate differences from only a few neurons. More ACC neurons

increased their firing rate than decreased their firing rate during the cue epoch (**Figure 3.6**, Error+1, ACC). Although the time between trials was brief, this firing rate increase did not seem to be solely a response to the omission of reward, but rather it seemed to serve a more functional role. Supporting this, two trials after the error (**Figure 3.5**, Error+2, rule cue epoch, ACC firing rate change: 6% [4%, 8%]), the average firing rate of the ACC neurons also showed an increase in firing rate during the preparatory epoch, but not during the intertrial interval, fixation, or when the test stimulus was shown. Similar to the first trial after the error, there were more neurons that increased their firing rate in response to an error two trials in the past than decreased (**Figure 3.6**, Error+2, ACC).

In contrast, the population of dlPFC neurons only showed a significant increase in firing rate during the rule epoch (the preparatory epoch) on the first trial after an error (**Figure 3.5**, Error History, dlPFC, Error+1, average change in dlPFC neurons firing rate: 5% [3%, 7%]) and not on the subsequent trials after the error (**Figure 3.5**, Error+2, Error+3, Error+4, and Error+5). The average increase in firing by the dlPFC neurons on errors one or two trials in the past was smaller than the ACC neurons (**Figure 3.5**, average difference between ACC and dlPFC, Error+1: 4% [1%, 7%], $p < 0.05$; Error+2: 6% [4%, 9%], $p < 0.05$).

A different pattern emerged when considering the effect of changing the rule. On the first trial after the rule changed, dlPFC neurons on average increased their firing rate by 8% [5%, 11%] when the rule was cued and 9% [5%, 12%] after

the test stimulus was cued (**Figure 3.5**, Repetition1). This was also not due to a few extreme neurons in the population. More dlPFC neurons increased their firing rate in response to the rule change than decreased (**Figure 3.6**, Repetition1, dlPFC). On the next trial (**Figure 3.5**, Repetition2), much like ACC on the second trial after an error, the dlPFC population firing rate only significantly changed when the rule was cued (rule cue epoch, 6% [3%, 9%]), but not in any other time epoch during the trial.

ACC neurons followed a similar pattern of change on the first and second rule repetition (**Figure 3.5**, Repetition1: rule cue epoch, ACC average change in firing rate 3% [0%, 6%], test stimulus epoch, 4% [1%, 7%], Repetition2, rule cue epoch: 3% [0%, 6%]), but these changes were smaller than dlPFC in the rule cue and test stimulus epochs of the first rule repetition trial (Repetition1, average difference between ACC and dlPFC, rule cue epoch: -5% [-8%, 1%], $p < 0.05$, test stimulus epoch: 4%, [-8, 0%], $p < 0.05$), but not the subsequent repetitions (all $p > 0.05$).

Finally, ACC neurons show little difference in firing rate between congruent and incongruent stimuli and any change in neural activity tends to be stronger for the congruent, not the incongruent condition (**Figure 3.5**, ACC incongruent). dlPFC neurons did show changes in firing rate for incongruent versus congruent stimuli, but these changes were not preferentially biased toward congruent or incongruent stimuli (**Figure 3.5**, dlPFC incongruent and **Figure 3.6**, dlPFC congruency), indicating that they were more likely related to the

visual features of the test stimulus, rather than reflecting increased cognitive demand.

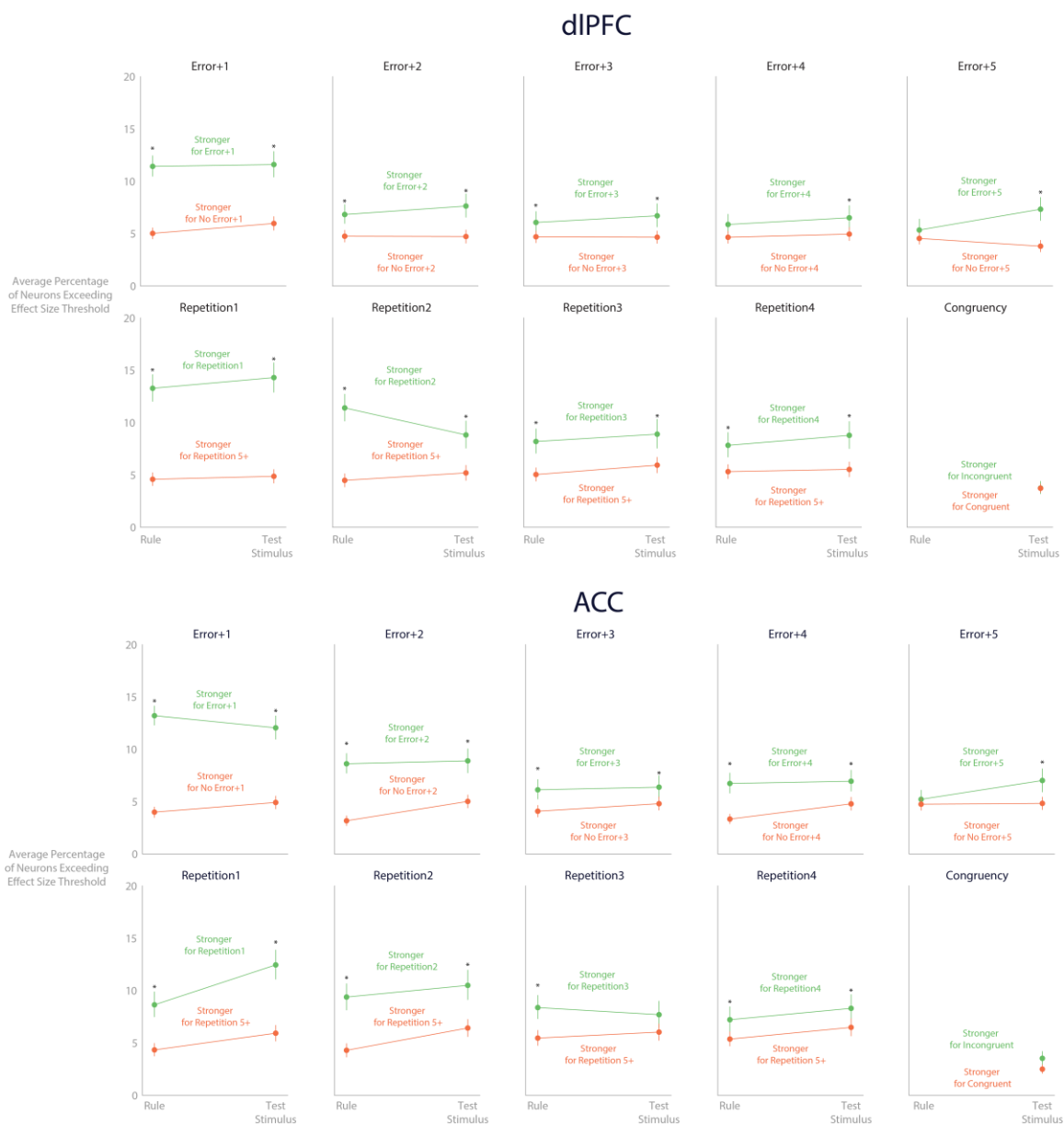


Figure 3.6. The majority of neurons increased their firing rate in response to recent errors and the change of the rule during the cue epoch.

Green lines represent the average percentage of neurons that increased their firing rate during the rule cue epoch or test stimulus epoch in response to a cognitively demanding factor. Orange lines represent the average percentage of neurons that decreased their firing rate in response to a cognitively demanding factor. The average percentage was calculated by computing the

percentage of neurons that exceeded an effect size threshold (e.g the percentage of neurons that increased by 1% for a cognitively demanding situation or the percentage of neurons that decreased by 1% for a cognitively demanding situation) over a range of thresholds (1-150% for increases and decreases). The integral over the range of effect size thresholds divided by the total range yielded the average percentage of neurons that increased or decreased. Uncertainty about this estimate was captured by repeating this procedure over 10000 estimates generated from the fitted models of each neuron (parametric bootstrap).

3.3.5 Does the ACC care about the number of trials from error (error distance)

or the recent history of errors?

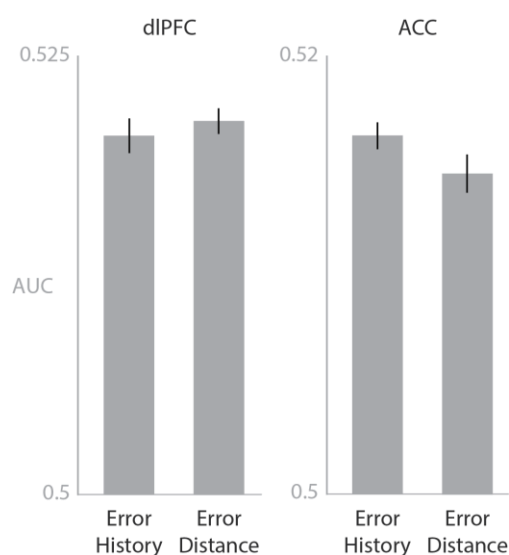


Figure 3.7 Taking into account the past history of errors (Error History) rather than the number of trials from the error (Error Distance) improves spike prediction accuracy in ACC, but not dIPFC.

Spike prediction accuracy is measured in terms of area under the curve (AUC) and averaged over all neurons in the population of interest (dIPFC, left column, ACC, right column). Confidence intervals are 95% confidence intervals derived from the five fold cross-validation used to evaluate spike prediction accuracy.

We next investigated whether the effect of the recent error history was a function of the number of errors made in the past five trials (Error History) – that is, whether the monkey making consecutive errors influenced the firing rate – or was more simply a function of the number of trials from the error (Error Distance).

To determine which was the better model, we compared the spike prediction accuracy of the two different models (Error History vs. Error Distance) using the area under the curve metric (AUC, see Methods for further details on the metric and specific models used). For dlPFC neurons, the average spike prediction accuracy for the population was similar between the Error History and the Error Distance (**Figure 3.7**, dlPFC) and the model including Error Distance predicted better for 47% of the neurons compared to 45% for Error History (Models that predicted spikes worse than chance at 0.5 were considered to have no effect and excluded). In contrast, Error History was the better predictor on average for ACC neurons (**Figure 3.7**, ACC) and predicted better for 47% of the ACC neurons (compared to 41% for Error Distance). While admittedly, this is hardly decisive for deciding between Error History and Error Distance, it is worth noting that even in a well-trained task, many ACC neurons were better fit by a model that takes into account the number of errors in the recent trials.



Figure 3.8 Representative neurons showing rule-related activity in ACC (left two columns) and dlPFC (right two columns) relative to the rule cue onset and test stimulus onset.

Figure conventions are the same as Figure 3.3. There are two cues for each rule, represented in different shades of the same color for the same rule. The color rule cues are in pink and the orientation rule cues are in purple. dlPFC neurons typically show individual cue related activity compared to ACC neurons.

3.3.6 Can the current context affect ACC neurons?

We next investigated the role of task rule in dlPFC and ACC. While it has been established that dlPFC neurons can respond selectively to task rules, even if those rules are cued by different modalities (Wallis et al., 2001), only one previous study has investigated the effect of rule on ACC neurons and importantly, that rule cue was signaled by error (Johnston et al., 2007). Given that task information can be signaled by sensory modalities and rule selectivity is crucial to many current theories of ACC function (Alexander and Brown, 2011; Shenhav et al., 2013), we wanted to know if ACC would respond to a visually cued rule. In our task, each

rule was signaled by two different visual cues, allowing us to differentiate rule selectivity from differences caused by visual features of the rule stimulus.

Figure 3.8 shows six representative neurons that responded differentially to rule in ACC (left column) and dlPFC (right column). Each of these neurons have roughly similar responses to both rule cues, although there are some differences between the individual cues for each rule, particularly in dlPFC, presumably due to different visual features of the rule cue such as in example neuron 2 and 8. Firing rate differences between the rules for both ACC and dlPFC were also comparable (**Figure 3.9**, top) and the number of neurons selective for the rule cue increased during the cue interval of the trial (**Figure 3.9**, bottom), indicating that they were relevant for the task. Furthermore, including rule in the generalized linear model substantially improved the prediction of spikes for each area (**Figure 3.10**). Indeed, a model with the rule factor by itself on average predicted better than the cognitive demand factors by themselves (**Figure 3.10b,e**), models including the rule and one or both of the cognitive demand factors predicted better than one or both of the cognitive demand factors (**Figure 3.10b,e**), and the best predicting model for each neuron included the rule factor more than the other factors (**Figure 3.10c,f**). Moreover, the best predicting models for each neuron included the rule and at least one other cognitive demand factor for 55% of ACC neurons and 61% of dlPFC neurons, suggesting that most ACC and dlPFC neurons were well modeled by consideration of the rule and a change in cognitive demand.

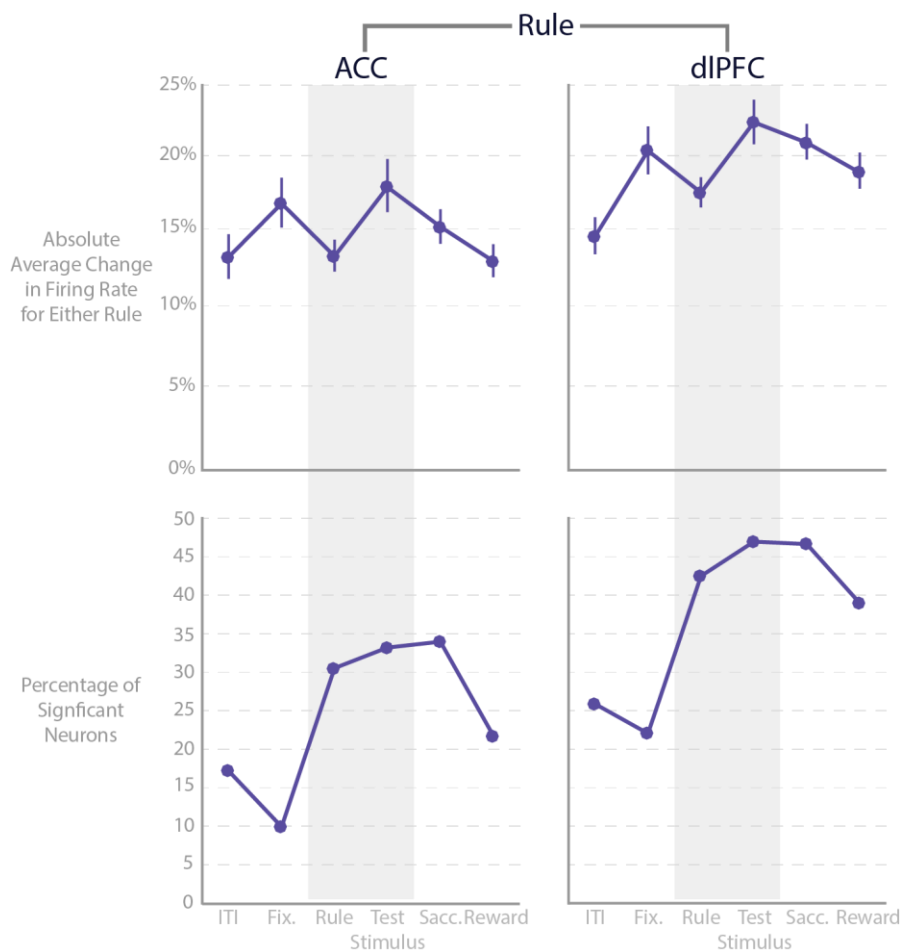


Figure 3.9 Average rule-related differences and percentage of significantly changing neurons for the rule.

Figure conventions are the same as Figure 3.5, except that in the topmost row percentage change in firing rate is the absolute change in firing rate for either rule. This is to capture the rule-related change regardless if the neuron fired more for the orientation or color rule.

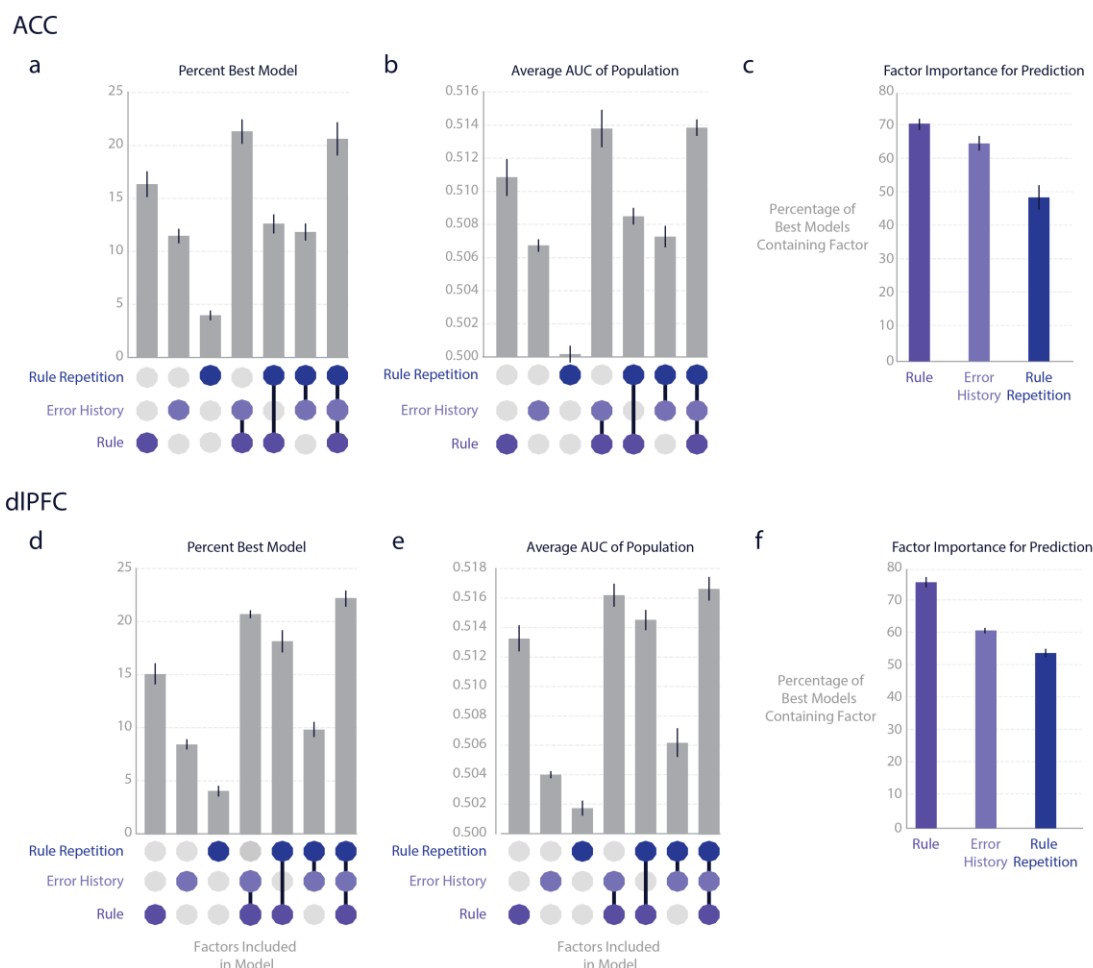


Figure 3.10 Comparison of spike prediction accuracy for a set of models for ACC (top row) and dlPFC (bottom row) during the rule cue epoch.

We consider whether neurons are better predicted by models containing individual factors (rule, rule repetition, error history) or by a combination of the factors. UpSet diagrams, which are an extension of Venn Diagrams, display the combination of the factors included in the model in a, b, d, and e. (a,d) Percentage of neurons for which that model was the best predicting model. (b,e) Average AUC for that model over all neurons. (c,f) The percentage of best predicting models (in a and d) that contained that individual factor.

3.4 Discussion

We report three main results. First, in a visually cued task switch, dlPFC neurons respond more strongly than ACC neurons in response to changing the contextual rule. Second, ACC activity is more responsive to and is better predicted by errors in recent trials than dlPFC. Third, ACC neurons can respond to rules even when

the rule is signaled by a visual cue (and not by an error) and furthermore, their activity is better predicted by a combination of recent error history and rule.

A recent model by Shenhav et al. (2013) proposed that ACC identifies the appropriate control signal (in our experiment, the contextual rule) and predicts changes in that signal (i.e. a task switch). Supporting this, Johnston et al. (2007) found that in a uncued error-driven task switch, rule-selective ACC neurons discriminated between the rule conditions more strongly and earlier than rule-selective dlPFC neurons around the time of the switch – a pattern which reversed (dlPFC neurons more strongly and led ACC) after the same task was repeated approximately 10 or more times. Our results are more similar to the pattern Johnston et al. (2007) observed after 10 or more repetitions of the same rule. This highlights an important subtlety not captured by the model of Shenhav et al.; namely, that in a visually cued task switch, dlPFC is more important for identifying and predicting the task to be performed than ACC. Different prefrontal subdivisions may be important for different types of switching. It is also possible that the ACC is not important for switching between tasks at all. For example, Kennerley et al. (2006) found that lesioning the ACC in a motor-reward reversal task did not impair their subjects ability to switch between motor-reward associations.

Our results may also be further evidence of an important functional distinction between the prefrontal subdivisions. Rushworth and colleagues (2006; 2011) proposed that prefrontal subdivisions learn different types of

associations: dlPFC is more important for stimulus-response associations and anterior cingulate for response-outcome associations. Our results are partially consistent with this proposal because ACC, in our study and in the Johnston et al. (2007) study, was responsive to the recent pattern of errors and ACC seems to play a more important role in switching between the tasks when the task switch is signaled by an error. However, Rushworth's distinction does not account for the role of context. We have shown that context signals, whether signaled by error or visual cue, can have a meaningful impact on the firing rate of ACC neurons.

Our results are inconsistent with another recent study by Ebitz and Platt (2015), that suggested ACC was important for signaling goal-related task conflict. Ebitz and Platt found that task-relevant visual distractors induced higher firing rates in ACC neurons than task-irrelevant distractors or the absence of distractors. They suggested that this conflict was of the same sort that would be observed in a task switch, in which goal-irrelevant information from the previous rule would conflict with the current rule. However, our study also goes against this interpretation. If ACC were primarily involved in signaling task conflict, then we would have expected to see much stronger ACC activity around the time of the switch compared to dlPFC and more neurons selective for the switch – at least compared to the activity we found induced by errors. It is possible that, in our well-trained visually cued task, this task conflict was not as strong, and we did observe some increase in activity around the switch; however, the number of errors around the switch indicates that switching between the tasks was still

challenging. Furthermore, we had the advantage of comparing two prefrontal areas, dlPFC and ACC. We would expect the conflict induced by task switching to have at least an equal effect on ACC firing rate as dlPFC and/or the response to error.

We did not observe any response conflict induced by the congruency of the stimulus. 70% of our trials had incongruent stimuli, so it is possible that the monkeys were always expecting incongruent trials. However, as discussed in the introduction, most electrophysiologic studies have failed to find evidence of response conflict in the dorsal ACC of non-human primates (Ebitz and Platt, 2015; Ito et al., 2003; Nakamura et al., 2005), so we did not expect to find response conflict in our data. Several human functional neuroimaging studies and one electrophysiologic study have found an effect of response conflict on both the current trial and the past trial (Kerns et al., 2004; MacDonald et al., 2000; Sheth et al., 2012). Given that the recent history of errors also seems to have an effect on ACC activity, it would be interesting to see the relative contributions of the past history of congruency versus those of the history of errors. At the very least, our study and others show that it is important to account for the recent error history when considering ACC functioning, because of its large effect on the firing rate of the current trial.

3.5 Materials and Methods

This dataset and experiment were previously described in a report focusing on the dlPFC local field potentials (Buschman et al., 2012). Some information from

that report is summarized here with additional detail as it pertains to this analysis.

3.5.1 Subjects and Recordings

Two monkeys — a male *Macaca fascicularis* (Monkey CC) and a female *Macaca mulatta* (Monkey ISA) — were subjects. We recorded from extracellular electrodes in ACC (areas 24c and 32) and dlPFC (area 9/46). There were 34 total recording sessions (11 for monkey CC, 23 for monkey ISA) with most sessions containing simultaneous recordings in ACC and dlPFC. Up to eight electrodes were placed in both ACC and dlPFC each session with a maximum of 16 simultaneous electrodes. 262 ACC neurons (117 neurons in monkey CC, 145 neurons in monkey ISA) and 313 dlPFC neurons (99 neurons in monkey CC, 214 neurons in monkey ISA) were recorded. The average firing rate of dlPFC neurons was 7.4 Hz (interquartile range: 1.7 to 10.1 Hz) and the average firing rate of ACC neurons was 6.7 Hz (interquartile range: 2.0 to 9.6 Hz). Further details of the recording and spike sorting can be found in (Buschman et al., 2012).

3.5.2 Task

Each trial began with the presentation of a fixation spot. After the monkeys acquired fixation, one of four rule cues was presented as a border stimulus around the screen — two for the color rule, two for the orientation rule — along with two response targets to the left and right of the fixation spot. The color rule cues indicated that the monkey should pay attention to the color (red or blue) of the upcoming test stimulus to make the correct saccade response, the orientation

rule cues indicated the monkey should pay attention to the orientation (vertical or horizontal) of the test stimulus. Each rule was cued in consecutive blocks of trials with at least 20 trials in each block — the rule switching with a 5% or 10% probability (monkey ISA and CC, respectively) after 20 trials. Rules appeared with equal frequency during the session. By cueing the rule on each trial, we can disambiguate the neuronal response to switches between the rules from errors on previous trials, because the task switches are not error-driven.

After the rule cue, the monkeys maintained fixation for a randomized duration (monkey CC: 227 to 496-ms, monkey ISA: 86–367 ms) until the test stimulus appeared on the screen. A “congruent” test stimulus meant the correct saccade direction was the same regardless of the rule cue (e.g. if the test was vertical and blue, the correct saccade direction is the right target). An “incongruent” test stimulus required knowledge of both the rule and test stimulus to make the correct response. Separation of test stimulus and rule cue allowed us to disambiguate the contributions of congruency and response direction from the rule cues in terms of timing. This is important because ACC neurons may be responsive to response conflict (Botvinick et al., 2004, 2001; Kerns et al., 2004; Sheth et al., 2012) — the increased demand caused by multiple potential responses. 70% of the trials had congruent test stimuli and 30% of the trials had incongruent test stimuli, so the monkey could not anticipate the response conflict.

The two monkeys performed an average of 2473 correct trials per recording session (range: 689 to 4093 trials). They successfully switched between blocks of rules in each session an average of 64 times (average of 41 correct switches for Monkey CC, 76 for Monkey ISA). The average number of correct color-to-orientation rule switches and orientation-to-color rule switches is 32 trials per session (color-to-orientation range: 9 to 54, orientation-to-color range: 9 to 55 trials per session).

Correct trials for which the previous trial was an error averaged 129 trials per session. The average number of color rule trials with an error on the previous trial is 64 and the average number of orientation rule trials with an error in the previous trial is 64 (color range: 11 to 174 trials, orientation range: 16 to 138 trials). All correct trials were rewarded with juice.

3.5.3 Behavioral Analysis

Reaction time and error analysis were previously reported in (Buschman et al., 2012). We expanded upon the analysis of errors by fitting a binomial generalized linear model with a logit link function with a 1 encoding a correct response and a 0 encoding an incorrect response in the task.

The model has five covariates from the task: **Rule**, **Error History**, **Rule Repetition**, and **Congruency**. **Rule** is an indicator function with 1 corresponding to the Orientation Rule and a 0 corresponding to the Color Rule. **Error History** is a lagged indicator that corresponds to whether the subject made an error in the previous $N-1$, $N-2$, $N-3$, $N-4$, $N-5$ trials where N represents

the current trial – 1 for an error, 0 for no error. **Rule Repetition** is an indicator function corresponding to the number of repetitions of the rule in the current block up to four repetitions (0 corresponds to repetitions of 5 or more trials, 1 corresponds to 1,2,3, or 4 repetitions of the same rule respectively). **Congruency** is an indicator function with 1 indicating an incongruent test stimulus and 0 corresponding to a congruent test stimulus.

In **Figure 3.2**, we present the effects of errors as a percentage change, $100 * (e^{\beta} - 1)$, in odds ratio – the probability of a correct response divided by the probability of an incorrect response – where the coefficient β is the linear coefficient estimated from the model. Effects are presented on a linear scale so as to give equal visual weight to decreases in odds ratios as increases in odds ratios, but units are labeled on the axis as the percentage change.

3.5.4 Permutation Analysis

Average firing rate differences between a high cognitive demand condition and the corresponding low cognitive demand condition in **Figure 3.4** were compared using a permutation test. We formed a null distribution by shuffling trial labels between the high cognitive demand condition of interest and the low cognitive demand condition and then recomputing the difference of the average firing rates in those conditions. We repeated this 10,000 times. A p-value was obtained by comparing the absolute observed difference between conditions to the shuffled null distribution of absolute differences. These p-values were

corrected using the false discovery rate (Benjamini and Hochberg, 1995) with $q=0.5$.

3.5.5 Spiking Model Parameters and Fitting

Generalized linear models were used for the results presented in **Figures 3.5-3.7** and **Figures 3.9-3.10**. Models were fit to each neuron using a Poisson distribution and a log link function to describe the relative contribution of factors to the instantaneous spike rate of each neuron. Spikes were parameterized by an indicator function over time in the trial with a 1 representing a spike and 0 representing no-spike in a 1-ms time bin. Covariates **Rule**, **Rule Repetition**, **Error History** and **Congruency** were parameterized in the same way as the behavioral analysis described in 3.5.3. **Response Direction** encoded the direction of the saccade with a leftward saccade corresponding to a 1 and a rightward saccade corresponding to a 0. We used the model *Rule + Error History + Rule Repetition* for within trial time epoch before the test stimulus (ITI, Fixation, and Rule) and the model *Rule + Error History + Rule Repetition + Congruency + Response Direction* for within trial time epochs after the test stimulus was cued (Test Stimulus, Saccade, Reward).

We fit only trials where the subject made a correct response. Trials with incorrect responses, fixation breaks, or reaction times less than 100 ms and greater than 313 ms were also excluded from the analysis.

Estimated effect sizes, such as those in **Figures 3.5** and **3.7**, are given percentage change from the low cognitive demand condition. As in the behavioral

analysis, this corresponds to $100 * (e^{\beta} - 1)$ where the coefficient β is the linear coefficient estimated from the model. Effects are presented on a linear scale so as to give equal visual weight to decreases in odds ratios as increases in odds ratios, but units are labeled on the axis as the percentage change.

3.5.6 Spike Prediction

To estimate how well the models were expected to generalize to new datasets, we used 5-fold cross-validation. Trials for each recording session were randomly assigned to five groups, four of which were used to fit the model and fifth used to validate the model. This was then repeated for each fold. In order to evaluate how well the model predicted on the test fold, we used the receiver operating characteristic (ROC). Using the model fit on the training folds, we can estimate a predicted instantaneous firing rate for the test fold. This instantaneous firing rate can be separated into two distributions: one corresponding to predicted instantaneous firing rates when a spike occurred and one corresponding to predicted instantaneous firing rates when a spike did not occur. If the model predicts well, then these two populations should be more discriminable than if the model did not predict well. The ROC gives us a measure of this discriminability by telling us the ratio of true positives and false negatives along the extent of the data, forming a ROC curve. We can then summarize this measure using the area under the ROC curve.

For **Figure 3.7**, we compared the predictions of two models over the cue epoch:

1. Rule + Error History + Rule Repetition + Congruency + Response

Direction.

2. Rule + Error Distance + Rule Repetition + Congruency + Response

Direction.

The **Error Distance** factor was encoded by an indicator function on the number of trials since an error occurred — up to five trials. So, like **Rule Repetition**, 0 corresponds to five or more trials since an error occurred, 1 corresponds to 1,2,3, or 4 trials since an error occurred.

For **Figure 3.10**, we compared eight models in the preparatory epoch before the test stimulus was cued:

1. *Rule*
2. *Error History*
3. *Rule Repetition*
4. *Rule + Error History*
5. *Rule + Rule Repetition*
6. *Error History + Rule Repetition*
7. *Rule + Error History + Rule Repetition*
8. *No Effect*

Where No Effect corresponds to a model with only an intercept term, which encodes the average firing rate over that interval. We do not display the No Effect Model in **Figure 3.10**, but it does affect the results. For example, in **Figure**

3.10a, the percentages do not add up to 100% because, for a subset of the neurons, the best predicting model for those neurons was the No Effect model.

CHAPTER IV: NEW TOOLS FOR WEB-ENABLED INTERACTIVE VISUALIZATIONS OF ELECTROPHYSIOLOGICAL DATA

4.1. Summary

Electrophysiology datasets in neuroscience are becoming richer and more complex as data is collected on multiple scales, dataset sizes increase, and more sophisticated questions are asked of the data. Visualization is an essential tool for understanding these datasets at all stages of analysis, but current practices in visualization of electrophysiological data are limited in their ability to efficiently compare between visualizations (such as between a raster plot of neuronal spiking to a visualization of a regression model of the same neuron) and filter complex data (for example, by limiting a visualization to specific brain areas on demand). Such difficulties are only magnified as the amount of data increases.

This chapter describes a set of composable, web-enabled interactive visualization tools developed for use in electrophysiological studies. These tools were developed to facilitate (1) exploratory data analysis, (2) checking of raw data and statistical modeling assumptions, and (3) data presentation in the context of large, complex and multi-scale neuroscience data. Data from several experiments were used to test the tools. These visualization tools are viewable in the web browser and open-source, making them easily shareable online and allowing for modification and development by the neuroscience community.

4.2. Introduction

Current theories of brain functioning ascribe different roles to different scales: neurons, cortical layers, brain areas, networks between brain areas. For example, the Communication-through-Coherence Hypothesis postulates that communication in the brain happens primarily through phase coordination between groups of neurons (Fries, 2005). This phase coordination between groups of neurons may differ between different layers, frequencies, within-brain areas, and between brain areas (Buffalo et al., 2011; Buschman et al., 2012; Gregoriou et al., 2009). Through the use of multiple electrode arrays and laminar probes, we are beginning to collect data at these different scales and understand how they interact (Miller and Wilson, 2008). However, as electrode technology progresses, our understanding of the data is not limited by the amount of data we can collect, but by our ability to efficiently understand and model relationships in the data.

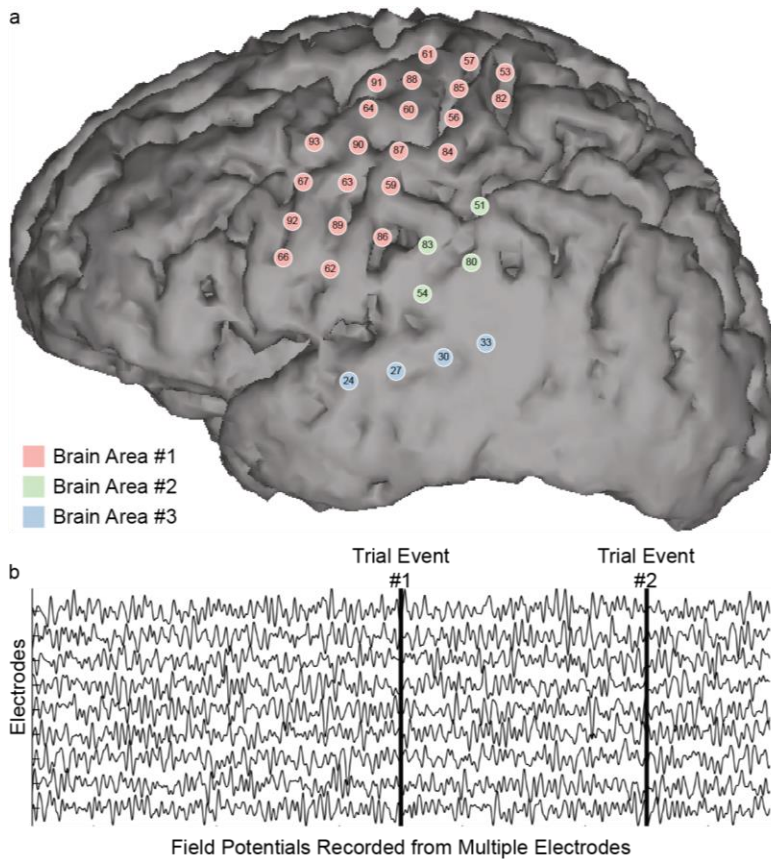


Figure 4.1 Example of an electrophysiological dataset.

(a) A human brain with electrode positions from intracranial electrodes marked as circles with numbers inside. The colors of the electrodes represent different brain areas. (b) Field potentials recorded from electrodes in part (a). Each line represents a field potential from a different electrode in part (a). In a typical analysis, these signals may be aggregated at different levels such as by brain area in part (a). They may also be compared to various events that occur over the time course such as trial event #1 and trial event #2.

Take, for example, a typical analysis of an electrocorticography (ECoG) dataset in which grids of intracranial electrodes are placed across large portions of cortex. These grids span multiple brain areas (**Figure 4.1a**) and are often combined with microelectrode grids to measure both local field potentials and action potentials from individual neurons (**Figure 4.1b**). Given enough data, this allows us to ask questions about the properties at different spatial scales

(units, multiunits, local field potentials, brain region summaries) and how they relate (e.g. correlation and coherence between local field potentials, local field potentials and neurons, neurons and neurons). Moreover, we can ask questions about how these change over time and/or relate to experimental conditions (e.g. comparing trial event #1 versus trial event #2 in **Figure 4.1b**). This results in a dataset with many complex interrelations.

Understanding a dataset such as this becomes even more challenging as we record from more electrodes. For example, when assessing relationships between recorded signals, the number of possible associations scales quadratically with the number of signals. That is, 10 electrodes means analyzing 100 relationships between electrodes. Implantation of multielectrode arrays with upwards of 100 electrodes is becoming common (Einevoll et al., 2012; Miller and Wilson, 2008; Siegel et al., 2015) and the number of simultaneously recorded neurons is projected to double every seven years (Stevenson and Kording, 2011).

Visualization of data is one way that we can reduce data complexity — allowing us to make multiple simultaneous comparisons, easing the cognitive burden on working memory by efficiently encoding properties of the data into features salient to the visual system (Cleveland and McGill, 1984; Healey and Enns, 2012). In addition, visualization is important in the understanding and checking of statistical assumptions — it helps reveal differences between the expected structure of the data (the model) and the observed data (Anscombe, 1973; Tukey, 1977). This is important, from the initial stages of analysis to

publication, for revising our assumptions and models and for understanding and communicating where and how our models do not adequately explain the data (Gelman, 2004).

However, current practice with electrophysiologic data relies on static visualization — requiring the generation of figures for each particular view. This makes it difficult to explore and check the data efficiently. For example, Liu and Heer (2014) found that even a 500 millisecond delay between visualizations could reduce the amount of the dataset explored and affect the number of hypotheses and observations formed.

Adding interactivity allows the user to change perspectives and modify analyses on demand, facilitating comprehension and hypothesis generation (Liu and Heer, 2014). Neuroimaging studies, which generate large datasets with complex interrelations, make extensive use of interactive visualization tools (e.g. the Freeview module in Freesurfer, Pysurfer, SPM), but there are no such tools for electrophysiology studies. One can design user interfaces using MATLAB, but these are hard to share and require commercial software.

We present a set of three tools aimed at providing basic interactive visualizations for electrophysiology studies: **SpectraVis** is a tool aimed at exploring task-related functional networks over time and frequency; **RasterVis** is a tool for dynamically displaying and sorting spike raster plots and peri-event histograms; and **GLMVis** is a tool for displaying coefficients from generalized linear models (GLMs) — which are commonly used to describe the receptive

fields of neurons. Each visualization allows examination of the electrophysiological signals (or summary statistic of the signal) over time relative to task-relevant events, comparison of different subjects or recording sessions, and aggregation or filtering of signals. The visualizations are composable — two or more of the visualizations can be linked together to give a more comprehensive view of the dataset — and static visualizations can be exported for use in papers. Finally, all visualizations are web-based and open-source, making them easily shareable and operating system independent, and allowing for modification and repurposing by the neuroscience community.

4.3 Materials and Methods

4.3.1 Design

In order to make our set of tools accessible to a large number of users, we identified a set of design principles that would make them maximally useful to developers — who may want to extend the visualization code based on our toolkit — and to the end-users of the visualizations (Sherif et al., 2015). To that end, our approach is to create interactive visualizations that are:

1. **Configurable** — so visualizations can dynamically display different datasets or be preset to a particular view state.
2. **Shareable** — so others can easily view the visualizations online or in print.
3. **Modular** — so the visualizations can be used independently or linked together to provide an integrated view of an electrophysiological dataset.

4. **Extendable** — so others can implement their own visualization algorithms and modify the visualizations for their own use.

4.3.2 Configurable

Configurability ensures that developers will be able to set up the visualizations using their own datasets and customize settings for their own needs. The visualizations are configurable in three ways: parameters can be passed through the URL, parameters can be preset using Javascript via the init function for each visualization, and data and data labels can be loaded using the JSON file format.

The JSON file format (see **Figure 4.2b**) is a readable, XML-like format that allows the visualization to display different datasets — the visualization dynamically adjusts the axes, labels, and the display for each dataset based on the JSON file it receives. Each visualization has a standardized format for the JSON file, details of which are documented on the wiki located in the Github repository.

Importantly, JSON files can be exported from MATLAB data structures (using, for example, the open-source toolbox [JSONlab](#)) and Python — providing a bridge between commonly used analysis tools and the visualizations. An example workflow might be to perform data analysis in MATLAB, format the data into MATLAB structures that correspond with the visualization format, use JSONlab to export the MATLAB structures to the JSON format, and use the visualization tools to explore the implications of the analysis on the dataset (**Figure 4.2a**). This is often an iterative process — requiring several cycles of data analysis and data visualization — which highlights the utility of the interactive visualizations.

Each successive analysis may require an adjustment: an addition of an experimental condition, investigation of a different statistic, or fixing a mistake in the analysis. Example MATLAB scripts for exporting JSON in the correct format are included in the Github repositories to make it easier for the user to get started.

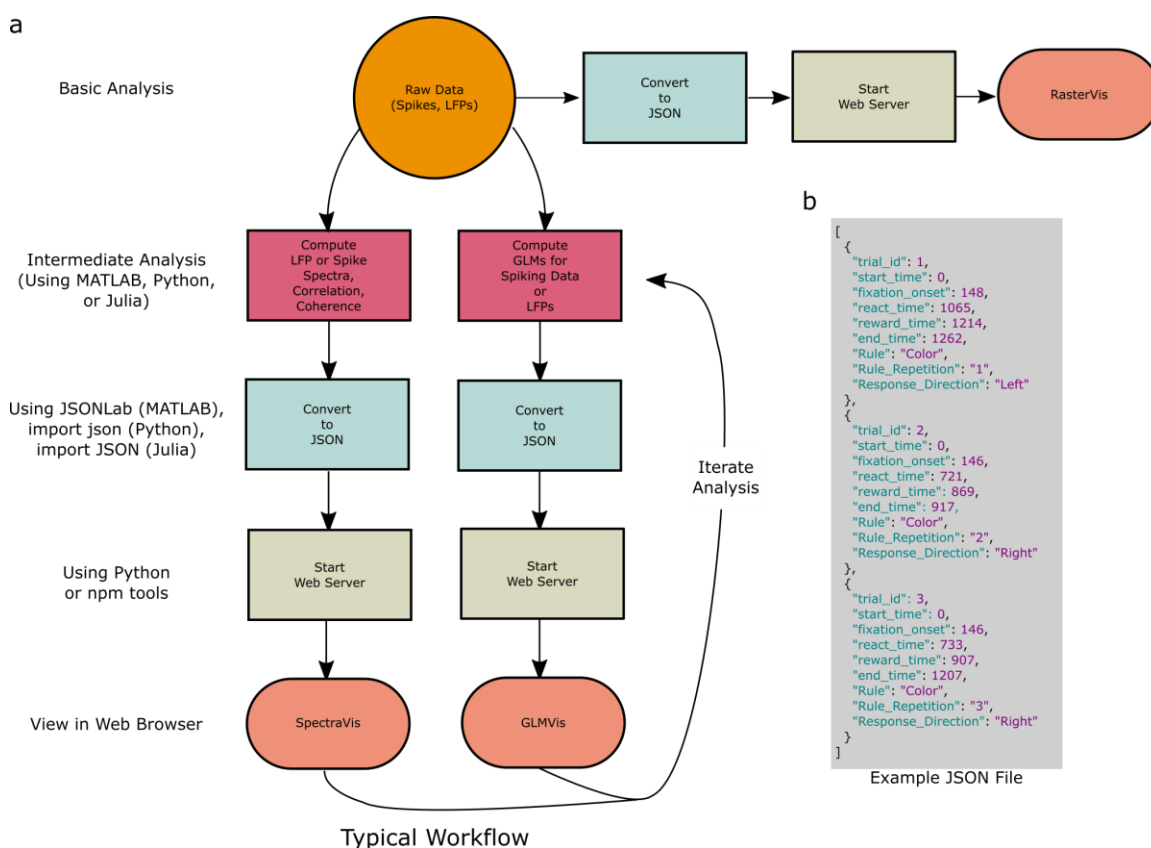


Figure 4.2. An example workflow (a) and JSON data structure (b).

(a) A typical analysis involves examining the raw data (basic analysis, such as examining spike rasters), performing intermediate analyses (e.g. computing spectra, coherences, regression models), and comparing the results of those analyses to the raw data (model checking). Typically, this process is iterative, so intermediate and basic analyses must be repeated. The three visualizations, RasterVis, GLMVis, and SpectraVis, aid in the iterative process by allowing rapid exploration of the raw data and intermediate analyses. To view the visualizations, data from the analyses must be output in the JSON format. Then a web server must be started to host the JSON files. This can be done locally or over the web. The visualizations can then be viewed in a web browser. (b) The JSON data format is a structured, easily understood data format for the visualizations. This example shows a part of a JSON file for RasterVis.

4.3.3 Shareable

To make the visualizations shareable, the visualizations were written with modern web technologies — HTML, CSS, and Javascript. The Javascript code relies heavily on the D3 visualization library (Bostock et al., 2011). The visualizations can be deployed via a local or remotely hosted web server and viewed with any modern browsers (Firefox 4+, Chrome 4+, Safari 4+, Opera 9.5+ and IE9+). As a result, the visualizations require no specialized software (beyond a browser) to view.

Users can share a particular state of the visualization using permanent links (permalinks) — each visualization has a button which provides the URL containing the parameters necessary to generate the current view. For example, SpectraVis can show correlation networks across time. If a user wanted to share a snapshot of the correlation network at a specific time (e.g. 100 ms after stimulus onset), clicking on the link button would provide a URL that could then be shared with colleagues.

Additionally, static visualizations can be saved for publication purposes. Each visualization includes a button to download the current view of the visualization in scalable vector graphics (SVG) format. This format has the advantage that it can be resized without loss of resolution — making it useful for both presentations and publications — and can be imported into a graphics program of choice such as Inkscape or Adobe Illustrator for further modification. The New York Times, which frequently uses interactive graphics online and in

print, has used this workflow [successfully](#) and we used it for many of the figures in this chapter as well.

4.3.4 Modular and Extendable

Each visualization is self-contained and works independently of the other visualizations. The visualizations can be selectively linked together by using the permalinks — which allow specification of a particular state of the linked visualization. For example, GLMVis might display a neuron’s receptive field response to several experimental stimuli. By a simple modification of the code, this can be linked to the neuron’s raster plot in RasterVis — showing the spiking response of the neuron to each experimental stimulus. This makes the visualizations composable — the visualizations can be mixed and matched to provide a desired view of the dataset.

The visualizations’ internal code is also constructed modularly — separating the internal visualization modules from data loading modules and from user interface elements such as buttons. Developers can import and export these modules selectively or make their own modules, making the visualization customizable to the developers’ needs. For example, in SpectraVis, a developer might want to customize the layout of the correlation networks, spatially grouping nodes by brain area or another desired metric. Constructing the code modularly allows a developer to implement this new layout without interfering with the rest of the code internals.

Finally, each visualization has its own online software repository. The repositories are hosted on Github and can be downloaded and installed — including all software dependencies — using the node package manager (npm). This ensures that the development tools, such as deploying a local web server (allowing the user to view the visualization on their own computer without having to host it remotely), are included. This helps developers extending the visualizations to get started developing as quickly as possible. These repositories are also open-sourced under the [GNU General Public License \(version 2\)](#), meaning the code is available to anyone to use and develop as long as the code remains open-source.

4.4 Results

Here we describe the functionality and interface for the visualizations and explain why they are useful for analyzing electrophysiological data.

4.4.1 SpectraVis

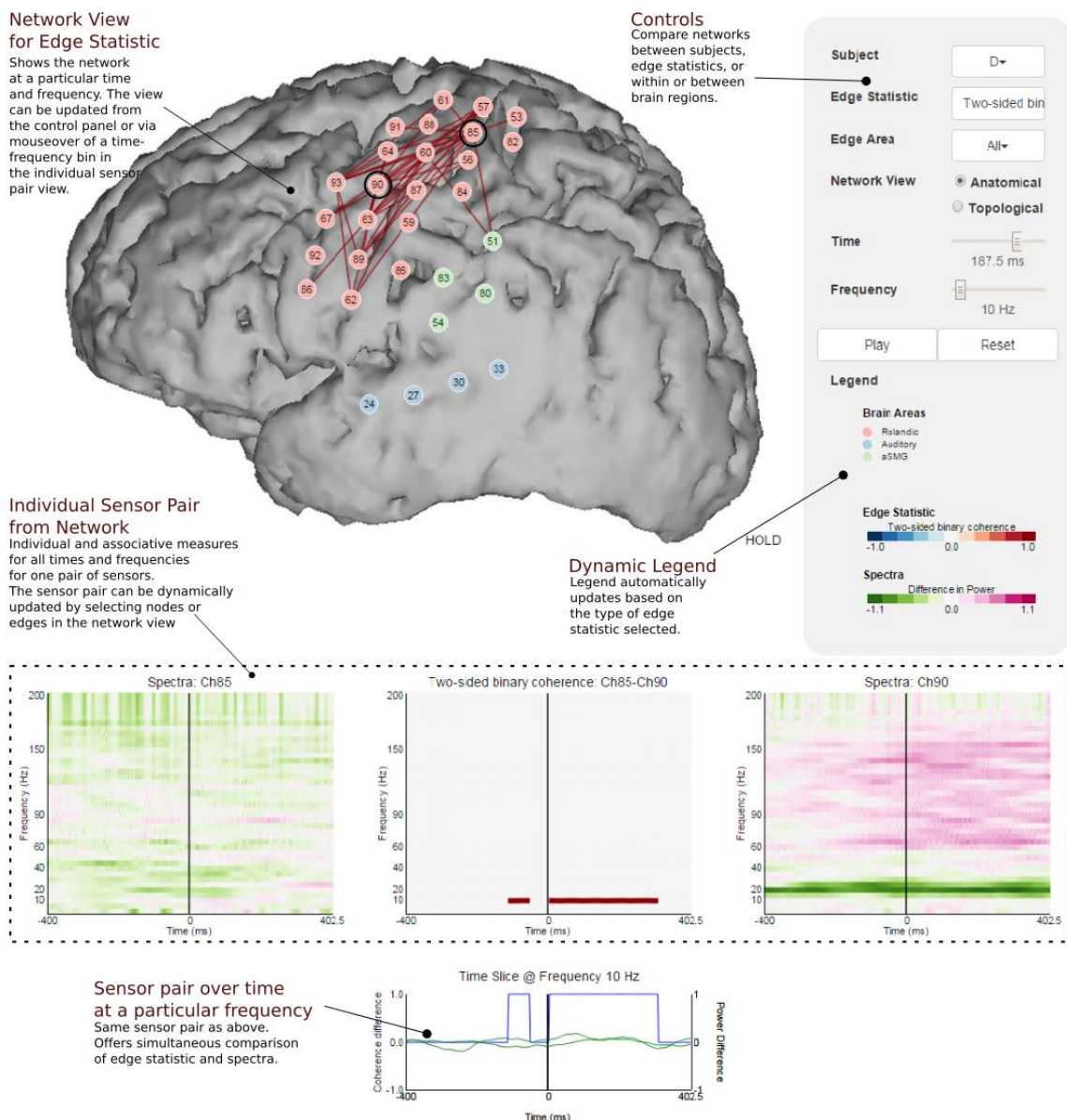


Figure 4.3. A screenshot of the SpectraVis interface.

There are three main parts of the user interface: the network view, the individual sensor pair view, and the controls. The controls alter the network view. Using the controls, the user can change the subject or metric used for the network, display the network at other time-frequency bins, or change the spatial layout of the network, or “play” the network forward in time — a movie of how the network changes. A dynamic legend which updates based on the data and the edge statistic used is below the controls. Users can click on nodes or edges of the network in the network view to get a more detailed view in the individual sensor pair view, displaying all the time-frequency bins of the spectra and coherences (or other associative measure such as correlation) corresponding to the sensor pair selected. Mousing over a time-frequency bin in the individual sensor pair view will display the network at that time-frequency bin in the network

view. The individual sensor pair view also shows the change over time of the edge statistic and spectra at the current frequency of the network view (bottom).

Functional network analysis is a growing area of neuroscience research, driven in part by technological improvements allowing us to record from more sensors simultaneously. However, as researchers record from more sensors, network analyses can become unwieldy and hard to interpret, because the number of possible network connections scales quadratically with the number of sensors (e.g. electrodes). Further, we expect neural processes to form dynamic networks that vary over time, frequency, and spatial scales (e.g. within and between brain regions), adding numerous dimensions to network analyses.

SpectraVis is an interactive visualization aimed at enhancing exploratory analysis of networks by allowing the user to efficiently: (1) compare task-related functional networks over time and frequency, (2) compare individual and associative measures on all sensor pairs (e.g. spectra, coherences), and (3) compare different measures of association (e.g. correlation vs. coherence, binary vs. weighted networks). The different views of SpectraVis are dynamically linked, highlighting relationships between the metrics in response to user interaction.

Figure 4.3 shows a typical view of SpectraVis. The network view shows the anatomical location of the sensors (circles with sensor number) and edges (lines) weighted by the edge statistic (color of the line, measure of association between the sensors). In this example, the edges are binary, representing significant changes in local field potential coherence between *Speech* — subjects reading aloud the words of a famous speech or nursery rhyme — and *Silence* at a particular frequency (10 Hz) and time (187.5 ms after speech onset). The network

has dense connectivity within and between primary motor and primary somatosensory cortices (M1 and S1). Users can compare between binary edge statistics (see **Figure 4.4**, middle and right image), which categorically declare associations between sensors, and weighted edge statistics (see **Figure 4.4**, left image), which use continuous measures such as the raw coherence difference and z-scored coherence difference, specified via the edge statistic dropdown.

The controls can also be used to examine the evolution of the network over time using either the time slider, which can be dragged to a time of interest, or the play button, which will automatically advance the time slider. Examining the network over time can potentially reveal differences in network structure that could result from an experimental cue or event. SpectraVis enables quick comparison between all time points. The user can also compare networks at different frequency bands (for example, comparing a 10 Hz alpha band network to a 20 Hz beta band network) using the frequency slider. This is important because different frequency bands may have different functional roles (Ainsworth et al., 2012; Engel and Fries, 2010; Kopell et al., 2010; Palva and Palva, 2007).

One difficulty of analyzing networks is interpreting the edges between sensors, particularly if the network is a weighted network and there are many sensors. There often is not enough room in a visualization to display all the edges without much overlap. To solve this problem, we use two strategies: layout and filtering.

The network layout toggle controls where nodes are positioned (and consequently the edges between nodes). The *anatomical* layout places the nodes according to the anatomical position defined in the JSON files (**Figure 4.4**, left and middle image). For example, in an ECoG dataset the network nodes often correspond to electrodes, which can be displayed over an image of the brain to give the end-user a sense for the sulci and gyri underlying each electrode. In some cases the anatomical locations of the nodes may be less important than their position induced by the network topology: for example, a node with strong connections to other nodes may serve as a hub. To help with this kind of interpretation, SpectraVis offers a *topological* layout that models the nodes and edges as a physical system to limit the number of overlapping edges (**Figure 4.4**, right image). Node numerical labels are preserved across choices of layout.

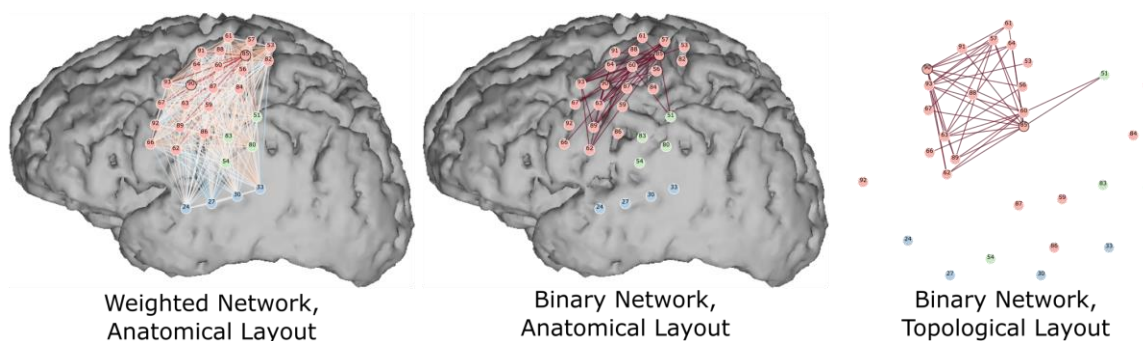


Figure 4.4 Different layouts for understanding associative networks.

Left layout draws edges between all nodes. The color of the edges corresponds to a relative weight — in this case a difference of coherence between speech and no-speech conditions in the experiment. Middle layout only shows the edges that correspond to statistically significant changes in coherence (binary network). This network is easier to understand (compare to the left weighted network) because there are fewer edges, although it is subject to the choice of statistical thresholding — there might be meaningful changes that are not shown due to the choice of threshold or vice versa. A topological layout (right layout) removes the constraint of spatial anatomical location and attempts to position the nodes so that connected nodes are closer together and overlapping of edges is minimal, so the user can better see which edges and nodes are well-connected (hubs).

The second strategy to make edges more visible allows the user to isolate subsets of the network by filtering edges and sensors, thus reducing the number of comparisons needed in any one view. Using the edge filter dropdown, the user can isolate the edges between sensors that reside within the same brain area (e.g. only auditory cortex - auditory cortex sensor pairs) or between sensors that have non-matching brain areas (e.g. only auditory cortex – motor cortex sensor pairs).

Once the desired network view has been obtained, users can get further detail by clicking on a pair of sensors. This loads a sensor view (dotted box) which depicts the relationship (spectra and coherences) between a selected pair of sensors (circled in black, network view, sensors 85 and 90) at all times and frequencies. Here, the edge between M1 (sensor 90) and S1 (sensor 85) represents a 10 Hz increase in speech coherence relative to silence. The increase co-occurs with higher frequency beta (15-25 Hz) power suppression on the M1 sensor. The user can investigate the relationship between the sensor pair and the network view by mousing over a time-frequency bin in the sensor view, which correspondingly updates the network view to the time-frequency bin under the cursor.

4.4.2 RasterVis



Figure 4.5 A screenshot of the RasterVis interface.

Controls in the upper left hand corner allow for easing linking and exporting of figures. The current neuron displayed is also labeled next to the RasterVis title. The left column of the interface contains the control panel, where users can control the figure displayed. Users can manually scroll through the available neurons or search for specific neurons using the text box. Below that, drop down menus allow sorting by experimental factor or aligning the timing of the spikes to an event of interest (in this case the Rule Cue, whose onset is marked by the pink to green transition). Binning of the peri-event time histogram is controlled by the Line Smoothing scroll bar. The spikes and peri-event time histogram can be toggled on and off using the Show lines and Show spikes checkbox. The right hand column displays the raster plot and the peri-event time histogram. Trials are arranged in rows with black filled-in circles representing the time of the spike relative to the event of interest. The background colors — purple, pink, green, etc. — for each row represent the onset and offset of a trial event such as visual stimulus appearing. Blank trials where there is no background color represent trials in which the subject did not complete the trial (because of a break in fixation in this case). The black line represents the perievent histogram — which spans the entire height of the figure (The full length of the figure is cut-off because the figure spans more than the screen size. The user can scroll to see the entire figure or toggle off the display of the spikes, which shortens the figure to just display the peri-event time histogram). Mousing over a trial shows a tool-tip display that gives further information about that trial condition.

RasterVis incorporates two canonical visualizations for single and multiunit spiking data — the raster plot and peri-event time histogram. The raster plot shows spike times for each trial relative to a trial event. The peri-event time histogram sums the raster over trials, showing the count of spikes that occurred in each time bin relative to the time of a trial event (Ventura et al., 2002).

Because these two types of visualizations are familiar and represent the “raw” spiking data, they are an ideal building-block visualization. Furthermore, they can be used to compare raw spiking data to statistical model-generated data in order to check statistical modeling assumptions — so they can be useful in understanding how statistical models capture or do not capture features of the data.

RasterVis uses interactivity and animation to supplement the raster plot and peri-event time histogram in order to make it easier for the user to accomplish typical tasks in the analysis of spiking data (see **Figure 4.5** for a screenshot of the RasterVis interface).

For example, RasterVis allows for dynamic alignment of spike times and “on-the-fly” computation of peri-event histograms relative to experimental trial events (e.g. visual stimuli, timing of rewards, presentation of fixation points). Animated transitions emphasize how spike timing relative to one trial event relates to another trial event. This helps a user quickly compare the timing of individual spikes and aggregate spiking (via histogram) to different cues (**Figure 4.6**, top vs. right row) and conditions. Different levels of aggregation of the spikes over

time for the histogram can be compared as well (**Figure 4.6**, left column vs. right column).

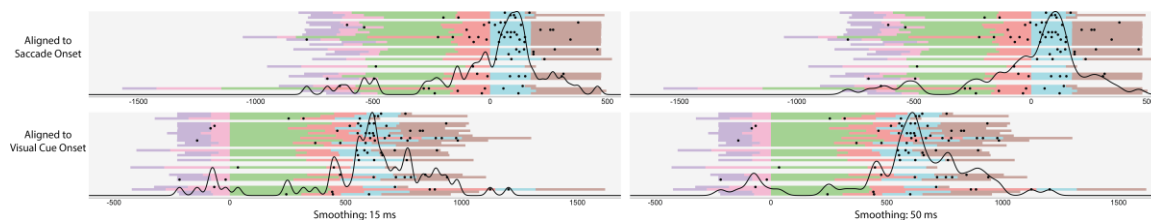


Figure 4.6. RasterVis can align the raster plots to different trial events (saccade onset in darker pink vs. visual stimulus onset in light blue) and aggregate the spikes with different amounts of precision (15 ms standard deviation Gaussian smoothed kernel density estimate left, 50 ms standard deviation Gaussian smoothed kernel density estimate right).

RasterVis can dynamically sort trials by experimental task factors (**Figure 4.7**, left vs. right column). This creates on-demand plots for each condition within the task factor. For example, if a task factor is a visual cue with two experimental conditions — the color cue and the orientation cue — sorting by the visual cue creates two plots for the color condition and the orientation condition (**Figure 4.7**, left column). This is essential for multidimensional analysis, which involves comparison of several different factors and conditions.

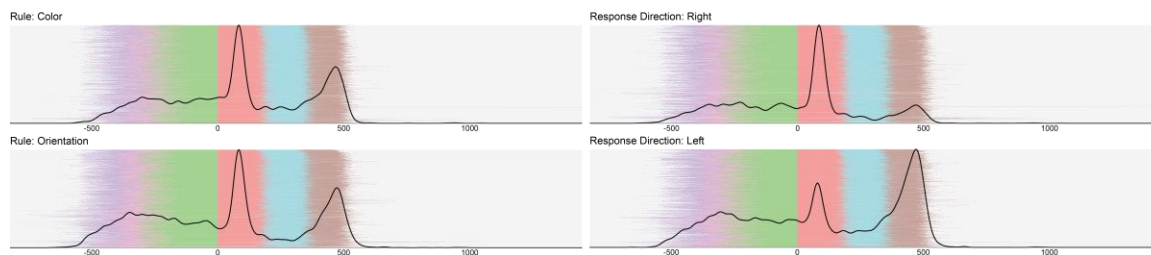


Figure 4.7 Dynamic sorting by task factors.

This example shows the user sorting by two different experiment task factors for a single neuron: The “Rule” factor (left column) and the “Response Direction” factor (right column). The Rule factor shows the same pattern for both conditions, but the Response Direction factor shows a differential response for the right response vs. the left response.

Finally, users can quickly search for neurons by subject, recording session, brain area or name. This is useful for fast comparison between neurons, linking to other visualizations (other visualizations can directly link to a specific neuron by name via a parameter passed via the URL), and general exploratory analysis of the dataset.

4.4.3 GLMVis

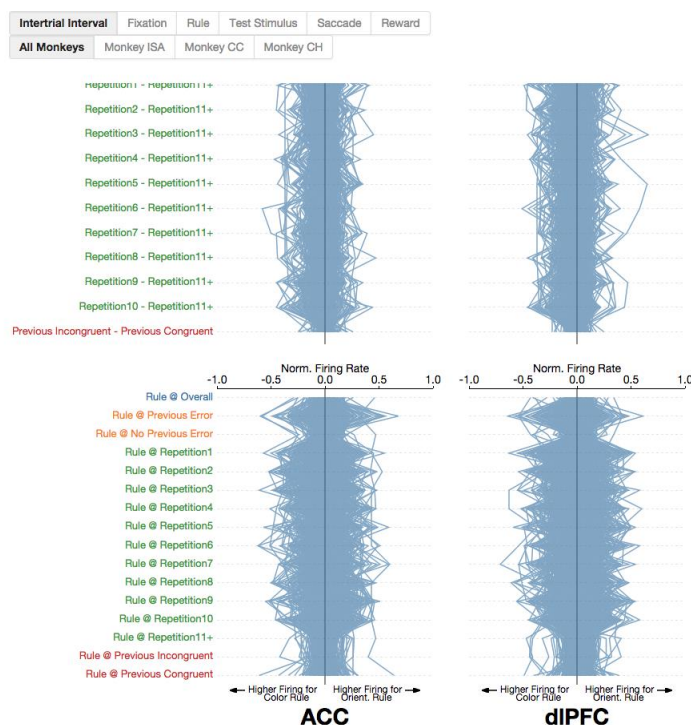


Figure 4.8. A screenshot of the GLMVis interface.

The top row shows the controls — buttons which change the model displayed (in this case relative to different stimuli) or filter the neurons by subject. Below are the parallel coordinate plots, which are separated by brain area (left column ACC, right column dlPFC). Each blue line represents a neuron. Each dotted parallel line represents a dimension that has been fit by the GLM (they correspond to a particular trial condition). The labels on the left group the conditions by color, which correspond to the factor the condition belongs to. For example, the Rule by Rule Repetition interaction is colored green, because Rule @ Repetition₁, Rule @ Repetition₂, etc. all correspond to the same factor.

A common analysis framework for characterizing the spiking response of neurons is the generalized linear model (GLM) (Fernandes et al., 2014; Harris et al., 2003; Mayo et al., 2015; Park et al., 2014; Pillow, 2005; Truccolo, 2004). GLMs can simultaneously estimate effects of experimental conditions, spike history (refractory period, bursting), non-linear firing rate changes over time, and dependence on other neurons (Truccolo, 2004) — making them useful for analyzing a wide range of experiments. GLMs are especially useful in situations where conditions of interest are interdependent, making them difficult to tease apart using simple tools like peri-event time histograms (MacDonald et al., 2011).

One consequence of being able to estimate many factors simultaneously is that the relationship of the effects becomes hard to understand because of the number of dimensions — particularly if the factors change over time and there are many neurons. Moreover, understanding the relationship between multiple factors may be important to understanding *mixed selectivity* neurons (Cromer et al., 2010; Fusi et al., 2016; Rigotti et al., 2010). These neurons are sensitive to a combination of sensory, motor and cognitive processes, appear in higher-order association brain regions such as parietal and prefrontal cortex (Park et al., 2014; Rigotti et al., 2013), and may underlie the computation of complex behavior (Rigotti et al., 2010).

Therefore, we built GLMVis, an interactive visualization for GLMs, that: (1) shows the relationship between the multiple dimensions of the model fit over time, (2) allows filtering of neurons by effect size, brain area, and experimental

subject, and (3) can be used to compare estimates from different models. To show the relationship between multiple dimensions, we use parallel coordinate plots (Inselberg, 1985; Wegman, 1990) — a compact representation of multivariate data that links each dimension on parallel axes by a line.

Figure 4.8 shows a screenshot of the GLMVis interface. Each axis is a black horizontal line that corresponds to a dimension of the GLM. Non-parallel lines connect the dimensions and represent a single neuron. The intersection of the axes and non-parallel lines is the effect size of the neuron at that dimension. The user can investigate correlations between dimensions in two ways: clicking on a line, which highlights only that neuron along the dimensions of the model (**Figure 4.9c**, **Figure 4.9d**), or by “brushing” along a desired axis — holding and dragging the mouse to filter neurons by effect size in the range of values of the dimension (**Figure 4.9a** no brushing, **Figure 4.9b** with brushing). Multiple axes can be “brushed” in order to compare the associations between effects in different dimensions. To further isolate the neurons involved, the user can use dropdown menus to filter the neurons by brain area or experimental subject or compare different models (**Figure 4.9d**).

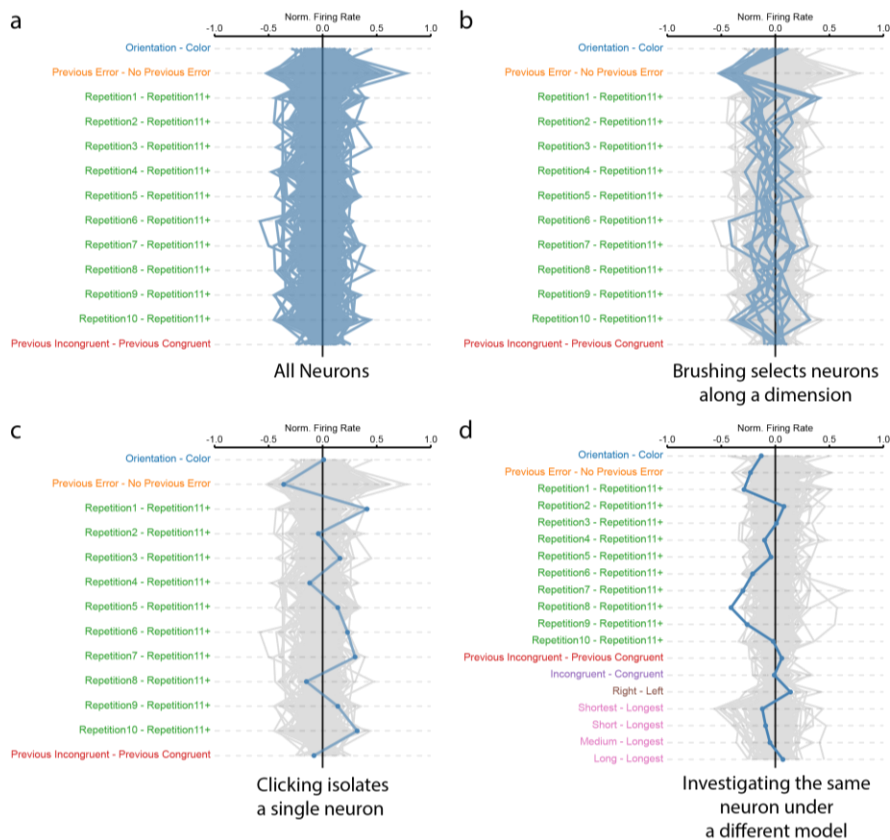


Figure 4.9 Interacting with parallel coordinate plots on GLMVis.

(a) Parallel coordinate plot with no brushing. (b) User brushes along the Previous Error – No Previous Error dimension, selecting a group of neurons that co-vary with the Repetition1 – Repetition11+ dimension. (c) User selects a single neuron that varies along the Previous Error – No Previous Error dimension and Repetition1 – Repetition11+ dimension. (d) User investigates how this model changes with the inclusion of more task factors.

Finally, the user can use GLMVis in conjunction with RasterVis to better

understand how the model fits the data. Because parameters can be passed to

RasterVis via URL — that is, a URL link can specify the state of RasterVis such as

one that corresponds to a dimension of interest for GLMVis — one can easily

modify GLMVis such that clicking on a dimension that corresponds to a

particular neuron can take the user to that neuron’s raster plot sorted by the

dimension of interest. Furthermore, RasterVis can be modified such that the user

can make a side-by-side comparison of the actual data and the model-generated

data, allowing for a deeper understanding of the reported effect in conjunction with how well that reported effect captures the structure of the data. This type of deeper understanding between model and data is hard to achieve with static figures, particularly when there is a lot of data and there are many dimensions, because figures for each set of models and data must be generated and then searched for on a file system. Interactivity and the combination of RasterVis and GLMVis allows the user to quickly move back and forth between model and data, gaining insights they might not have otherwise because of the ability to make fast comparisons.

4.5 Discussion

We developed a novel interactive visualization toolkit for investigating electrophysiological data. This toolkit allows users to quickly explore raw data via RasterVis and intermediate analysis such as receptive fields and networks via GLMVis and SpectraVis. We believe these tools will be important going forward as electrode technology progresses and scientists form more complicated hypotheses.

4.5.1 Importance of Visualization for Open Neuroscience

Online interactive visualization tools such as ours may provide a way for quick exploration of datasets online — enabling users to understand the datasets before performing more in-depth analyses. Indeed, the Allen Brain Institute — which shares massive neuroscience datasets online — makes extensive use of online visualizations to enable users to find the appropriate datasets. Because our tools

encompass many common types of analysis for electrophysiological data, we hope our tools and future extensions can be used in a similar manner.

Sharing datasets is important because (1) it can help ensure the reproducibility of results, (2) it makes the data available for meta-analyses, (3) the data can be used as benchmarks for computational models, and (4) the data can be used in new ways, maximizing its utility (Poldrack and Gorgolewski, 2014). This is particularly important for datasets that are hard to collect, such as those from non-human primates.

One challenge for the sharing of datasets is providing users with a way to find the datasets they want. Datasets provided in numerical form in non-standardized formats are hard to navigate and limit the usefulness of sharing the data. As electrophysiology dataset sharing becomes more common, it will be important to have tools to do preliminary investigations of these open datasets.

4.5.2 Future Directions

As data formats for sharing electrophysiologic data are standardized, we would like to change our JSON data structures to match those formats in order to make visualizing data as simple as possible. Unfortunately, there is no dominant standard currently.

We would also like to provide additional “plugin” layout options for SpectraVis, GLMVis, and RasterVis. In particular, there are numerous open source network layouts such as [Group-in-a-box layouts](#), which clusters nodes according to group membership, and [edge bundling layouts](#), which group similar

edges together — all with the goal of improving understanding of the network structure. Likewise, with GLMVis, alternative views of the GLMs such as scatter plot matrices (SPLOMs) and dimensionality reduction algorithms such as t-Distributed Stochastic Neighbor Embedding (t-SNE) (Van der Maaten and Hinton, 2008) could help identify multivariate patterns in the data.

Lastly, we would like to add more visualizations to the toolbox. Laminar electrodes, which have contacts spaced along the shank of the electrode and provide cortical layer information, pose an interesting challenge in terms of incorporating the extra dimension of depth information. As more studies incorporate laminar electrodes, finding effective visualizations and filtering of networks between different cortical layers, with the many possible associations between the layers, could be another good use case for interactive visualizations.

CHAPTER V: CONCLUSION

5.1 Summary

One important focus of this dissertation is to functionally dissociate the roles of prefrontal subdivisions with respect to the control of attention.

In Chapter II, I showed evidence that groups of neurons within dlPFC are linked together in a rule-dependent manner via synchronous oscillations. Moreover, the specific frequency of these oscillations might relate to the selection of the current rule (beta frequencies) or de-selection of the irrelevant rule (alpha frequencies). ACC did not show the same context-dependent linking of neurons via synchronous oscillations.

In Chapter III, I showed that – unlike dlPFC neurons and contrary to the conclusion of several recent studies (Ebitz and Platt, 2015; Johnston et al., 2007; Shenhav et al., 2013) – individual ACC neurons show little change in firing rate in response to the switching of rule. Instead, ACC neuronal activity is driven by the past history of errors. Additionally, I found that ACC neurons respond to visually cued rules as well as the past history of errors. dlPFC neurons were only sensitive to only the most recent error.

Finally, in Chapter IV, I developed visualization tools for the analysis of large, complex electrophysiological data. The three visualization tools – RasterVis, GLMVis, and SpectraVis – are aimed at making exploratory analysis and model checking of electrophysiological data more efficient through the use of

interactivity and making data analyses more shareable and transparent using web technologies.

5.2 Significance

The body of work presented in this dissertation is significant in several ways.

First, the study in Chapter II is the first evidence of a rule-based role for synchronous oscillations within the prefrontal cortex. It presents a new framework for thinking about the mechanisms of attentional control within the prefrontal cortex. Previous studies have considered the effects of oscillations between distant regions in the brain. The results of Chapter II suggest that there could be an even more local effect of synchronous oscillations – coordinating groups of neurons within the same anatomical brain region. Prior studies investigating context-dependent dynamics in the prefrontal cortex have also only focused on the average effects of neuronal firing rate. Chapter II shows that there might be an additional layer of structure imposed by prefrontal oscillations that is important for selecting the relevant rule.

Second, the results of Chapter III make an important contribution to our understanding of the prefrontal subdivisions. Current theories of prefrontal cortex attribute different functions to anatomical subdivisions (Dias et al., 1996; Miller and Cohen, 2001; Rushworth et al., 2011; Rushworth and Behrens, 2008). Because these functions are thought to underlie some of our more complex and diverse behavior, research is needed to tease apart the specific contributions of prefrontal subdivisions. Despite the wealth of studies on ACC, there is little

agreement on its function (Shenhav et al., 2013) – primarily due to the diversity of findings of its involvement in processing errors, reward, conflict and attention. This has led to a number of attempts to unify these findings under a single overarching function of cognitive demand (Alexander and Brown, 2015, 2011; Holroyd and Yeung, 2012; Shenhav et al., 2013), but the complexity of this function requires careful accounting of the numerous factors that could affect ACC. Our study is unique in that we are able to study the relative effect of errors, reward, conflict, and attention. We show that not all cognitively demanding situations produce changes in ACC activity. We also provide further evidence that ACC neurons are involved in higher-level cognitive functions. Neurons in ACC had properties consistent with tracking the current context and using that information to proactively boost information about the rule when errors are made in the recent past. This is significant because it helps distinguish its functioning from other reinforcement learning associated areas like the subcortical basal ganglia.

Last, the interactive visualizations developed in Chapter IV are the first interactive visualization tools developed for multi-electrode neurophysiological data. Interactive visualization tools should become more important as datasets become larger and more complex, because they allow users to navigate between alternate views with minimal delay and make comparisons between complicated representations. The interactive visualizations in Chapter IV serve as more than

proof-of-concept. The visualizations are functional and freely available on Github for use, modification or inspiration for future visualizations.

5.3 Future Directions

5.3.1 The Role of Alpha Oscillations

Chapter II suggested that synchronized alpha oscillations may have a role in de-selecting the more dominant rule. Although alpha oscillations are often associated with inhibition (Palva and Palva, 2007), it is not clear how oscillations in the alpha frequency band relate to the beta band synchronization. Do the alpha oscillations directly suppress beta synchronization within prefrontal cortex, or is it interaction with distal cortical and subcortical areas that prevent the beta band selection from occurring? Alpha could be generated by excitatory-inhibitory (or possibly purely excitatory) interactions in the deeper layers of a cortical column, it could be entrained by thalamus, or it could be through an interaction with thalamus (Buffalo et al., 2011; Jones et al., 2000; Silva et al., 1991; Sun and Dan, 2009; van Aerde et al., 2009). Computational modeling work and further experimental work will be important in establishing possible mechanisms by which this could happen.

5.3.2 Cognitive Demand in Monkeys versus Humans

A central finding of Chapter III is that ACC neurons respond to the past history of errors, not to response or cognitive conflict. However, it is important to acknowledge that the non-human primate brain is different from the human brain. Non-human primate studies to date have not found evidence of response

conflict (Ebitz and Platt, 2015; Ito et al., 2003; Nakamura et al., 2005), but numerous human functional neuroimaging studies have found evidence of response conflict (Kerns et al., 2004; MacDonald et al., 2000) and crucially, one human electrophysiologic study (Sheth et al., 2012). This has led to speculation about whether there are fundamental differences – both functional and anatomical – that could lead to the discrepancy between studies of the non-human and human primate brains (Cole et al., 2009). Therefore, it is important that there be more electrophysiology studies of the human ACC. It is possible that human ACC neurons are more responsive to the switching of context than those in the monkey, but those human studies also need to take into account the effect of the past history of errors.

5.3.3 Task Switching and the Auditory Connections of ACC

A principal argument for the primacy of errors and reinforcement learning in the ACC is its anatomical connections: strong dopamine inputs, connections to primary motor areas and the ventral spinal horn, and lack of direct connection to visual areas (Rushworth et al., 2011; Rushworth and Behrens, 2008). Consistent with this, Johnston et al. (2007) found that ACC neurons more strongly discriminate the task context compared to dlPFC around the time of the switch in error-driven task switching and in Chapter III, I have found that dlPFC neurons have greater activity than ACC neurons around the time of the switch in visually cued task switching. This suggests that ACC is more important for error-driven switches and dlPFC is more important for visually cued switches. However, no

study thus far has considered auditory cues. ACC (areas 25 and 32) has strong auditory connections with the rostral superior temporal gyrus (Barbas et al., 1999; Medalla and Barbas, 2014, 2010). dlPFC, in contrast, has a more variable connection to auditory areas – following a rostral-caudal gradient of strong-to-weak that is inversely related to the strength of visual connections (Barbas et al., 1999; Medalla and Barbas, 2014). One possibility is that an auditorily cued task switch may result in stronger ACC activation than dlPFC – which would argue against a purely reinforcement learning view of ACC. Future research should investigate the role of auditory cues on ACC.

5.3.4 Building Better Interactive Visualizations

Interactive visualizations are unfamiliar as of now to the neuroscientific community and any barrier to setup and use of software will prevent widespread adoption. More user-focused testing is needed to identify which features of the visualization are useful, elements of the user interface that are unintuitive or hard to discover, and common stumbling blocks to the setup of the visualizations. Although user-focused testing is common with commercial level software, a big challenge going forward will be to figure out ways to get feedback on the software without commercial level resources. Dedicated early adopters often drive open source software development of tools, which is one reason that it is important that the tools are available on Github. It will be interesting to see if the tools developed in this dissertation and elsewhere are able to build the community and resources necessary to be useful.

Another area for future development is finding the appropriate balance of web technologies to provide fast user interactivity. As discussed in Chapter IV, delays in visualizations in response to user interaction can result in less engagement and exploration on the part of the user. Currently, the tools in Chapter IV use SVG – which is a vectorized image format. This format does not perform well if many data elements are displayed on the screen. HTML5 Canvas and WebGL are two alternative formats that have much better performance with many elements, but tradeoff nice features such as ease of programming, some forms of user interaction, and easy export into graphics programs such as Adobe Illustrator or Inkscape. Additionally, displaying many data elements is not always useful in terms of the user understanding the visualization. Future development work will need to consider these tradeoffs and figure out the appropriate blend of web technologies in order to provide smooth user interactions

BIBLIOGRAPHY

Aertsen, A.M., Gerstein, G.L., Habib, M.K., Palm, G., 1989. Dynamics of neuronal firing correlation: modulation of “effective connectivity.” *Journal of Neurophysiology* 61, 900–917.

Ainsworth, M., Lee, S., Cunningham, M.O., Traub, R.D., Kopell, N.J., Whittington, M.A., 2012. Rates and Rhythms: A Synergistic View of Frequency and Temporal Coding in Neuronal Networks. *Neuron* 75, 572–583.
doi:10.1016/j.neuron.2012.08.004

Akam, T., Kullmann, D.M., 2014. Oscillatory multiplexing of population codes for selective communication in the mammalian brain. *Nature Reviews Neuroscience* 15, 111–122.

Akam, T., Kullmann, D.M., 2010. Oscillations and Filtering Networks Support Flexible Routing of Information. *Neuron* 67, 308–320.
doi:10.1016/j.neuron.2010.06.019

Akam, T.E., Kullmann, D.M., 2012. Efficient “Communication through Coherence” Requires Oscillations Structured to Minimize Interference between Signals. *Public Library of Science Computational Biology* 8, e1002760.
doi:10.1371/journal.pcbi.1002760

Alexander, W.H., Brown, J.W., 2015. Hierarchical Error Representation: A Computational Model of Anterior Cingulate and Dorsolateral Prefrontal Cortex. *Neural Computation* 27, 2354–2410. doi:10.1162/NECO_a_00779

Alexander, W.H., Brown, J.W., 2011. Medial prefrontal cortex as an action-outcome predictor. *Nature Neuroscience* 14, 1338–1344. doi:10.1038/nn.2921

Alexander, W.H., Brown, J.W., 2010. Computational Models of Performance Monitoring and Cognitive Control. *Topics in Cognitive Science* 2, 658–677.
doi:10.1111/j.1756-8765.2010.01085.x

Allport, D.A., Styles, E.A., Hsieh, S., 1994. Shifting intentional set: Exploring the dynamic control of tasks., in: *Attention and Performance XV: Conscious and Nonconscious Information Processing*. The MIT Press.

Amemori, K., Graybiel, A.M., 2012. Localized microstimulation of primate pregenual cingulate cortex induces negative decision-making. *Nature Neuroscience* 15, 776–785. doi:10.1038/nn.3088

Androulidakis, A.G., Doyle, L.M., Yarrow, K., Litvak, V., Gilbertson, T.P., Brown, P., 2007. Anticipatory changes in beta synchrony in the human corticospinal

system and associated improvements in task performance. *European Journal of Neuroscience* 25, 3758–3765.

Anscombe, F.J., 1973. Graphs in statistical analysis. *The American Statistician* 27, 17–21.

Axmacher, N., Schmitz, D.P., Wagner, T., Elger, C.E., Fell, J., 2008. Interactions between medial temporal lobe, prefrontal cortex, and inferior temporal regions during visual working memory: a combined intracranial EEG and functional magnetic resonance imaging study. *The Journal of Neuroscience* 28, 7304–7312.

Babiloni, C., Babiloni, F., Carducci, F., Cincotti, F., Vecchio, F., Cola, B., Rossi, S., Miniussi, C., Rossini, P.M., 2004. Functional frontoparietal connectivity during short-term memory as revealed by high-resolution EEG coherence analysis. *Behavioral Neuroscience* 118, 687.

Barbas, H., Ghashghaei, H., Dombrowski, S.M., Rempel-Clower, N.L., 1999. Medial prefrontal cortices are unified by common connections with superior temporal cortices and distinguished by input from memory-related areas in the rhesus monkey. *Journal of Comparative Neurology* 410, 343–367.

Barbas, H., Pandya, D.N., 1989. Architecture and intrinsic connections of the prefrontal cortex in the rhesus monkey. *The Journal of Comparative Neurology* 286, 353–375. doi:10.1002/cne.902860306

Bates, J.F., Goldman-Rakic, P.S., 1993. Prefrontal connections of medial motor areas in the rhesus monkey. *Journal of Comparative Neurology* 336, 211–228.

Benjamini, Y., Hochberg, Y., 1995. Controlling the false discovery rate: a practical and powerful approach to multiple testing. *Journal of the Royal Statistical Society. Series B (Methodological)* 289–300.

Berens, P., 2008. Feature selectivity of the gamma-band of the local field potential in primate primary visual cortex. *Frontiers in Neuroscience* 2, 199–207. doi:10.3389/neuro.01.037.2008

Bostock, M., Ogievetsky, V., Heer, J., 2011. D³ data-driven documents. *Visualization and Computer Graphics, IEEE Transactions on* 17, 2301–2309.

Botvinick, M.M., Braver, T.S., Barch, D.M., Carter, C.S., Cohen, J.D., 2001. Conflict monitoring and cognitive control. *Psychological Review* 108, 624.

Botvinick, M.M., Cohen, J.D., Carter, C.S., 2004. Conflict monitoring and anterior cingulate cortex: an update. *Trends in Cognitive Sciences* 8, 539–546. doi:10.1016/j.tics.2004.10.003

Brown, J.W., Braver, T.S., 2005. Learned predictions of error likelihood in the anterior cingulate cortex. *Science* 307, 1118–1121.

Brutlag, J., 2009. Speed matters for Google web search. Google. June.

Buffalo, E.A., Fries, P., Landman, R., Buschman, T.J., Desimone, R., 2011. Laminar differences in gamma and alpha coherence in the ventral stream. *Proc. Nat. Acad. Sci. USA* 108, 11262–11267. doi:10.1073/pnas.1011284108

Burchell, T.R., Faulkner, H.J., Whittington, M.A., 1998. Gamma frequency oscillations gate temporally coded afferent inputs in the rat hippocampal slice. *Neuroscience Letters* 255, 151–154. doi:10.1016/S0304-3940(98)00676-4

Buschman, T.J., Denovellis, E.L., Diogo, C., Bullock, D., Miller, E.K., 2012. Synchronous Oscillatory Neural Ensembles for Rules in the Prefrontal Cortex. *Neuron* 76, 838–846. doi:10.1016/j.neuron.2012.09.029

Buschman, T.J., Miller, E.K., 2009. Serial, Covert Shifts of Attention during Visual Search Are Reflected by the Frontal Eye Fields and Correlated with Population Oscillations. *Neuron* 63, 386–396. doi:10.1016/j.neuron.2009.06.020

Buschman, T.J., Miller, E.K., 2007. Top-Down Versus Bottom-Up Control of Attention in the Prefrontal and Posterior Parietal Cortices. *Science* 315, 1860–1862. doi:10.1126/science.1138071

Bush, G., Luu, P., Posner, M.I., 2000. Cognitive and emotional influences in anterior cingulate cortex. *Trends in Cognitive Sciences* 4, 215–222. doi:10.1016/S1364-6613(00)01483-2

Card, S.K., Mackinlay, J.D., Shneiderman, B., 1999. Readings in information visualization: using vision to think. Morgan Kaufmann.

Carter, C.S., Braver, T.S., Barch, D.M., Botvinick, M.M., Noll, D., Cohen, J.D., 1998. Anterior Cingulate Cortex, Error Detection, and the Online Monitoring of Performance. *Science* 280, 747–749. doi:10.1126/science.280.5364.747

Carter, C.S., Veen, V. van, 2007. Anterior cingulate cortex and conflict detection: An update of theory and data. *Cognitive, Affective, & Behavioral Neuroscience* 7, 367–379. doi:10.3758/CABN.7.4.367

Caselli, L., Chelazzi, L., 2011. Does the Macaque Monkey Provide a Good Model for Studying Human Executive Control? A Comparative Behavioral Study of Task Switching. *Public Library of Science ONE* 6, e21489. doi:10.1371/journal.pone.0021489

Cleveland, W.S., McGill, R., 1985. Graphical perception and graphical methods for analyzing scientific data. *Science* 229, 828–833.

Cleveland, W.S., McGill, R., 1984. Graphical perception: Theory, experimentation, and application to the development of graphical methods. *Journal of the American Statistical Association* 79, 531–554.

Cohen, M.R., Maunsell, J.H.R., 2009. Attention improves performance primarily by reducing interneuronal correlations. *Nature Neuroscience* 12, 1594–1600. doi:10.1038/nn.2439

Cole, M.W., Schneider, W., 2007. The cognitive control network: Integrated cortical regions with dissociable functions. *NeuroImage* 37, 343–360. doi:10.1016/j.neuroimage.2007.03.071

Cole, M.W., Yeung, N., Freiwald, W.A., Botvinick, M., 2009. Cingulate cortex: Diverging data from humans and monkeys. *Trends in Neurosciences* 32, 566–574. doi:10.1016/j.tins.2009.07.001

Cromer, J.A., Roy, J.E., Miller, E.K., 2010. Representation of multiple, independent categories in the primate prefrontal cortex. *Neuron* 66, 796–807.

Dias, R., Robbins, T.W., Roberts, A.C., 1996. Dissociation in prefrontal cortex of affective and attentional shifts 380. *Nature* 69–72. doi:10.1038/380069a0

Dove, A., Pollmann, S., Schubert, T., Wiggins, C.J., Von Cramon, D.Y., 2000. Prefrontal cortex activation in task switching: an event-related fMRI study. *Cognitive Brain Research* 9, 103–109.

Ebitz, R.B., Platt, M.L., 2015. Neuronal Activity in Primate Dorsal Anterior Cingulate Cortex Signals Task Conflict and Predicts Adjustments in Pupil-Linked Arousal. *Neuron* 85, 628–640. doi:10.1016/j.neuron.2014.12.053

Einevoll, G.T., Franke, F., Hagen, E., Pouzat, C., Harris, K.D., 2012. Towards reliable spike-train recordings from thousands of neurons with multielectrodes. *Current Opinion in Neurobiology* 22, 11–17. doi:10.1016/j.conb.2011.10.001

Engel, A.K., Fries, P., 2010. Beta-band oscillations—signalling the status quo? *Current Opinion in Neurobiology* 20, 156–165.

Fekete, J.-D., Van Wijk, J.J., Stasko, J.T., North, C., 2008. The value of information visualization, in: *Information Visualization*. Springer, pp. 1–18.

Fernandes, H.L., Stevenson, I.H., Phillips, A.N., Segraves, M.A., Kording, K.P., 2014. Saliency and Saccade Encoding in the Frontal Eye Field During Natural Scene Search. *Cerebral Cortex* 24, 3232–3245. doi:10.1093/cercor/bht179

- Freeman, J., 2015. Open source tools for large-scale neuroscience. *Current Opinion in Neurobiology* 32, 156–163. doi:10.1016/j.conb.2015.04.002
- Freeman, J., Vladimirov, N., Kawashima, T., Mu, Y., Sofroniew, N.J., Bennett, D.V., Rosen, J., Yang, C.-T., Looger, L.L., Ahrens, M.B., 2014. Mapping brain activity at scale with cluster computing. *Nature Methods* 11, 941–950. doi:10.1038/nmeth.3041
- Freunberger, R., Klimesch, W., Griesmayr, B., Sauseng, P., Gruber, W., 2008. Alpha phase coupling reflects object recognition. *Neuroimage* 42, 928–935.
- Fries, P., 2005. A mechanism for cognitive dynamics: neuronal communication through neuronal coherence. *Trends in Cognitive Sciences* 9, 474–480. doi:10.1016/j.tics.2005.08.011
- Fries, P., Reynolds, J.H., Rorie, A.E., Desimone, R., 2001. Modulation of oscillatory neuronal synchronization by selective visual attention. *Science* 291, 1560.
- Fusi, S., Miller, E.K., Rigotti, M., 2016. Why neurons mix: high dimensionality for higher cognition. *Current Opinion in Neurobiology* 37, 66–74. doi:10.1016/j.conb.2016.01.010
- Fuster, J.M., 1973. Unit activity in prefrontal cortex during delayed-response performance: neuronal correlates of transient memory. *Journal of Neurophysiology*.
- Gao, J.S., Huth, A.G., Lescroart, M.D., Gallant, J.L., 2015. Pycortex: an interactive surface visualizer for fMRI. *Frontiers in Neuroinformatics* 9. doi:10.3389/fninf.2015.00023
- Gehring, W.J., Fencsik, D.E., 2001. Functions of the Medial Frontal Cortex in the Processing of Conflict and Errors. *The Journal of Neuroscience* 21, 9430–9437.
- Gelman, A., 2004. Exploratory Data Analysis for Complex Models. *Journal of Computational and Graphical Statistics* 13, 755–779. doi:10.1198/106186004X11435
- Gelman, A., Unwin, A., 2013. Infovis and statistical graphics: different goals, different looks. *Journal of Computational and Graphical Statistics* 22, 2–28.
- Gilbertson, T., Lalo, E., Doyle, L., Di Lazzaro, V., Cioni, B., Brown, P., 2005. Existing motor state is favored at the expense of new movement during 13-35 Hz oscillatory synchrony in the human corticospinal system. *The Journal of Neuroscience* 25, 7771–7779.

- Gould, I.C., Rushworth, M.F., Nobre, A.C., 2011. Indexing the graded allocation of visuospatial attention using anticipatory alpha oscillations. *Journal of Neurophysiology* 105, 1318–1326.
- Gregoriou, G.G., Gotts, S.J., Zhou, H., Desimone, R., 2009. High-Frequency, Long-Range Coupling Between Prefrontal and Visual Cortex During Attention. *Science* 324, 1207–1210. doi:10.1126/science.1171402
- Gross, J., Schmitz, F., Schnitzler, I., Kessler, K., Shapiro, K., Hommel, B., Schnitzler, A., 2006. Anticipatory control of long-range phase synchronization. *European Journal of Neuroscience* 24, 2057–2060.
- Haegens, S., Nácher, V., Hernández, A., Luna, R., Jensen, O., Romo, R., 2011a. Beta oscillations in the monkey sensorimotor network reflect somatosensory decision making. *Proc. Nat. Acad. Sci. USA* 108, 10708.
- Haegens, S., Nácher, V., Luna, R., Romo, R., Jensen, O., 2011b. α -Oscillations in the monkey sensorimotor network influence discrimination performance by rhythmical inhibition of neuronal spiking. *Proc. Nat. Acad. Sci. USA* 108, 19377–19382.
- Harris, K.D., Csicsvari, J., Hirase, H., Dragoi, G., Buzsáki, G., 2003. Organization of cell assemblies in the hippocampus. *Nature* 424, 552–556.
- Hayden, B.Y., Platt, M.L., 2010. Neurons in anterior cingulate cortex multiplex information about reward and action. *The Journal of Neuroscience* 30, 3339–3346.
- Healey, C.G., Booth, K.S., Enns, J.T., 1996. High-speed visual estimation using preattentive processing. *ACM Transactions on Computer-Human Interaction (TOCHI)* 3, 107–135.
- Healey, C.G., Enns, J.T., 2012. Attention and Visual Memory in Visualization and Computer Graphics. *IEEE Transactions on Visualization and Computer Graphics* 18, 1170–1188. doi:10.1109/TVCG.2011.127
- Heer, J., Robertson, G.G., 2007. Animated transitions in statistical data graphics. *IEEE Transactions on Visualization and Computer Graphics* 13, 1240–1247.
- Heer, J., Shneiderman, B., 2012. Interactive dynamics for visual analysis. *Queue* 10, 30.
- Holroyd, C.B., Coles, M.G.H., 2002. The neural basis of human error processing: reinforcement learning, dopamine, and the error-related negativity. *Psychological Review* 109, 679–709.

- Holroyd, C.B., Yeung, N., 2012. Motivation of extended behaviors by anterior cingulate cortex. *Trends in Cognitive Sciences* 16, 122–128. doi:10.1016/j.tics.2011.12.008
- Huth, A.G., Nishimoto, S., Vu, A.T., Gallant, J.L., 2012. A Continuous Semantic Space Describes the Representation of Thousands of Object and Action Categories across the Human Brain. *Neuron* 76, 1210–1224. doi:10.1016/j.neuron.2012.10.014
- Hyafil, A., Summerfield, C., Koehlin, E., 2009. Two mechanisms for task switching in the prefrontal cortex. *The Journal of Neuroscience* 29, 5135–5142.
- Inselberg, A., 1985. The plane with parallel coordinates. *The Visual Computer* 1, 69–91.
- Ito, S., Stuphorn, V., Brown, J.W., Schall, J.D., 2003. Performance monitoring by the anterior cingulate cortex during saccade countermanding. *Science* 302, 120–122.
- Jacobson, S., Trojanowski, J.Q., 1977. Prefrontal granular cortex of the rhesus monkey. I. Intrahemispheric cortical afferents. *Brain Research* 132, 209–233.
- Jensen, O., Gelfand, J., Kounios, J., Lisman, J.E., 2002. Oscillations in the alpha band (9–12 Hz) increase with memory load during retention in a short-term memory task. *Cerebral Cortex* 12, 877–882.
- Johnston, K., Levin, H.M., Koval, M.J., Everling, S., 2007. Top-Down Control-Signal Dynamics in Anterior Cingulate and Prefrontal Cortex Neurons following Task Switching. *Neuron* 53, 453–462. doi:10.1016/j.neuron.2006.12.023
- Jones, S.R., Pinto, D.J., Kaper, T.J., Kopell, N., 2000. Alpha-Frequency Rhythms Desynchronize over Long Cortical Distances: A Modeling Study. *Journal of Computational Neuroscience* 9, 271–291. doi:10.1023/A:1026539805445
- Kajikawa, Y., Schroeder, C.E., 2011. How local is the local field potential? *Neuron* 72, 847–858.
- Katzner, S., Nauhaus, I., Benucci, A., Bonin, V., Ringach, D.L., Carandini, M., 2009. Local Origin of Field Potentials in Visual Cortex. *Neuron* 61, 35–41. doi:10.1016/j.neuron.2008.11.016
- Kennerley, S.W., Behrens, T.E., Wallis, J.D., 2011. Double dissociation of value computations in orbitofrontal and anterior cingulate neurons. *Nature Neuroscience* 14, 1581–1589.

Kennerley, S.W., Dahmubed, A.F., Lara, A.H., Wallis, J.D., 2009. Neurons in the frontal lobe encode the value of multiple decision variables. *Journal of Cognitive Neuroscience* 21, 1162–1178.

Kennerley, S.W., Walton, M.E., Behrens, T.E.J., Buckley, M.J., Rushworth, M.F.S., 2006. Optimal decision making and the anterior cingulate cortex. *Nature Neuroscience* 9, 940–947. doi:10.1038/nn1724

Keren, G., Lewis, C., 1979. Partial omega squared for ANOVA designs. *Educational and Psychological Measurement* 39, 119.

Kerns, J.G., Cohen, J.D., MacDonald, A.W., Cho, R.Y., Stenger, V.A., Carter, C.S., 2004. Anterior cingulate conflict monitoring and adjustments in control. *Science* 303, 1023–1026.

Klimesch, W., 1999. EEG alpha and theta oscillations reflect cognitive and memory performance: a review and analysis. *Brain Research Reviews* 29, 169–195.

Klimesch, W., Sauseng, P., Hanslmayr, S., 2007. EEG alpha oscillations: the inhibition-timing hypothesis. *Brain Research Reviews* 53, 63–88.

Kopell, N., Kramer, M.A., Malerba, P., Whittington, M.A., 2010. Are different rhythms good for different functions? *Frontiers in Human Neuroscience* 4.

Lakatos, P., Karmos, G., Mehta, A.D., Ulbert, I., Schroeder, C.E., 2008. Entrainment of Neuronal Oscillations as a Mechanism of Attentional Selection. *Science* 320, 110–113. doi:10.1126/science.1154735

Liang, H., Bressler, S.L., Ding, M., Truccolo, W.A., Nakamura, R., 2002. Synchronized activity in prefrontal cortex during anticipation of visuomotor processing. *Neuroreport* 13, 2011–2015.

Liu, Z., Heer, J., 2014. The effects of interactive latency on exploratory visual analysis. *IEEE Transactions on Visualization and Computer Graphics* 20, 2122–2131.

Luk, C.-H., Wallis, J.D., 2013. Choice Coding in Frontal Cortex during Stimulus-Guided or Action-Guided Decision-Making. *The Journal of Neuroscience* 33, 1864–1871. doi:10.1523/JNEUROSCI.4920-12.2013

Luks, T.L., Simpson, G.V., Feiwell, R.J., Miller, W.L., 2002. Evidence for Anterior Cingulate Cortex Involvement in Monitoring Preparatory Attentional Set. *NeuroImage* 17, 792–802. doi:10.1006/nimg.2002.1210

MacDonald, A.W., Cohen, J.D., Stenger, V.A., Carter, C.S., 2000. Dissociating the role of the dorsolateral prefrontal and anterior cingulate cortex in cognitive control. *Science* 288, 1835–1838.

MacDonald, C.J., Lepage, K.Q., Eden, U.T., Eichenbaum, H., 2011. Hippocampal “time cells” bridge the gap in memory for discontinuous events. *Neuron* 71, 737–749.

MacLeod, C.M., 1991. Half a century of research on the Stroop effect: An integrative review. *Psychological Bulletin* 109, 163.

Mathewson, K.E., Lleras, A., Beck, D.M., Fabiani, M., Ro, T., Gratton, G., 2011. Pulsed out of awareness: EEG alpha oscillations represent a pulsed-inhibition of ongoing cortical processing. *Frontiers in Psychology* 2.

Matsumoto, K., Suzuki, W., Tanaka, K., 2003. Neuronal correlates of goal-based motor selection in the prefrontal cortex. *Science* 301, 229–232.

Matsumoto, M., Matsumoto, K., Abe, H., Tanaka, K., 2007. Medial prefrontal cell activity signaling prediction errors of action values. *Nature Neuroscience* 10, 647–656. doi:10.1038/nn1890

Mayo, J.P., DiTomasso, A.R., Sommer, M.A., Smith, M.A., 2015. Dynamics of visual receptive fields in the macaque frontal eye field. *Journal of Neurophysiology* 114, 3201–3210. doi:10.1152/jn.00746.2015

McCullagh, P., Nelder, J.A., 1989. *Generalized linear models*. Chapman & Hall/CRC.

Medalla, M., Barbas, H., 2014. Specialized prefrontal “auditory fields”: organization of primate prefrontal-temporal pathways. *Frontiers in Neuroscience* 8, 10–3389.

Medalla, M., Barbas, H., 2010. Anterior Cingulate Synapses in Prefrontal Areas 10 and 46 Suggest Differential Influence in Cognitive Control. *The Journal of Neuroscience* 30, 16068–16081. doi:10.1523/JNEUROSCI.1773-10.2010

Medalla, M., Barbas, H., 2009. Synapses with Inhibitory Neurons Differentiate Anterior Cingulate from Dorsolateral Prefrontal Pathways Associated with Cognitive Control. *Neuron* 61, 609–620. doi:10.1016/j.neuron.2009.01.006

Michelet, T., Bioulac, B., Guehl, D., Goillandeau, M., Burbaud, P., 2009. Single medial prefrontal neurons cope with error. *Public Library of Science One* 4, e6240.

- Miller, E.K., Cohen, J.D., 2001. An integrative theory of prefrontal cortex function. *Annual Review of Neuroscience* 24, 167–202.
- Miller, E.K., Wilson, M.A., 2008. All My Circuits: Using Multiple Electrodes to Understand Functioning Neural Networks. *Neuron* 60, 483–488. doi:10.1016/j.neuron.2008.10.033
- Milner, B., 1963. Effects of different brain lesions on card sorting: The role of the frontal lobes. *Archives of Neurology* 9, 90.
- Mitchell, J.F., Sundberg, K.A., Reynolds, J.H., 2009. Spatial attention decorrelates intrinsic activity fluctuations in macaque area V4. *Neuron* 63, 879–888.
- Monsell, S., 2003. Task switching. *Trends in Cognitive Sciences* 7, 134–140.
- Nakamura, K., Roesch, M.R., Olson, C.R., 2005. Neuronal activity in macaque SEF and ACC during performance of tasks involving conflict. *Journal of Neurophysiology* 93, 884–908.
- Nettleton, J.S., Spain, W.J., 2000. Linear to Supralinear Summation of AMPA-Mediated EPSPs in Neocortical Pyramidal Neurons. *Journal of Neurophysiology* 83, 3310–3322.
- Nichols, T.E., Holmes, A.P., 2002. Nonparametric permutation tests for functional neuroimaging: a primer with examples. *Human Brain Mapping* 15, 1–25.
- Niki, H., Watanabe, M., 1979. Prefrontal and cingulate unit activity during timing behavior in the monkey. *Brain Research* 171, 213–224.
- Oswal, A., Litvak, V., Sauleau, P., Brown, P., 2012. Beta reactivity, prospective facilitation of executive processing, and its dependence on dopaminergic therapy in Parkinson's disease. *The Journal of Neuroscience* 32, 9909–9916.
- Palva, S., Palva, J.M., 2011. Functional roles of alpha-band phase synchronization in local and large-scale cortical networks. *Frontiers in Psychology* 2.
- Palva, S., Palva, J.M., 2007. New vistas for α -frequency band oscillations. *Trends in Neurosciences* 30, 150–158.
- Park, I.M., Meister, M.L.R., Huk, A.C., Pillow, J.W., 2014. Encoding and decoding in parietal cortex during sensorimotor decision-making. *Nature Neuroscience* 17, 1395–1403. doi:10.1038/nn.3800

- Pesaran, B., Nelson, M.J., Andersen, R.A., 2008. Free choice activates a decision circuit between frontal and parietal cortex. *Nature* 453, 406.
- Petersen, S.E., Fox, P.T., Posner, M.I., Mintun, M., Raichle, M.E., 1989. Positron emission tomographic studies of the processing of single words. *Journal of Cognitive Neuroscience* 1, 153–170.
- Pfurtscheller, G., 2001. Functional brain imaging based on ERD/ERS. *Vision Research* 41, 1257–1260.
- Pfurtscheller, G., 1981. Central beta rhythm during sensorimotor activities in man. *Electroencephalography and clinical neurophysiology* 51, 253–264.
- Pillow, J.W., 2005. Prediction and Decoding of Retinal Ganglion Cell Responses with a Probabilistic Spiking Model. *Journal of Neuroscience* 25, 11003–11013. doi:10.1523/JNEUROSCI.3305-05.2005
- Poldrack, R.A., Gorgolewski, K.J., 2014. Making big data open: data sharing in neuroimaging. *Nature Neuroscience* 17, 1510–1517. doi:10.1038/nn.3818
- Rainer, G., Rao, S.C., Miller, E.K., 1999. Prospective coding for objects in primate prefrontal cortex. *The Journal of Neuroscience* 19, 5493–5505.
- Ray, W.J., Cole, H.W., 1985. EEG alpha activity reflects attentional demands, and beta activity reflects emotional and cognitive processes. *Science* 228, 750.
- Rigotti, M., Barak, O., Warden, M.R., Wang, X.-J., Daw, N.D., Miller, E.K., Fusi, S., 2013. The importance of mixed selectivity in complex cognitive tasks. *Nature advance online publication*. doi:10.1038/nature12160
- Rigotti, M., Rubin, D.B.D., Wang, X.J., Fusi, S., 2010. Internal representation of task rules by recurrent dynamics: the importance of the diversity of neural responses. *Frontiers in Computational Neuroscience* 4.
- Rogers, R.D., Monsell, S., 1995. Costs of a predictable switch between simple cognitive tasks. *Journal of Experimental Psychology: General* 124, 207.
- Rudebeck, P.H., Walton, M.E., Smyth, A.N., Bannerman, D.M., Rushworth, M.F.S., 2006. Separate neural pathways process different decision costs. *Nature Neuroscience* 9, 1161–1168. doi:10.1038/nn1756
- Ruge, H., Jamadar, S., Zimmermann, U., Karayanidis, F., 2013. The many faces of preparatory control in task switching: reviewing a decade of fMRI research. *Human Brain Mapping* 34, 12–35.

- Rushworth, M.F.S., Behrens, T.E.J., 2008. Choice, uncertainty and value in prefrontal and cingulate cortex. *Nature Neuroscience* 11, 389–397. doi:10.1038/nn2066
- Rushworth, M.F.S., Hadland, K.A., Gaffan, D., Passingham, R.E., 2003. The effect of cingulate cortex lesions on task switching and working memory. *Journal of Cognitive Neuroscience* 15, 338–353.
- Rushworth, M.F.S., Noonan, M.P., Boorman, E.D., Walton, M.E., Behrens, T.E., 2011. Frontal Cortex and Reward-Guided Learning and Decision-Making. *Neuron* 70, 1054–1069. doi:10.1016/j.neuron.2011.05.014
- Sadaghiani, S., Scheeringa, R., Lehongre, K., Morillon, B., Giraud, A.L., Kleinschmidt, A., 2010. Intrinsic connectivity networks, alpha oscillations, and tonic alertness: a simultaneous electroencephalography/functional magnetic resonance imaging study. *The Journal of Neuroscience* 30, 10243–10250.
- Sakai, K., Passingham, R.E., 2003. Prefrontal interactions reflect future task operations. *Nature Neuroscience* 6, 75–81.
- Salazar, R.F., Dotson, N.M., Bressler, S.L., Gray, C.M., 2012. Content-Specific Fronto-Parietal Synchronization During Visual Working Memory. *Science* 338, 1097–1100. doi:10.1126/science.1224000
- Salinas, E., Sejnowski, T.J., 2000. Impact of Correlated Synaptic Input on Output Firing Rate and Variability in Simple Neuronal Models. *The Journal of Neuroscience* 20, 6193–6209.
- Sauseng, P., Klimesch, W., Stadler, W., Schabus, M., Doppelmayr, M., Hanslmayr, S., Gruber, W.R., Birbaumer, N., 2005. A shift of visual spatial attention is selectively associated with human EEG alpha activity. *European Journal of Neuroscience* 22, 2917–2926.
- Scheffers, M.K., Coles, M.G.H., 2000. Performance monitoring in a confusing world: Error-related brain activity, judgments of response accuracy, and types of errors. *Journal of Experimental Psychology: Human Perception and Performance* 26, 141–151. doi:10.1037/0096-1523.26.1.141
- Schwartz, M.L., Goldman-Rakic, P.S., 1984. Callosal and intrahemispheric connectivity of the prefrontal association cortex in rhesus monkey: relation between intraparietal and principal sulcal cortex. *Journal of Comparative Neurology* 226, 403–420.
- Sejnowski, T.J., Paulsen, O., 2006. Network oscillations: emerging computational principles. *The Journal of Neuroscience* 26, 1673.

- Seo, H., Lee, D., 2007. Temporal Filtering of Reward Signals in the Dorsal Anterior Cingulate Cortex during a Mixed-Strategy Game. *The Journal of Neuroscience* 27, 8366–8377. doi:10.1523/JNEUROSCI.2369-07.2007
- Shen, C., Ardid, S., Kaping, D., Westendorff, S., Everling, S., Womelsdorf, T., 2014. Anterior Cingulate Cortex Cells Identify Process-Specific Errors of Attentional Control Prior to Transient Prefrontal-Cingulate Inhibition. *Cerebral Cortex* bh028. doi:10.1093/cercor/bhu028
- Shenhav, A., Botvinick, M.M., Cohen, J.D., 2013. The Expected Value of Control: An Integrative Theory of Anterior Cingulate Cortex Function. *Neuron* 79, 217–240. doi:10.1016/j.neuron.2013.07.007
- Sherif, T., Kassis, N., Rousseau, M.-Ã., Adalat, R., Evans, A.C., 2015. BrainBrowser: distributed, web-based neurological data visualization. *Frontiers in Neuroinformatics* 8. doi:10.3389/fninf.2014.00089
- Sheth, S.A., Mian, M.K., Patel, S.R., Asaad, W.F., Williams, Z.M., Dougherty, D.D., Bush, G., Eskandar, E.N., 2012. Human dorsal anterior cingulate cortex neurons mediate ongoing behavioural adaptation. *Nature* 488, 218–221. doi:10.1038/nature11239
- Shima, K., Tanji, J., 1998. Role for cingulate motor area cells in voluntary movement selection based on reward. *Science* 282, 1335.
- Siegel, M., Buschman, T.J., Miller, E.K., 2015. Cortical information flow during flexible sensorimotor decisions. *Science* 348, 1352–1355.
- Siegel, M., Donner, T.H., Engel, A.K., 2012. Spectral fingerprints of large-scale neuronal interactions. *Nature Reviews Neuroscience*.
- Silva, L.R., Amitai, Y., Connors, B.W., 1991. Intrinsic oscillations of neocortex generated by layer 5 pyramidal neurons. *Science* 251, 432–435.
- Singer, W., 2013. Cortical dynamics revisited. *Trends in Cognitive Sciences* 17, 616–626. doi:10.1016/j.tics.2013.09.006
- Spence, I., Lewandowsky, S., 1991. Displaying proportions and percentages. *Applied Cognitive Psychology* 5, 61–77.
- Stevenson, I.H., Kording, K.P., 2011. How advances in neural recording affect data analysis. *Nature Neuroscience* 14, 139–142. doi:10.1038/nn.2731
- Stuss, D.T., Benson, D.F., 1984. Neuropsychological studies of the frontal lobes. *Psychological Bulletin* 95, 3.

Sun, W., Dan, Y., 2009. Layer-specific network oscillation and spatiotemporal receptive field in the visual cortex. *Proc. Nat. Acad. Sci. USA* 106, 17986–17991. doi:10.1073/pnas.0903962106

Swann, N., Tandon, N., Canolty, R., Ellmore, T.M., McEvoy, L.K., Dreyer, S., DiSano, M., Aron, A.R., 2009. Intracranial EEG reveals a time- and frequency-specific role for the right inferior frontal gyrus and primary motor cortex in stopping initiated responses. *The Journal of Neuroscience* 29, 12675–12685.

Truccolo, W., 2004. A Point Process Framework for Relating Neural Spiking Activity to Spiking History, Neural Ensemble, and Extrinsic Covariate Effects. *Journal of Neurophysiology* 93, 1074–1089. doi:10.1152/jn.00697.2004

Tukey, J.W., 1993. Graphic Comparisons of Several Linked Aspects: Alternatives and Suggested Principles. *Journal of Computational and Graphical Statistics* 2, 1. doi:10.2307/1390951

Tukey, J.W., 1977. *Exploratory data analysis*.

Tversky, B., Morrison, J.B., Betrancourt, M., 2002. Animation: can it facilitate? *International journal of human-computer studies* 57, 247–262.

van Aerde, K.I., Mann, E.O., Canto, C.B., Heistek, T.S., Linkenkaer-Hansen, K., Mulder, A.B., van der Roest, M., Paulsen, O., Brussaard, A.B., Mansvelder, H.D., 2009. Flexible spike timing of layer 5 neurons during dynamic beta oscillation shifts in rat prefrontal cortex. *The Journal of Physiology* 587, 5177–5196. doi:10.1113/jphysiol.2009.178384

Van der Maaten, L., Hinton, G., 2008. Visualizing data using t-SNE. *Journal of Machine Learning Research* 9, 85.

Van Dijk, K.R.A., Sabuncu, M.R., Buckner, R.L., 2012. The influence of head motion on intrinsic functional connectivity MRI. *NeuroImage* 59, 431–438. doi:10.1016/j.neuroimage.2011.07.044

Ventura, V., Carta, R., Kass, R.E., Gettner, S.N., Olson, C.R., 2002. Statistical analysis of temporal evolution in single-neuron firing rates. *Biostatistics* 3, 1–20.

Von Stein, A., Chiang, C., König, P., 2000. Top-down processing mediated by interareal synchronization. *Proc. Nat. Acad. Sci. USA* 97, 14748.

Wallis, J.D., Anderson, K.C., Miller, E.K., 2001. Single neurons in prefrontal cortex encode abstract rules. *Nature* 411, 953–956.

Wegman, E.J., 1990. Hyperdimensional data analysis using parallel coordinates. *Journal of the American Statistical Association* 85, 664–675.

White, I.M., Wise, S.P., 1999. Rule-dependent neuronal activity in the prefrontal cortex. *Experimental Brain Research* 126, 315–335.

Womelsdorf, T., Schoffelen, J.-M., Oostenveld, R., Singer, W., Desimone, R., Engel, A.K., Fries, P., 2007. Modulation of Neuronal Interactions Through Neuronal Synchronization. *Science* 316, 1609–1612. doi:10.1126/science.1139597

Woodward, T.S., Ruff, C.C., Ngan, E.T.C., 2006. Short- and long-term changes in anterior cingulate activation during resolution of task-set competition. *Brain Research* 1068, 161–169. doi:10.1016/j.brainres.2005.10.094

Worden, M.S., Foxe, J.J., Wang, N., Simpson, G.V., 2000. Anticipatory biasing of visuospatial attention indexed by retinotopically specific-band electroencephalography increases over occipital cortex. *The Journal of Neuroscience* 20, 1–6.

Yeterian, E.H., Pandya, D.N., 1994. Laminar origin of striatal and thalamic projections of the prefrontal cortex in rhesus monkeys. *Experimental Brain Research* 99, 383–398.

Zhang, Y., Wang, X., Bressler, S.L., Chen, Y., Ding, M., 2008. Prestimulus cortical activity is correlated with speed of visuomotor processing. *Journal of Cognitive Neuroscience* 20, 1915–1925.

CURRICULUM VITAE

Eric L. Denovellis (DOB: 8-17-1985)

CONTACT INFORMATION	677 Beacon St. Boston University Boston, MA 02215 USA	<i>Email:</i> edeno@bu.edu <i>Website:</i> ericdeno.com <i>Github:</i> github.com/edeno
RESEARCH INTERESTS	Interactive data visualization, statistical methods for large datasets, prefrontal cortex, cognitive flexibility, task switching, machine learning, computational neuroscience	
EDUCATION	<p>Boston University, Boston, Massachusetts USA <i>Graduate Program for Neuroscience</i></p> <p>Ph.D. in Computational Neuroscience, March, 2016</p> <p>Thesis: "Task switching in the prefrontal cortex"</p> <p>Advisor: Daniel Bullock</p> <p>University of California, Santa Barbara, Santa Barbara, California USA</p> <p>B.S., Mathematics and B.A., Philosophy with High Honors, June 2007</p>	
ACADEMIC EXPERIENCE	<p>Boston University, Boston, Massachusetts USA</p> <p><i>Graduate Student</i> September, 2009 - June, 2016 Includes doctoral and masters level coursework in mathematics, statistics, computational modeling, and neuroscience as well as research into the neural correlates of task switching.</p> <p><i>Teaching Fellow</i> January, 2014 - May, 2014 CAS NE 340 - Introduction to Computational Models of Skilled Decision and Action. Gave lecture on Matlab. Assisted in computer lab.</p> <p><i>Teaching Fellow</i> January, 2011 - May, 2011 CAS CN 570 - Neural and Computational Models of Conditioning, Reinforcement, Motivation and Rhythm. Gave lecture on task switching. Led MATLAB tutorial and designed the course final project.</p> <p>University of California, Santa Barbara, Santa Barbara, California USA</p> <p><i>Campus Learning Assistance Services - Mathematics Tutor</i> September, 2005 - June, 2007 Assisted students with mathematics homework for lower level courses.</p>	
SERVICE	<p><i>CELEST Student Organization Co-President</i> May, 2011 - March, 2016 In charge of organizing CELEST student events (CELEST is an NSF-funded Science of Learning Center), scheduling the speaker series, Matlab tutorials for CELEST summer program for college students.</p> <p><i>Computational Neuroscience Student Organization Treasurer</i> May, 2010 - March, 2011 In charge of budgeting funds and reimbursing students.</p>	

- PUBLICATIONS** Buschman, T.J.*, **Denovellis, E.L.***, Diogo, C.*, Bullock, D., and Miller, E.K. (2012). Synchronous Oscillatory Neural Ensembles for Rules in the Prefrontal Cortex. *Neuron*. 76, 1–9.
- * Co-first authors**
- CONFERENCE PROCEEDINGS** **Denovellis, E.L.**, Buschman, T.J., Diogo, C., Bullock, D., and Miller, E.K. Point process models of anterior cingulate and dorsolateral prefrontal cortical neurons during cognitive control. Program No. 599.12. 2012 Neuroscience Meeting Planner. New Orleans, LA: Society for Neuroscience, 2012. Online.
- Buschman, T.J., **Denovellis, E.L.**, Diogo, C., Bullock, D., and Miller, E.K. Dynamic, synchronous, sub-networks in prefrontal cortex encode stimulus-response rules. Program No. 599.12. 2012 Neuroscience Meeting Planner. New Orleans, LA: Society for Neuroscience, 2012. Online.
- Buschman, T.J., **Denovellis, E.L.**, Diogo, C., Bullock, D., and Miller, E. (2012). Dynamic networks in frontal cortex support the cognitive flexibility to switch between rules. Poster presented at the Computational and systems neuroscience (Cosyne) meeting, Salt Lake City, UT.
- Denovellis, E.L.**, Buschman, T.J., Diogo, C., Bullock, D., and Miller, E.K. Rule-based task switching in the anterior cingulate and prefrontal cortex. Program No. 405.18. 2011 Neuroscience Meeting Planner. Washington, DC: Society for Neuroscience, 2011. Online.
- TALKS** Data visualization tools: from classroom to science. Inter Science of Learning Centers Conference Workshop. San Diego, CA June 2015
- Synchronous Neural Ensembles for Rules in the Prefrontal Cortex. The 5th Annual Dana and Betty Fisher Retreat of the Picower Institute. Red Jacket Resort. South Yarmouth, MA June 2012.
- Neural Dynamics of Cognitive Flexibility. Fall 2011 Picower Plastic Lunch Series. Massachusetts Institute of Technology. Cambridge, MA October 2011.
- PROFESSIONAL EXPERIENCE** **Mercer Advisors**, Santa Barbara, California USA
- Pension Consultant I* **October, 2007 - July, 2009**
- In charge of designing and advising clients on pension plans for three national offices. Carried out statistical analysis of pension plans. Attended conferences to keep abreast of IRS rule changes. Designed a computer program to enhance the efficiency of pension plan design and analysis.
- PROFESSIONAL MEMBERSHIPS** Society for Neuroscience **May, 2011 - Present**
- HONORS AND AWARDS** Phi Beta Kappa, Lambda Chapter
- SKILLS**
- Statistical Packages: MATLAB, R
 - Languages: Javascript